Fundamentals of Nonlinear Optics

ECED 6400 Lecture Notes

January 11, 2018

Contents

Chapter 1

Introduction

In this course, we will be describing all optical phenomena classically within the framework of *macroscopic Maxwell's equations* written in terms of *macroscopic* electromagnetic fields. The latter are obtained by averaging rapidly varying microscopic fields over spatial scales much larger than characteristic material microstructure scales (atomic size, lattice scale, etc). The averaging procedure is examined in detail in standard electrodynamics textbooks[1]. Within the framework of such a phenomenological approach, which circumvents a detailed microscopic light-matter interaction description, *external* or *driving* volume charge and current densities, $\rho_{\rm ex}$ and $\mathbf{J}_{\rm ex}$, give rise to the electromagnetic fields obeying the Maxwell equations in the form

$$\nabla \cdot \mathbf{D} = \rho_{\rm ex}, \tag{1.1}$$

$$\nabla \cdot \mathbf{B} = 0, \tag{1.2}$$

$$\nabla \times \mathbf{E} = -\partial_t \mathbf{B} \tag{1.3}$$

and

$$\nabla \times \mathbf{H} = \mathbf{J}_{\rm ex} + \partial_t \mathbf{D}. \tag{1.4}$$

The set of equations (1.1) through (1.4) is not closed, however, until we provide any information about the material media. Such information is furnished by supplying phenomenological constitutive relations among the four fields, $\mathbf{E}$, $\mathbf{D}$, $\mathbf{B}$, and $\mathbf{H}$. Without much loss of generality we will assume hereafter that all material media are nonmagnetic, which holds true for virtually all natural media at optical frequencies [2]. We can then represent the magnetic constitutive relation in its simplest form as

$$\mathbf{B} = \mu_0 \mathbf{H}, \tag{1.5}$$

with μ_0 being the free space permeability in the SI units we will be employing hereafter. A general electric constitutive relation states

$$\mathbf{D} = \epsilon_0 \mathbf{E} + \mathbf{P}; \qquad \mathbf{P} = \mathbf{P}(\mathbf{E}), \tag{1.6}$$

[1] J. D. Jackson, *Classical Electrodynamics* (Wiley, New York, NY, 1999) 3rd edition.

[2] This criterion, however, breaks down for some artificial materials, the so-called metamaterials, which we will not consider in this course.

where ϵ_0 is the free space permittivity and $\mathbf{P}$ is a macroscopic polarization field. The latter is in turn a function of the applied electric field. For sufficiently weak applied fields, $\mathbf{P}$ is a linear function of $\mathbf{E}$; this is a regime of *linear optics*. However, even in the linear optics regime, the dependence of the polarization on the applied electric field can be rather complicated to account for possible medium anisotropy and–temporal and sometimes even spatial–dispersion. While the former implies that the medium response in a particular direction can be affected by the electric field components orthogonal to this direction, the latter acknowledges the fact that the medium response at a given space-time point can depend on the applied electric field in the past (temporal dispersion) and/or on the fields in the neighborhood of the spatial point (spatial dispersion). We will study all these cases in detail in the subsequent chapters.

As the magnitude of the applied electric field increases, the linear relationship between $\mathbf{P}$ and $\mathbf{E}$ breaks down and we enter the realm of *nonlinear optics*. If the electric field intensity is far below a critical value, $E_{\rm cr} \sim 10^9$ V/cm needed to ionize a material atom, the resulting polarization can be expressed as a series in increasing powers of the electric field. Schematically, such a series can be expressed as

$$P = \epsilon_0(\chi^{(1)}E + \chi^{(2)}E^2 + \chi^{(3)}E^3 + \ldots), \tag{1.7}$$

where we ignored the vector nature of the fields as well as dispersion, for simplicity. The expansion coefficients, $\chi^{(1)}$ and $\chi^{(2)}$, etc., are identified as linear and nonlinear susceptibilities, respectively. The linear and nonlinear susceptibilities should be treated as phenomenological constants in our classical description. The condition $E \ll E_{\rm cr}$ is typically met with a vast majority of laser sources which rarely generate fields in excess of 10^6 V/cm. However, even if the applied field does not exceed $E_{\rm cr}$, the power series expansion can fail, provided the carrier frequency of the field lies close to any internal resonance of the medium. In the latter case, the material response tends to saturate at high enough field intensities. The proper quantitative description of such nonlinear saturation phenomena calls for a quantum mechanical treatment of the medium. Whenever, the power expansion of $\mathbf{P}$ is valid, though, we shall refer to the lowest-order term in the expansion as a linear contribution and designate the rest to be *nonlinear polarization* such that

$$\mathbf{P} = \mathbf{P}_{\rm L} + \mathbf{P}_{\rm NL}. \tag{1.8}$$

Next, the external charge and current densities are not independent from each other. Rather they are related by another fundamental law, the charge conservation law, which takes the form of a well-known continuity equation viz.,

$$\partial_t \rho_{\rm ex} + \nabla \cdot \mathbf{J}_{\rm ex} = 0. \tag{1.9}$$

The external $\rho_{\rm ex}$ and $\mathbf{J}_{\rm ex}$ drive the electromagnetic fields which, in turn, induce *internal* charge and current densities, ρ and $\mathbf{J}$, inside a medium. The induced charges and currents can be of either free (conduction) or bound (polarized) type and they also obey the continuity equation,

$$\partial_t \rho + \nabla \cdot \mathbf{J} = 0. \tag{1.10}$$

We stress that charge conservation (1.9) amounts to a fundamental law which does not follow from Maxwell's equations. The electromagnetic energy conservation law,

however, does follow from the Maxwell equations by the same token as the mechanical energy conservation follows from Newton's laws.

To derive the electromagnetic energy conservation law or the Poynting theorem, we take dot products of the both sides of Eqs. (1.3) and (1.4) with $\mathbf{H}$ and $\mathbf{E}$, respectively, and use the constitutive relations (1.5) and (1.6), yielding

$$\mathbf{H} \cdot (\nabla \times \mathbf{E}) = -\mu_0 \mathbf{H} \cdot \partial_t \mathbf{H} \tag{1.11}$$

and

$$\mathbf{E} \cdot (\nabla \times \mathbf{H}) = \mathbf{J}_{\text{ex}} \cdot \mathbf{E} + \epsilon_0 \mathbf{E} \cdot \partial_t \mathbf{E} + \mathbf{E} \cdot \partial_t \mathbf{P}. \tag{1.12}$$

On subtracting Eq. (1.11) from Eq. (1.12) term by term, we obtain

$$\tfrac{\epsilon_0}{2} \partial_t E^2 + \tfrac{\mu_0}{2} \partial_t H^2 + \mathbf{J}_{\text{ex}} \cdot \mathbf{E} = \mathbf{E} \cdot (\nabla \times \mathbf{H}) - \mathbf{H} \cdot (\nabla \times \mathbf{E}) - \mathbf{E} \cdot \partial_t \mathbf{P}. \tag{1.13}$$

Further, using the vector identity

$$\nabla \cdot (\mathbf{E} \times \mathbf{H}) = \mathbf{H} \cdot (\nabla \times \mathbf{E}) - \mathbf{E} \cdot (\nabla \times \mathbf{H}) \tag{1.14}$$

we arrive, after minor algebra, at a differential form of the electromagnetic energy conservation equation

$$\partial_t w_{em} + \nabla \cdot \mathbf{S} = -\mathbf{J}_{\text{ex}} \cdot \mathbf{E} - \mathbf{E} \cdot \partial_t \mathbf{P}. \tag{1.15}$$

Here the electromagnetic energy density w_{em} is defined in the same way as in free space,

$$w_{em} = \tfrac{1}{2} \epsilon_0 E^2 + \tfrac{1}{2} \mu_0 H^2, \tag{1.16}$$

and we introduced the electromagnetic energy flux density, the so-called Poynting vector, by the expression

$$\mathbf{S} = \mathbf{E} \times \mathbf{H}. \tag{1.17}$$

Equation (1.15) is often referred to as Poynting's theorem. In essence, it implies that the time rate of change of the electromagnetic energy density is determined by the energy flux density minus losses associated with external as well as internal currents. The second term on the r.h.s of Eq. (1.15) describes Ohmic losses associated with external currents and the third one is identified with the energy loss caused by induced polarization currents, including the ones associated with the generation of nonlinear polarizations. To reexpress the right-hand side of Eq. (1.15) in a more symmetric from, we can explicitly define the induced polarization currents as

$$\mathbf{J} = \partial_t \mathbf{P}, \tag{1.18}$$

and introduce the corresponding induced charge densities as

$$\rho = -\nabla \cdot \mathbf{P}, \tag{1.19}$$

such that the continuity equation (1.10) is respected. We emphasize that our separation of the charges into external (driving) and internal (induced) is much more natural at optical frequencies than the standard separation into free and bound charges. The latter

is a rather arbitrary division[3] which can be confusing at optical frequencies, especially for metals[4]. We will then unify free and bound induced charges and currents under the umbrella of ρ and $\mathbf{J}$.

To better understand Eq. (1.15), we transform it into the integral form

$$\frac{dW_{em}}{dt} = -\oint_{\sigma} d\boldsymbol{\sigma} \cdot \mathbf{S} - \int_{v} dv(\mathbf{J}_{\rm ex} + \mathbf{J}) \cdot \mathbf{E}. \tag{1.20}$$

where

$$W_{em} = \int_{v} dv w_{em}, \tag{1.21}$$

is the total energy of electromagnetic field inside a given volume v, and we used a divergence theorem to convert a volume integral on the the r.h.s of (1.20) into the surface one. Equation (1.20) then implies that the total energy change inside a finite region of the medium can occur as a result of the energy outflow through the boundary surface of the region as well as via energy losses inside the region associated with driving and induced currents. This situation is schematically illustrated in Fig. 1.

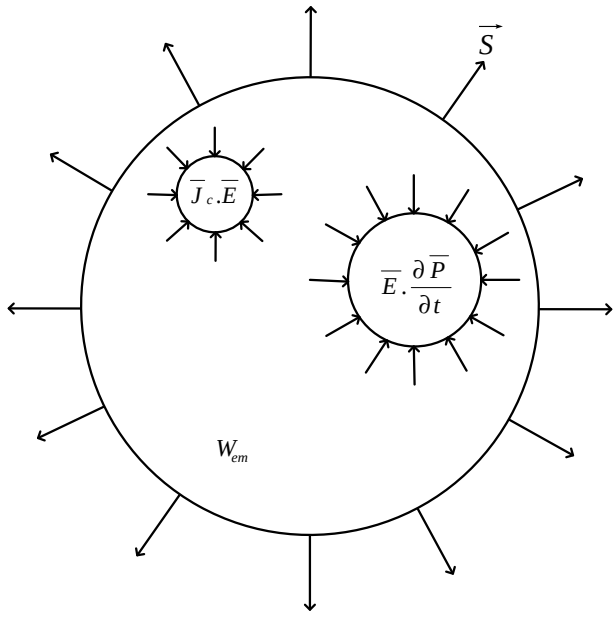

Figure 1.1: Schematic illustration of energy conservation in nonlinear media.

In many practical situations in nonlinear optics one deals with pulse or beam fields with their carriers oscillating at optical frequencies. Such fast oscillations can never be detected by even the fastest modern detectors whose response time is much larger

[3] Yu. A. Illinskii, L. V. Keldysh, *Electromagnetic response of material media* (Plenum Press, New York, NY, 1994).

[4] S. A. Maier, *Plasmonics, Fundamentals and Applications* (Springer, Berlin, 2007).

that an optical period. Consequently, it makes sense to talk about the field quantities averaged over many optical cycles – it is those quantities that can actually be registered in optical measurements anyway. In the absence of external currents, $\mathbf{J}_{\rm ex} = 0$, we can rewrite the time-averaged Poynting theorem as

$$\langle \partial_t w_{em} \rangle + \nabla \cdot \langle \mathbf{S} \rangle = - \langle \mathbf{E} \cdot \partial_t \mathbf{P} \rangle \,. \tag{1.22}$$

Here we define time-averaged quantities such as the average Poynting vector by the expression

$$\langle \mathbf{S} \rangle = \langle \mathbf{E} \times \mathbf{H} \rangle \equiv \frac{1}{T} \int_{t-T/2}^{t+T/2} dt \, (\mathbf{E} \times \mathbf{H}), \tag{1.23}$$

where T is an optical period. In case of monochromatic fields, which can be conveniently represented via complex amplitudes as

$$\mathbf{E} = \tfrac{1}{2}(\boldsymbol{\mathcal{E}} e^{-i\omega t} + c.\, c.), \tag{1.24}$$

and

$$\mathbf{H} = \tfrac{1}{2}(\boldsymbol{\mathcal{H}} e^{-i\omega t} + c.\, c.), \tag{1.25}$$

Eq. (1.23) can be shown to reduce to

$$\langle \mathbf{S} \rangle = \tfrac{1}{2} \mathrm{Re}(\boldsymbol{\mathcal{E}} \times \boldsymbol{\mathcal{H}}^*). \tag{1.26}$$

Chapter 2

Plane electromagnetic waves in linear media

2.1 Plane waves in free space

In the absence of external charges and currents, Maxwell's equations in free space take the form

$$\nabla \cdot \mathbf{E} = 0, \tag{2.1}$$

$$\nabla \cdot \mathbf{H} = 0, \tag{2.2}$$

$$\nabla \times \mathbf{E} = -\mu_0 \partial_t \mathbf{H}, \tag{2.3}$$

and

$$\nabla \times \mathbf{H} = \epsilon_0 \partial_t \mathbf{E}. \tag{2.4}$$

Linearity, stationarity, and homogeneity of Maxwell's equations in free space point to the existence of plane-wave solutions in the form

$$\mathbf{E}(\mathbf{r}, t) = \mathrm{Re}\{\boldsymbol{\mathcal{E}} e^{i(\mathbf{k}\cdot\mathbf{r}-\omega t)}\}, \qquad \mathbf{H}(\mathbf{r}, t) = \mathrm{Re}\{\boldsymbol{\mathcal{H}} e^{i(\mathbf{k}\cdot\mathbf{r}-\omega t)}\}. \tag{2.5}$$

By linearity of Maxwell's equations in free space, we can drop the real part and deal with complex phasors describing the waves directly. The real part can be taken at the end of all calculations to yield physical (real) electric and magnetic fields of a plane wave.

The Maxwell equations in the plane-wave form can be rewritten as

$$\mathbf{k} \cdot \boldsymbol{\mathcal{E}} = 0, \tag{2.6}$$

$$\mathbf{k} \cdot \boldsymbol{\mathcal{H}} = 0, \tag{2.7}$$

$$\mathbf{k} \times \boldsymbol{\mathcal{E}} = \omega \mu_0 \boldsymbol{\mathcal{H}}, \tag{2.8}$$

and

$$\mathbf{k} \times \boldsymbol{\mathcal{H}} = -\omega \epsilon_0 \boldsymbol{\mathcal{E}}. \tag{2.9}$$

In Eqs. (2.6) – (2.9) we dropped plane-wave phasors on both sides.

Next, we can exclude the magnetic field from the fourth Maxwell equation leading to

$$\mathbf{k} \times (\mathbf{k} \times \boldsymbol{\mathcal{E}}) = -\epsilon_0 \mu_0 \omega^2 \boldsymbol{\mathcal{E}}. \tag{2.10}$$

Rearranging the double cross-product on the left-hand side of Eq. (2.10), we arrive at

$$\mathbf{k}(\mathbf{k} \cdot \boldsymbol{\mathcal{E}}) - k^2 \boldsymbol{\mathcal{E}} = -\epsilon_0 \mu_0 \omega^2 \boldsymbol{\mathcal{E}}. \tag{2.11}$$

With the aid of Eq. (2.6), we obtain

$$(k^2 - \mu_0 \epsilon_0 \omega^2) \boldsymbol{\mathcal{E}} = 0, \tag{2.12}$$

implying that

$$k = \omega \sqrt{\epsilon_0 \mu_0} = \omega / c \tag{2.13}$$

where we introduced the speed of light in vacuum

$$c = \frac{1}{\sqrt{\epsilon_0 \mu_0}} = 3 \times 10^8 \text{ m/s}. \tag{2.14}$$

Equation (2.13) is a dispersion relation for plane electromagnetic waves in free space; it relates the wave number to the wave frequency. The complex amplitudes $\boldsymbol{\mathcal{E}}$ and $\boldsymbol{\mathcal{H}}$–which determine the directions of $\mathbf{E}$ and $\mathbf{H}$–are not independent, but are related by the Maxwell equations (2.8) or (2.9). For instance, from the knowledge of $\boldsymbol{\mathcal{E}}$ one can determine $\boldsymbol{\mathcal{H}}$ using Eq. (2.8),

$$\boldsymbol{\mathcal{H}} = \frac{(\mathbf{e}_k \times \boldsymbol{\mathcal{E}})}{\eta_0}, \tag{2.15}$$

where $\mathbf{e}_k = \mathbf{k}/k$ and η_0 is the **free space impedance** defined as

$$\eta_0 = \sqrt{\frac{\mu_0}{\epsilon_0}} \simeq 377\,\Omega. \tag{2.16}$$

By the same token, $\mathbf{E}_0$ can be inferred from $\mathbf{H}_0$ with the help of Eq. (2.9):

$$\boldsymbol{\mathcal{E}} = -\eta_0 (\mathbf{e}_k \times \boldsymbol{\mathcal{H}}). \tag{2.17}$$

It follows at once from Eqs. (2.15) and (2.17) that $\boldsymbol{\mathcal{E}}$, $\mathbf{k}$ and $\boldsymbol{\mathcal{H}}$ are mutually orthogonal for a plane wave in free space.

By convention, the wave polarization is associated with the time evolution of the electric field vector. Let us consider a plane wave propagating along the z-axis in free space. As, $\mathbf{k} = k\mathbf{e}_z$, and $\mathbf{E} \perp \mathbf{k}$, the electric field in the phasor form reads

$$\mathbf{E}(z,t) = \text{Re}\{(\mathbf{e}_x |\mathcal{E}_x| e^{i\phi_{0x}} + \mathbf{e}_y |\mathcal{E}_y| e^{i\phi_{0y}}) e^{i(kz - \omega t)}\}, \tag{2.18}$$

We will now show that, in general, the tip of the electric field vector moves around an ellipse as the time evolves. This general polarization is called **elliptic**. To proceed,

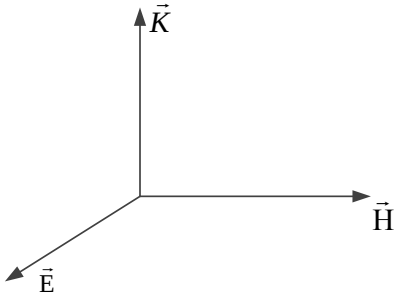

Figure 2.1: Mutual orientation of $\mathbf{E}$, $\mathbf{H}$ and $\mathbf{k}$ of a plane wave propagating in free space.

we rewrite the complex amplitude in the rectangular form as

$$\begin{aligned}\mathcal{E}_x\mathbf{e}_x + \mathcal{E}_y\mathbf{e}_y &= \underbrace{(\mathbf{e}_x|\mathcal{E}_x|\cos\phi_{0x} + \mathbf{e}_y|\mathcal{E}_y|\cos\phi_{0y})}_{\mathbf{U}} \\ &\quad + i\underbrace{(\mathbf{e}_x|\mathcal{E}_x|\sin\phi_{0x} + \mathbf{e}_y|\mathcal{E}_y|\sin\phi_{0y})}_{\mathbf{V}}. \end{aligned} \tag{2.19}$$

Note that $\mathbf{U}$ and $\mathbf{V}$ are not orthogonal which makes the situation tricky. We can however introduce a transformation from $\mathbf{U}$ and $\mathbf{V}$ to $\mathbf{u}$, $\mathbf{v}$ involving an auxiliary parameter θ such that

$$\mathbf{U} + i\mathbf{V} = (\mathbf{u} + i\mathbf{v})e^{i\theta}, \tag{2.20}$$

It follows at once from Eq. (2.20) that

$$\mathbf{U} = \mathbf{u}\cos\theta - \mathbf{v}\sin\theta, \qquad \mathbf{V} = \mathbf{u}\sin\theta + \mathbf{v}\cos\theta. \tag{2.21}$$

Inverting Eqs. (2.21), we obtain

$$\mathbf{u} = \mathbf{U}\cos\theta + \mathbf{V}\sin\theta, \qquad \mathbf{v} = \mathbf{U}\sin\theta - \mathbf{V}\cos\theta. \tag{2.22}$$

We can now use our freedom to choose θ wisely. In particular, choosing it such that $\mathbf{u}\cdot\mathbf{v} = 0$ (orthogonal axes), we obtain by taking the dot product of $\mathbf{u}$ and $\mathbf{v}$,

$$\tan 2\theta = \frac{2\mathbf{U}\cdot\mathbf{V}}{U^2 - V^2} \implies \theta = \frac{1}{2}\tan^{-1}\left(\frac{2\mathbf{U}\cdot\mathbf{V}}{U^2 - V^2}\right). \tag{2.23}$$

Here we made use of the trigonometric identities, $\sin 2\theta = 2\sin\theta\cos\theta$ and $\cos 2\theta = \cos^2\theta - \sin^2\theta$. By combining Eqs. (2.19) and (2.20), we can rewrite our field as

$$\mathbf{E}(z,t) = \mathrm{Re}\{(\mathbf{u} + i\mathbf{v})e^{i(kz-\omega t+\theta)}\}. \tag{2.24}$$

Using the orthogonality of $\mathbf{u}$ and $\mathbf{v}$, we can write the two orthogonal components of the field, E_u and E_v as

$$E_u = u\cos(kz - \omega t + \theta), \qquad E_v = v\sin(kz - \omega t + \theta). \tag{2.25}$$

It follows from Eq. (2.25) that

$$\frac{E_u^2}{u^2} + \frac{E_v^2}{v^2} = 1, \tag{2.26}$$

where u and v are given by Eq. (2.22) and θ by Eq. (2.23). Eq. (2.26) manifestly represents an ellipse with the semi-major axis making the angle θ with the x-axis as is shown in Fig. 3.6. The tip of $\mathbf{E}$ can move either clockwise or counterclockwise along

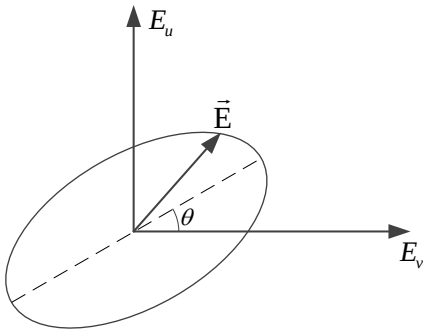

Figure 2.2: Illustrating elliptic polarization.

the ellipse; depending on the direction of motion of $\mathbf{E}$, the polarization is left-hand or right-hand elliptical. In the left-hand (right-hand) elliptical polarization, the fingers of your left (right) hand follow the direction of rotation and the thumb points to the wave propagation direction. Thus, for a general **elliptic** polarization, the electric field

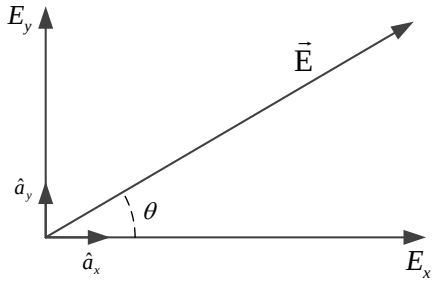

Figure 2.3: Illustrating linear polarization.

amplitude takes the form

$$\mathbf{E}(z,t) = \mathbf{e}_x|\mathcal{E}_x|\cos(kz - \omega t + \phi_{0x}) + \mathbf{e}_y|\mathcal{E}_y|\cos(kz - \omega t + \phi_{0y}). \tag{2.27}$$

Although, in general, the electric field is elliptically polarized, there are two important particular cases. The electric field is said to be **linearly** polarized if the phases of

two orthogonal components of the field in Eq. (2.18) are the same, $\phi_{0x} = \phi_{0y}$.
In this case,

$$\mathbf{E}(z,t) = (\mathbf{e}_x|\mathcal{E}_x| + \mathbf{e}_y|\mathcal{E}_y|)\cos(kz - \omega t + \phi_0), \tag{2.28}$$

and the electric field is always directed along the line making the angle

$$\alpha = \tan^{-1}(|\mathcal{E}_y|/|\mathcal{E}_x|) \tag{2.29}$$

with the x-axis as is shown in Fig. 3.7.
If the phases of the two orthogonal components in Eq. (2.19) differ by $\pi/2$, and $|E_{0x}| = |E_{0y}|$, the wave is said to be **circularly** polarized. In this case

$$\mathbf{E}(z,t) = |\mathcal{E}|[\mathbf{e}_x \cos(kz - \omega t + \phi_0) \mp \mathbf{e}_y \sin(kz - \omega t + \phi_0)]. \tag{2.30}$$

In a circularly polarized wave, the $\mathbf{E}$ has the same magnitude but is moving along

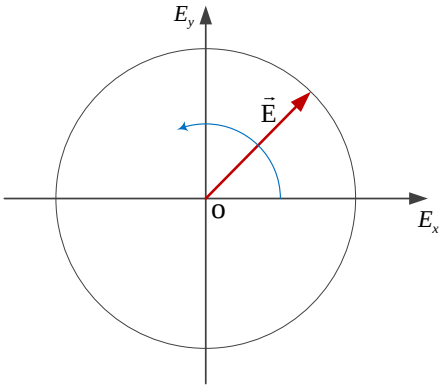

Figure 2.4: Illustrating circular polarization.

the circle. In the case of "-" sign in Eq. (2.30), $\mathbf{E}$ moves counterclockwise around the circle and the wave is **left circularly** polarized; for the "+" sign it is **right circularly** polarized.

2.2 Plane waves in homogeneous dielectrics

We now consider general phenomenological electric constitutive relations for stationary, homogeneous linear media. As a medium can be anisotropic and dispersive, we can introduce the relative permittivity and conductivity tensors, ϵ_{ij} and σ_{ij} and express $\mathbf{D}$ and $\mathbf{J}$ in terms of $\mathbf{E}$ as

$$D_i(\mathbf{r},t) = \epsilon_0 \sum_{j=x,y,z} \int_{-\infty}^{\infty} dt' \int d\mathbf{r}'\, \epsilon_{ij}(\mathbf{r} - \mathbf{r}', t - t') E_j(\mathbf{r}', t'), \tag{2.31}$$

and

$$J_i(\mathbf{r},t) = \sum_{j=x,y,z} \int_{-\infty}^{\infty} dt' \int d\mathbf{r}'\, \sigma_{ij}(\mathbf{r}-\mathbf{r}', t-t') E_j(\mathbf{r}', t'). \tag{2.32}$$

In Eqs. (2.31) and (2.32), the permittivity and conductivity tensors depend only on coordinate and time differences because of homogeneity and stationarity of the medium: All properties of such media are invariant with respect to translations in time and displacements in space.

The translational invariance of the system prompts the use of plane-wave expansions via Fourier transforms, i. e.,

$$\mathbf{D}(\mathbf{r},t) = \int d\omega \int d\mathbf{k}\, \boldsymbol{\mathcal{D}}(\mathbf{k},\omega) e^{i(\mathbf{k}\cdot\mathbf{r}-\omega t)}, \tag{2.33}$$

with similar expressions for the other fields. In physical terms, Fourier expansions give all possible plane waves allowed to propagate in such media; the Fourier coefficients specify field amplitudes of these plane waves. Introducing also Fourier expansions of the permittivity and conductivity tensors viz.,

$$\epsilon_{ij}(\mathbf{r},t) = \int d\omega \int d\mathbf{k}\, \epsilon_{ij}(\mathbf{k},\omega) e^{i(\mathbf{k}\cdot\mathbf{r}-\omega t)}, \tag{2.34}$$

and

$$\sigma_{ij}(\mathbf{r},t) = \int d\omega \int d\mathbf{k}\, \sigma_{ij}(\mathbf{k},\omega) e^{i(\mathbf{k}\cdot\mathbf{r}-\omega t)}, \tag{2.35}$$

we can use convolution properties of Fourier transforms to cast Eqs. (2.31) and (2.32) to

$$\mathcal{D}_i(\mathbf{k},\omega) = \epsilon_0 \sum_{j=x,y,z} \epsilon_{ij}(\mathbf{k},\omega) \mathcal{E}_j(\mathbf{k},\omega), \tag{2.36}$$

and

$$\mathcal{J}_i(\mathbf{k},\omega) = \sum_{j=x,y,z} \sigma_{ij}(\mathbf{k},\omega) \mathcal{E}_j(\mathbf{k},\omega). \tag{2.37}$$

Next, on taking Fourier transforms of Eqs. (1.6), and (1.18) and combining Eqs. (2.36) as well as (2.37), we can establish a relation between the permittivity and conductivity tensors in the Fourier space,

$$\epsilon_{ij}(\mathbf{k},\omega) = \delta_{ij} + \frac{i}{\epsilon_0 \omega} \sigma_{ij}(\mathbf{k},\omega). \tag{2.38}$$

Exercise 2.1. *Derive Eq. (2.38).*

Thus, we conclude that the permittivity and conductivity tensors are actually related and one can be eliminated in favor of the other. In condensed-matter calculations, it is the conductivity tensor that is typically employed. On the other hand, optical wave propagation in the media is more conveniently examined in terms of the permittivity tensor. In the absence of external charges and currents, the Maxwell equations (1.1) through (1.4) can be greatly simplified in the Fourier space to read

$$\mathbf{k} \cdot \boldsymbol{\mathcal{D}} = 0, \tag{2.39}$$

$$\mathbf{k} \cdot \boldsymbol{\mathcal{H}} = 0, \tag{2.40}$$

$$\mathbf{k} \times \boldsymbol{\mathcal{E}} = \mu_0 \omega \boldsymbol{\mathcal{H}}, \tag{2.41}$$

and

$$\mathbf{k} \times \boldsymbol{\mathcal{H}} = -\omega \boldsymbol{\mathcal{D}}. \tag{2.42}$$

Next, eliminating the magnetic field from Eqs. (2.39) - (2.42), and using the constitutive relation (2.36), we can express Eqs. (1.1) and (2.41) in the component form as

$$\sum_{i,j=x,y,z} k_i \epsilon_{ij}(\mathbf{k}, \omega) \mathcal{E}_j(\mathbf{k}, \omega) = 0, \tag{2.43}$$

and

$$\sum_{j=x,y,z} \left[k^2 \delta_{ij} - k_i k_j - \tfrac{\omega^2}{c^2} \epsilon_{ij}(\mathbf{k}, \omega) \right] \mathcal{E}_j(\mathbf{k}, \omega) = 0. \tag{2.44}$$

Eqs. (2.43) and (2.44) determine all possible plane electromagnetic waves supported by a given medium.

Exercise 2.2. *Show that Eqs. (2.43) and (2.44) are always compatible.*

Eq. (2.43 is called a generalized transversality condition, whereas Eq. (2.44) is a dispersion relation for the waves. The existence of nontrivial plane-wave solutions to Eq. (2.44) can be expressed in terms of a determinant condition as

$$\text{Det} \left[k^2 \delta_{ij} - k_i k_j - \tfrac{\omega^2}{c^2} \epsilon_{ij}(\mathbf{k}, \omega) \right] = 0. \tag{2.45}$$

Let us now consider the important limiting case of an isotropic dielectric. It can be inferred by inspection that the dielectric permittivity tensor of an isotropic medium can only be composed of δ_{ij} and $k_i k_j$ implying that

$$\epsilon_{ij}(\mathbf{k}, \omega) = \delta_{ij} A(k, \omega) + k_i k_j B(k, \omega), \tag{2.46}$$

where $A(k, \omega)$ and $B(k, \omega)$ are scalar functions. Instead of using A and B, however, it will prove convenient to divide ϵ_{ij} into a part transverse to the $\mathbf{e}_k = \mathbf{k}/k$ direction, and that longitudinal to $\mathbf{e}_k$. Such a decomposition can be accomplished via

$$\epsilon_{ij}(\mathbf{k}, \omega) = \epsilon_\perp(k, \omega) \left(\delta_{ij} - \tfrac{k_i k_j}{k^2} \right) + \epsilon_\parallel(k, \omega) \tfrac{k_i k_j}{k^2}. \tag{2.47}$$

On substituting from Eq. (2.47) into Eqs. (2.43) and (2.44), the latter can be transformed to

$$\epsilon_\parallel(k, \omega)(\mathbf{k} \cdot \boldsymbol{\mathcal{E}}) = 0, \tag{2.48}$$

and

$$\left[k^2 - \tfrac{\omega^2}{c^2} \epsilon_\perp(k, \omega) \right] \left[\boldsymbol{\mathcal{E}} - \tfrac{\mathbf{k}(\mathbf{k} \cdot \boldsymbol{\mathcal{E}})}{k^2} \right] - \left(\tfrac{\omega^2}{k^2 c^2} \right) \epsilon_\parallel(k, \omega) \mathbf{k} (\mathbf{k} \cdot \boldsymbol{\mathcal{E}}) = 0. \tag{2.49}$$

Eqs. (2.48) and (2.49) then imply the existence of a family of purely transverse plane waves,

$$\mathbf{k} \cdot \boldsymbol{\mathcal{E}} = 0, \tag{2.50}$$

with the dispersion relation,

$$k = \pm\tfrac{\omega}{c}\sqrt{\epsilon_\perp(k,\omega)}, \tag{2.51}$$

and a family of the waves which have longitudinal component(s) of the electric field, $\mathbf{k}\cdot\boldsymbol{\mathcal{E}} \neq 0$, with the dispersion relation determined by a *common* solution of Eq. (2.51) and of the following equation

$$\epsilon_\parallel(k,\omega) = 0. \tag{2.52}$$

In Eq. (2.51) the two signs on the right-hand side correspond to two plane waves at a given frequency ω propagating the the opposite directions.

Exercise. 2.3. *As we will see in Sec. 2.5., dielectric response of metals at high frequencies can be modeled by the permittivity*

$$\epsilon_{ij}(\omega) = \delta_{ij}\left(1 - \frac{\omega_p^2}{\omega^2}\right), \tag{2.53}$$

where ω_p is the so-called plasma frequency. Determine the frequency(s) and dispersion relation of longitudinal electromagnetic waves propagating in metals at such ultraviolet frequencies and interpret your results in physical terms. Show that transverse electromagnetic waves can only propagate if $\omega > \omega_p$. What is their dispersion relation?

Note that the dispersion relation (2.51) is, in general, in the implicit form due to spatial dispersion of the medium. It is then instructive to examine the limiting case of local media which lack spatial dispersion. In reality the vast majority of inorganic media are made of atoms or molecules with the size significantly smaller than the optical wavelength. Hence, spatial nonlocality of their dielectric response to the applied field is negligible, resulting in the absence of spatial dispersion in such media. Under the circumstances, the permittivity tensor can be simplified as

$$\epsilon_{ij}(\mathbf{r}-\mathbf{r}', t-t') = \delta(\mathbf{r}-\mathbf{r}')\epsilon_{ij}(t-t'). \tag{2.54}$$

It then follows at once from Eqs. (2.34) and (2.54) that the permittivity tensor in Fourier space is independent of k, implying that

$$\epsilon(\mathbf{k},\omega) = \epsilon(\mathbf{k}=0,\omega) \equiv \epsilon(\omega). \tag{2.55}$$

The dispersion relation for transverse electromagnetic waves can be expressed in the explicit form as

$$k = \pm\tfrac{\omega}{c}\sqrt{\epsilon_\perp(\omega)}, \tag{2.56}$$

and the generalized transversality condition states

$$\epsilon_\parallel(\omega) = 0. \tag{2.57}$$

In the following sections, we will explore several commonly occurring types of linear optical media.

2.2.1 Plane waves in homogeneous isotropic media with no spatial dispersion

Medium isotropy and locality imply a greatly simplified form of the permittivity tensor,

$$\epsilon_{ij}(\mathbf{k},\omega) = \epsilon(\omega)\delta_{ij}. \tag{2.58}$$

It then follows from Eqs. (2.47) and (2.58) that $\epsilon_{\|}(\omega) = \epsilon_{\perp}(\omega) = \epsilon(\omega)$. Assuming further that in the spectral range of interest, $\epsilon(\omega) \neq 0$, we conclude that in this case, the only allowed plane waves in such media must be transverse, governed by the dispersion relation

$$k = \pm\tfrac{\omega}{c}\sqrt{\epsilon(\omega)}, \tag{2.59}$$

Representing the dielectric function in terms of its real and imaginary parts,

$$\epsilon(\omega) = \epsilon'(\omega) + i\epsilon''(\omega), \tag{2.60}$$

we can express the wave number of the propagating wave as

$$k = \beta_{\pm} + i\alpha_{\pm}/2. \tag{2.61}$$

Here

$$\beta_{\pm} = \pm\tfrac{\omega}{c}\sqrt{\tfrac{\sqrt{\epsilon'^2+\epsilon''^2}+\epsilon'}{2}}, \tag{2.62}$$

and

$$\tfrac{1}{2}\alpha_{\pm} = \pm\tfrac{\omega}{c}\sqrt{\tfrac{\sqrt{\epsilon'^2+\epsilon''^2}-\epsilon'}{2}}. \tag{2.63}$$

Exercise 2.4. *Derive the equations (2.62) and (2.63).*

Let us choose the z-axis of our coordinate system along propagation direction of the wave, $\mathbf{k} = k\mathbf{e}_z$. It then follows from the Maxwell equations (2.39) through (2.42) that the electric and magnetic field amplitudes are related as

$$\boldsymbol{\mathcal{E}} = -\eta(\mathbf{e}_z \times \boldsymbol{\mathcal{H}}), \tag{2.64}$$

or, alternatively,

$$\boldsymbol{\mathcal{H}} = \frac{(\mathbf{e}_z \times \boldsymbol{\mathcal{E}})}{\eta}, \tag{2.65}$$

where η is a complex impedance of the lossy medium, defined as

$$\eta(\omega) = \sqrt{\frac{\mu_0}{\epsilon_0\epsilon(\omega)}} = \frac{\eta_0}{\sqrt{\epsilon(\omega)}}. \tag{2.66}$$

To illustrate the plane wave propagation in such a medium, let us focus now on a particular case of a linearly polarized in the x-direction plane wave which propagates in the positive z-direction. The electric and magnetic fields of the wave can then be represented as

$$\mathbf{E}(z,t) = \tfrac{1}{2}\mathbf{e}_x[\mathcal{E}e^{-\alpha_+ z/2}e^{i(\beta_+ z-\omega t)} + c.\,c.,] \tag{2.67}$$

and

$$\mathbf{H}(z,t) = \tfrac{1}{2}\mathbf{e}_y\left[\tfrac{\mathcal{E}}{|\eta|}e^{-\alpha_+ z/2}e^{i(\beta_+ z-\omega t-\theta_\eta)} + c.\,c\right], \tag{2.68}$$

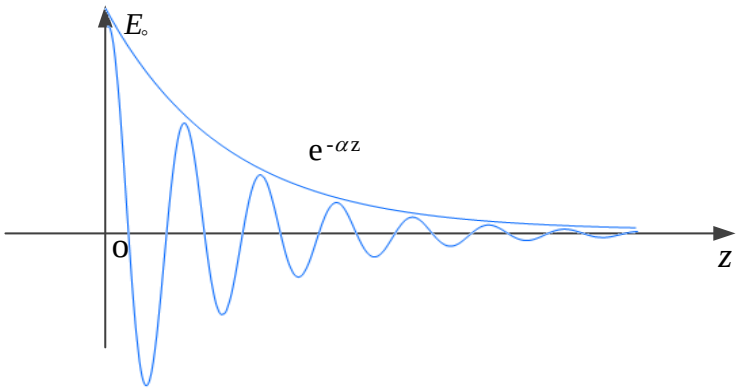

Figure 2.5: Inhomogeneous plane wave propagating in a lossy medium.

which describe inhomogeneous plane waves thanks to losses. Here we chose β_+ and α_+ which describe a plane wave propagating to the right and exponentially decaying on propagation into the medium; the magnitude and phase of the complex impedance can be expressed as

$$|\eta| = \frac{\eta_0}{(\epsilon'^2 + \epsilon''^2)^{1/4}}, \qquad \tan\theta_\eta = -\epsilon''/\epsilon'. \tag{2.69}$$

We can then infer from Eqs. (2.67) and (2.68) that the presence of losses introduces a phase lag between the magnetic and electric fields in such media as well.

Finally, we can work out the time-averaged energy flux density (Poynting vector), and hence the optical intensity, associated with the inhomogeneous plane wave. On substituting from Eqs. (2.67) and (2.68) into Eq. (1.26), we obtain for the optical intensity

$$I = |\langle S \rangle| = \frac{|\mathcal{E}|^2}{2|\eta|} e^{-z/\delta} \cos\theta_\eta. \tag{2.70}$$

Eq. (2.70) is known as Beer's absorption law, and by measuring the intensity extinction, one can infer the Beer absorption length, or skin depth

$$\delta = \frac{1}{\alpha_+}. \tag{2.71}$$

We note that Beer's absorption length is then a directly measurable quantity. We can also define a complex refractive index by the expression

$$\mathcal{N}(\omega) = \sqrt{\epsilon(\omega)} = n(\omega) + i\kappa(\omega), \tag{2.72}$$

where n is a real refractive index which can be determined from reflectivity measurements and κ is a so-called extinction coefficient, closely related to Beers' absorption length. In fact, it readily follows from Eqs. (2.59), (2.61) and (2.72) that

$$\delta^{-1}(\omega) = \frac{2\kappa(\omega)\omega}{c}. \tag{2.73}$$

The magnitudes of real and imaginary parts of ϵ can then be inferred from the knowledge of n and κ, i.e.,

$$\epsilon' = n^2 - \kappa^2, \qquad \epsilon'' = 2n\kappa. \tag{2.74}$$

In particular, in the transparent regions of the spectrum, where $\epsilon'' \ll \epsilon'$, $\epsilon' \simeq n^2$ and the optical intensity of a plane wave can be expressed as

$$I = \frac{\epsilon_0 n c}{2}|\mathcal{E}|^2. \tag{2.75}$$

2.2.2 Plane waves in uniaxial crystals

We will now explore the families of plane waves that can propagate in transparent dispersionless anisotropic media. Most crystals fall into this category in the optical frequency range. We will limit ourselves to the case of uniaxial crystals. Dielectric properties of uniaxial crystals along a special axis, usually defined by a unit vector $\mathbf{n}$, are different from those in any direction orthogonal to the axis. The special direction is called an optical axis of the crystal. In the absence of spatial dispersion, the dielectric permittivity tensor can only depend on δ_{ij} and $n_i n_j$ and can be conveniently expressed in terms of transverse $\epsilon_\perp$ and longitudinal $\epsilon_\parallel$ components as

$$\epsilon_{ij} = \epsilon_\perp(\delta_{ij} - n_i n_j) + \epsilon_\parallel n_i n_j. \tag{2.76}$$

One can always choose a coordinate systems such that the optical axis of the crystal coincides with one of the axes, the z-axis, say. In these coordinates, the dielectric tensor transforms to its canonical (diagonal) form represented by the matrix

$$\epsilon_{ij} = \begin{pmatrix} \epsilon_\perp & 0 & 0 \\ 0 & \epsilon_\perp & 0 \\ 0 & 0 & \epsilon_\parallel \end{pmatrix} \tag{2.77}$$

If $\epsilon_\parallel > \epsilon_\perp$, the crystal is said to be a positive uniaxial crystal, and if $\epsilon_\parallel < \epsilon_\perp$ the crystal is referred to as a negative uniaxial one.

Let us assume, for simplicity that the wave vector lies in the xz-plane, $\mathbf{k} = k_x\mathbf{e}_x + k_z\mathbf{e}_z$. It then follows from Eqs. (2.44) and Eq. (2.77) that

$$\left(k_z^2 - \tfrac{\omega^2}{c^2}\epsilon_\perp\right)\mathcal{E}_x - k_x k_z \mathcal{E}_z = 0, \tag{2.78}$$

$$-k_x k_z \mathcal{E}_x + \left(k_x^2 - \tfrac{\omega^2}{c^2}\epsilon_\parallel\right)\mathcal{E}_z = 0, \tag{2.79}$$

and

$$\left(k^2 - \tfrac{\omega^2}{c^2}\epsilon_\perp\right)\mathcal{E}_y = 0. \tag{2.80}$$

The generalized transversality condition (2.43) can then be cast into the form

$$k_x\epsilon_\perp\mathcal{E}_x + k_z\epsilon_\parallel\mathcal{E}_z = 0. \tag{2.81}$$

The analysis of Eqs. (2.78) through (2.81) reveals that there are two possible polarizations: ordinary and extraordinary one. For the ordinary polarization, it follows at once from Eq. (2.80) that the ordinarily polarized wave is transverse,

$$\boldsymbol{\mathcal{E}} = \mathcal{E}_y\mathbf{e}_y, \tag{2.82}$$

and ita dispersion relation is given by the expression

$$k_{\rm o} = \tfrac{\omega}{c}\sqrt{\epsilon_\perp}. \tag{2.83}$$

We observe that ordinary waves in uniaxial crystals have all the same properties as plane waves supported by transparent isotropic media.

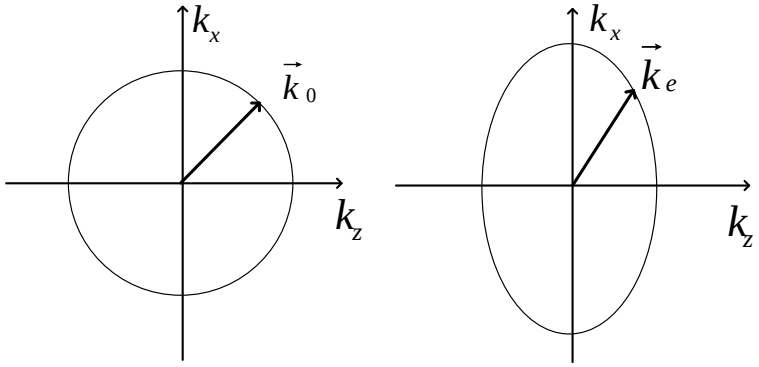

Figure 2.6: Graphical representation of the wave vectors of ordinary (left) and extraordinary (right) waves in a uniaxial crystal.

The polarization of the extraordinary waves can be inferred from

$$\boldsymbol{\mathcal{E}} = \mathcal{E}_x \mathbf{e}_x + \mathcal{E}_z \mathbf{e}_z, \tag{2.84}$$

where $\mathcal{E}_x$ and $\mathcal{E}_z$ are related by Eq. (2.81). We can also derive their dispersion relation from the determinant condition for Eqs. (2.78) and (2.79). The resulting dispersion relation reads

$$\frac{k_x^2 c^2}{\omega^2 \epsilon_\parallel} + \frac{k_z^2 c^2}{\omega^2 \epsilon_\perp} = 1. \tag{2.85}$$

Using $k_x = k_e \sin\theta$, and $k_z = k_{\rm e} \cos\theta$, we can cast Eq. (2.85) into the form

$$\frac{\omega^2}{k_{\rm e}^2 c^2} = \frac{\sin^2\theta}{\epsilon_\parallel} + \frac{\cos^2\theta}{\epsilon_\perp}. \tag{2.86}$$

Thus the wave vector magnitude of an extraordinary wave depends on its propagation direction which is a novel propagation feature arising in anisotropic media. The difference between ordinary and extraordinary waves can be best visualized by comparing their dispersion relations. It is seen from Eqs. (2.83) and (2.86) that in the k-plane the dispersion relations of ordinary and extraordinary waves can be represented by a sphere of radius $(\omega/c)\sqrt{\epsilon_\perp}$ and ellipse with the semi-axes $(\omega/c)\sqrt{\epsilon_\perp}$ and $(\omega/c)\sqrt{\epsilon_\parallel}$, respectively. The situation is schematically depicted in the figure above.

Exercise 2.5. *Using Maxwell's equations show that the wave vector of the extraordinary wave is not parallel to the Pointing vector,* $\mathbf{S} = \mathbf{E} \times \mathbf{H}$*. In other words, demonstrate that the direction of propagation of such a wave does not, in general, coincide with the direction of the energy flow.*

2.2.3 Faraday effect and polarization rotation

We will now consider light propagation in an isotropic, weakly dispersive–and hence lossless–dielectric medium with a weak homogeneous static magnetic field, $\mathbf{B}$, applied along the $z-$axis such that $\mathbf{B} = B\mathbf{e}_z$. We assume that the influence of magnetic field can be treated as a perturbation and we seek a phenomenological expression for a dielectric permittivity tensor of an isotropic medium with a small correction due to the magnetic field. The lowest-order correction is assumed to linear in the magnetic field. Therefore, the second-order permittivity tensor can only be comprised of δ_{ij} and a component linear in B_i. Recall that both $\mathbf{D}$ and $\mathbf{E}$ are physical vectors that change their sign upon reflections with respect to the origin of a coordinate system. It then follows from Eq. (2.31) that ϵ_{ij} should be invariant upon reflections. To respect the reflectional invariance of the permittivity tensor, the correction term can only be of the form $\sum_k e_{ijk}B_k$, where

$$e_{ijk} = \begin{cases} 1, & \text{clockwise permutation} \\ -1, & \text{counterclockwise permutation} \end{cases} \tag{2.87}$$

is an antisymmetric Levi-Chivita symbol; $e_{xyz} = 1$, $e_{yxz} = -1$ and so on up to a cyclic permutation. Thus, on phenomenological grounds, the dielectric permittivity tensor describing an isotropic dispersionless medium perturbed by a weak magnetic field can be written as

$$\epsilon_{ij}(\omega) = \epsilon(\omega)\delta_{ij} + ig(\omega)\sum_{k=x,y,z} e_{ijk}B_k, \qquad |gB| \ll \epsilon. \tag{2.88}$$

where $g(\omega)$ is a phenomenological constant. In the end of this chapter, we will derive Eq. (2.88) using a simple classical microscopic model of a medium. The permittivity tensor (2.88) can be written in a matrix form as

$$\epsilon_{ij}(\omega) = \begin{pmatrix} \epsilon(\omega) & ig(\omega)B & 0 \\ -ig(\omega)B & \epsilon(\omega) & 0 \\ 0 & 0 & \epsilon \end{pmatrix}. \tag{2.89}$$

Let us now assume, for simplicity that the wave propagates along the magnetic field, $\mathbf{k} = k\mathbf{e}_z$. It then follows from Eqs. (2.44) and (2.43) that

$$\left[k^2 - \tfrac{\omega^2}{c^2}\epsilon(\omega)\right]\mathcal{E}_x - ig(\omega)B\left(\tfrac{\omega^2}{c^2}\right)\mathcal{E}_y = 0, \tag{2.90}$$

$$ig(\omega)B\left(\tfrac{\omega^2}{c^2}\right)\mathcal{E}_x + \left[k^2 - \tfrac{\omega^2}{c^2}\epsilon(\omega)\right]\mathcal{E}_y = 0, \tag{2.91}$$

and

$$-\tfrac{\omega^2}{c^2}\mathcal{E}_z = 0. \tag{2.92}$$

Exercise 2.6. *Derive Eqs. (2.90) – (2.92) from Eqs. (2.44), (2.43), and (2.88).*
We can then show that up to the first order in $fB/\epsilon \ll 1$, wave vector magnitude of any wave existing in such media is given by

$$k_\pm = k \pm \Delta k, \tag{2.93}$$

where we introduced the notations

$$k = \frac{\omega}{c}\sqrt{\epsilon(\omega)}; \qquad \Delta k = \frac{\omega g(\omega) B}{2c\sqrt{\epsilon(\omega)}}. \tag{2.94}$$

The plane waves supported by the media must be circularly polarized, i. e.,

$$\mathcal{E}_z = 0, \qquad \mathcal{E}_y = \pm i\mathcal{E}_x, \tag{2.95}$$

where the upper (lower) sign on the right-hand side of Eq. (2.95) corresponds to the upper (lower) subscript on the left-hand side of Eq. (2.93). In other words, the medium supports left- and right-circularly polarized waves with slightly different wave numbers.

We will now explore how a linearly polarized wave evolves in the medium. Assuming the wave is polarized along the x-axis, say, at the entrance to the medium,

$$\mathbf{E}_0 = \tfrac{1}{2}\mathbf{e}_x\mathcal{E}_0 e^{-i\omega t} + c.c, \tag{2.96}$$

we can represent the incident electric field as

$$\mathbf{E}_0 = \tfrac{1}{2}\tfrac{\mathcal{E}_0}{\sqrt{2}}(\mathbf{e}_+ + \mathbf{e}_-)e^{-i\omega t} + c.c, \tag{2.97}$$

where

$$\mathbf{e}_\pm = \frac{\mathbf{e}_x \pm i\mathbf{e}_y}{\sqrt{2}}, \tag{2.98}$$

are the unit vectors associated with the two circular polarizations. We can now examine wave propagation in the medium. The electric field in any transverse plane $z = const$ can be written as

$$\mathbf{E} = (A\mathbf{e}_+ e^{ik_+ z} + B\mathbf{e}_- e^{ik_- z})e^{-i\omega t} + c.c. \tag{2.99}$$

It follows from the initial conditions that $A = B = \mathcal{E}_0/2\sqrt{2}$. Thus, we obtain subsequently the propagated wave expression in the form

$$\mathbf{E} = \tfrac{1}{2}\tfrac{\mathcal{E}_0}{\sqrt{2}}(\mathbf{e}_+ e^{i\Delta kz} + \mathbf{e}_- e^{-i\Delta kz})e^{i(kz-\omega t)} + c.c. \tag{2.100}$$

We can transform Eq. (2.100) to

$$\mathbf{E} = \tfrac{1}{2}\mathcal{E}_0\mathbf{e}_p(z)e^{i(kz-\omega t)} + c.c, \tag{2.101}$$

where

$$\mathbf{e}_p(z) = \mathbf{e}_x \cos\Delta kz - \mathbf{e}_y \sin\Delta kz. \tag{2.102}$$

Exercise 2.7. *Derive Eq. (2.101) from Eq. (2.100)*
It can be inferred from Eqs. (2.101) and (2.102) that the wave remains linearly polarized, but the plane of polarization rotates. Alternatively, one can conclude that the polarization vector rotates in the transverse plane as the wave propagates along the z-axis. This phenomenon is called Faraday rotation. The rate of rotation is customary characterized by the Verdet constant V defined by the expression

$$\Delta k = VB, \tag{2.103}$$

It then follows at once from Eqs. (2.94) and (2.103) that for a plane wave propagating along the magnetic field, the Verdet constant is given by

$$V = \frac{\omega g(\omega)}{2c\sqrt{\epsilon(\omega)}}. \tag{2.104}$$

Exercise 2.8. *Generalize the discussion of this section to the case when a plane wave propagates at an angle θ to the magnetic field. Derive a generalized dispersion relation and determine the Verdet constant in this case.*

2.3 Refraction and reflection of plane waves at the interface of homogeneous media

2.3.1 Reflection of plane waves at oblique incidence: Generalized Snell's law

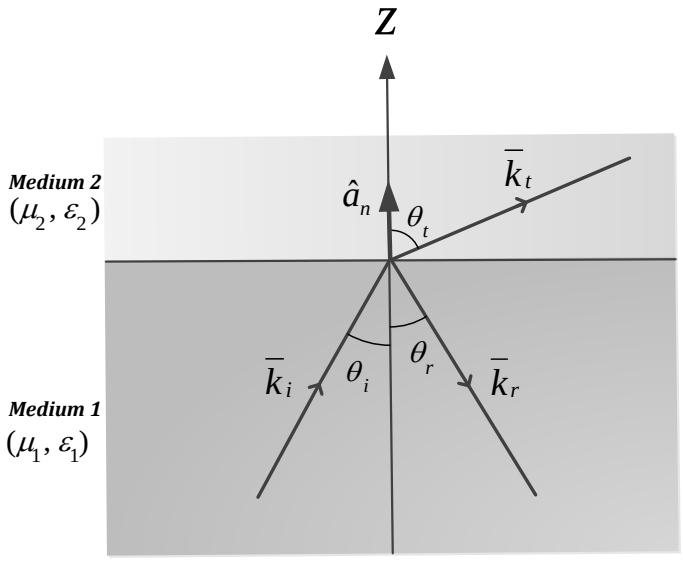

Figure 2.7: Illustrating Snell's law for oblique incidence of a plane wave.

We now explore refraction and reflection of plane electromagnetic waves at an interface of two homogeneous media. To reflect a typical physical situation, we will assume that a plane wave is incident from a transparent medium with the permittivity ϵ_1 onto a flat interface separating the medium from a lossy medium 2, characterized by the complex permittivity $\epsilon_2(\omega) = \epsilon_2'(\omega) + i\epsilon_2''(\omega)$. We choose a coordinate system with the

unit normal to the interface pointed along the z-axis. The geometry of the problem is sketched in Fig. 2.3.1. Note that the incidence, refraction, and transmission angles, θ_i, θ_r, and θ_t, respectively, are real angles only in the transparency window of the second medium, $\epsilon_2''(\omega) = 0$. Otherwise, all sines and cosines of θ_t are complex. For this reason, we will not use the angles hereafter. Rather, we will derive the Fresnel formulas for transmission and reflection amplitudes in terms of the corresponding projections of k-vectors which can, in general, be complex. Next, it will prove convenient hereafter to introduce the notations

$$k_1 = k_0 n_1, \qquad k_2 = k_0 \mathcal{N}_2, \tag{2.105}$$

where $k_0 = \omega/c$ and $\mathcal{N}_2$ is a complex refractive index of medium 2, c. f. Eq. (2.72). The boundary conditions at the flat interface $z = 0$ should hold at any point in the xz-plane and at any instant of time t, implying that

$$e^{i(\mathbf{k}_i \cdot \mathbf{r} - \omega_i t)}|_{z=0} = e^{i(\mathbf{k}_r \cdot \mathbf{r} - \omega_r t)}|_{z=0} = e^{i(\mathbf{k}_t \cdot \mathbf{r} - \omega_t t)}|_{z=0}. \tag{2.106}$$

Here the subscripts i, r, and t stand for incident, reflected and transmitted waves, respectively. It follows at once from Eq. (2.106) that

$$\omega_i = \omega_r = \omega_t = \omega, \tag{2.107}$$

that is the frequencies of the incident, reflected and transmitted waves must match. Further, it can be inferred from the boundary conditions (2.106) that

$$k_{ix} = k_{rx} = k_{tx} = k_x, \tag{2.108}$$

In other words, the in-plane components of the wave vectors must match as well. Notice that since medium 1 is assumed to be transparent, Eq. (2.108) stipulates that in-plane components of the wave vectors of all the involved waves be real. We stress that Eq. (2.108) is a generalized Snell's law. We shall also introduce the notations

$$k_{iz} = -k_{ir} = k_{1z}, \qquad k_{tz} = k_{2z}. \tag{2.109}$$

It then follows from Eqs. (2.105) (2.108), and (3.113) that

$$\mathbf{k}_i = k_x \mathbf{e}_x + k_{1z} \mathbf{e}_z, \tag{2.110}$$

$$\mathbf{k}_r = k_x \mathbf{e}_x - k_{1z} \mathbf{e}_z, \tag{2.111}$$

and

$$\mathbf{k}_t = k_x \mathbf{e}_x + k_{2z} \mathbf{e}_z, \tag{2.112}$$

where

$$k_{1z} = \sqrt{k_1^2 - k_x^2}, \quad \text{and} \quad k_{2z} = \sqrt{k_2^2 - k_x^2}. \tag{2.113}$$

It is easy to see from the geometry of Fig. 2.3.1 that in the transparency window of medium 2, all angles are real and Eq. (2.108 reduces to

$$\theta_i = \theta_r \equiv \theta_1, \qquad \theta_t \equiv \theta_2 \tag{2.114}$$

and

$$n_1 \sin\theta_1 = n_2 \sin\theta_2. \tag{2.115}$$

Put another way, the incidence and reflection angles should be equal and the Snell law should simplify to its familiar form for refraction at the interface of two transparent media.

2.3.2 Reflection of plane waves at oblique incidence: Fresnel Formulae

There are two important special cases of the incident polarization that should be distinguished: transverse magnetic (TM), or p-polarization, and transverse electric (TE), or s-polarization. In the first instance, the magnetic field of an incident wave is directed perpendicular to the plane of incidence, whereas in the second case it is the incident electric field that is orthogonal to this plane. We will examine the two cases separately. Note that an arbitrarily polarized incident field can be decomposed into a TM and TE polarized components which are mutually orthogonal.

Transverse magnetic (TM) or p-polarization. – Consider first the TM case. Magnetic fields of the incident, reflected and transmitted TM waves are assumed to be polarized along the y-axis, such that we can express their complex amplitudes as

$$\boldsymbol{\mathcal{H}}_s = H_s \mathbf{e}_y, \qquad s = i, r, t. \tag{2.116}$$

Since the magnetic field of a TM-polarized wave has only one component, it is convenient to express the electric field in terms of the magnetic one. It follows at once from the Maxwell equations (2.41) and (2.42) that

$$\boldsymbol{\mathcal{E}}_s = -\eta_s (\mathbf{e}_{ks} \times \boldsymbol{\mathcal{H}}_s), \tag{2.117}$$

where $\eta_{i,r} = \eta_0/\sqrt{\epsilon_1}$ and $\eta_t = \eta_0/\sqrt{\epsilon_2}$ are relevant media impedances. We can then infer from Eqs. (2.116) and (2.117) as well as Eqs. (2.109) through (2.113) that the complex amplitudes of the incident, reflected, and transmitted fields can be represented as

$$\begin{aligned} \boldsymbol{\mathcal{H}}_i &= H_i \mathbf{e}_y, \\ \boldsymbol{\mathcal{E}}_i &= \frac{\eta_0 H_i}{k_0 \epsilon_1} (k_{1z} \mathbf{e}_x - k_x \mathbf{e}_z), \end{aligned} \tag{2.118}$$

$$\begin{aligned} \boldsymbol{\mathcal{H}}_r &= H_r \mathbf{e}_y, \\ \boldsymbol{\mathcal{E}}_r &= \frac{\eta_0 H_r}{k_0 \epsilon_1} (-k_{1z} \mathbf{e}_x - k_x \mathbf{e}_z), \end{aligned} \tag{2.119}$$

and

$$\begin{aligned} \boldsymbol{\mathcal{H}}_t &= H_t \mathbf{e}_y, \\ \boldsymbol{\mathcal{E}}_t &= \frac{\eta_0 H_t}{k_0 \epsilon_2} (k_{2z} \mathbf{e}_x - k_x \mathbf{e}_z), \end{aligned} \tag{2.120}$$

respectively.

The boundary conditions for the tangential components of the fields across the interface state

$$H_i + H_r = H_t \tag{2.121}$$

and

$$\frac{H_i}{\epsilon_1} k_{1z} - \frac{H_r}{\epsilon_1} k_{1z} = \frac{H_t}{\epsilon_2} k_{2z}. \tag{2.122}$$

It then follows from Eqs. (2.121) and (2.122) that

$$H_r = \frac{\epsilon_2 k_{1z} - \epsilon_1 k_{2z}}{\epsilon_2 k_{1z} + \epsilon_1 k_{2z}} H_i, \tag{2.123}$$

and

$$H_t = \frac{2\epsilon_2 k_{1z}}{\epsilon_2 k_{1z} + \epsilon_1 k_{2z}} H_i. \tag{2.124}$$

Using (2.117) we arrive at the expressions for the electric fields in the form

$$E_i = \eta_1 H_i, \qquad E_r = \eta_1 H_r, \qquad E_t = \eta_2 H_t. \tag{2.125}$$

Finally, the complex reflectivity and transmittance can be represented as

$$r_{\rm p} \equiv \frac{E_r}{E_i} = \frac{\epsilon_2 k_{1z} - \epsilon_1 k_{2z}}{\epsilon_2 k_{1z} + \epsilon_1 k_{2z}}, \tag{2.126}$$

and

$$t_{\rm p} \equiv \frac{E_t}{E_i} = \frac{2\epsilon_2 k_{1z}}{\epsilon_2 k_{1z} + \epsilon_1 k_{2z}} \sqrt{\frac{\epsilon_1}{\epsilon_2}}. \tag{2.127}$$

Equations (2.126) and (2.127) are the celebrated Fresnel formulas for the TM case.

Let us now focus on the situation when the wave is incident normally to the interface, such that $k_x = 0$, $k_{sz} = k_s$, $s = 1, 2$. It then follows from Eqs. (2.105), (2.126) and (2.127) that

$$r_\perp = \frac{\mathcal{N}_2 - n_1}{\mathcal{N}_2 + n_1}, \qquad \text{and} \qquad t_\perp = \frac{2n_1}{\mathcal{N}_2 + n_1}. \tag{2.128}$$

There are two instructive limiting cases here. First, the second medium is transparent, $\mathcal{N}_2 = n_2$, such that the reflectivity and transmittance are purely real,

$$r_\perp = \frac{n_2 - n_1}{n_2 + n_1}, \qquad \text{and} \qquad t_\perp = \frac{2n_1}{n_2 + n_1}, \tag{2.129}$$

and the latter relations simply quantify the relative amplitudes of the reflected and transmitted waves. Note that no energy will be lost in transmission in this case.

Exercise 2.9. *A plane wave is normally incident at an interface separating two transparent media. Show that the electromagnetic energy fluxes on both sides of the interface are the same.*

Another interesting situation arises when medium 2 behaves as a good conductor in a certain spectral range. As is seen from Eqs. (2.38), 2.60), (2.72), and (2.74), $\kappa_2 \gg$

$\max(n_1, n_2)$ in this case. Thus, the reflectivity and transmittance may be approximated as

$$r_\perp \simeq 1 - \frac{2in_2}{\kappa_2} \quad \text{and} \quad t_\perp \simeq -\frac{2in_1}{\kappa_2}. \tag{2.130}$$

It follows that most of the incident wave power is reflected from the interface of a good conductor; only is its tiny fraction transmitted into the conductor.

Exercise 2.10. *Consider a plane wave incident normally at the interface separating air from a good conductor. Determine the portion of the incident wave power absorbed by the conductor.*

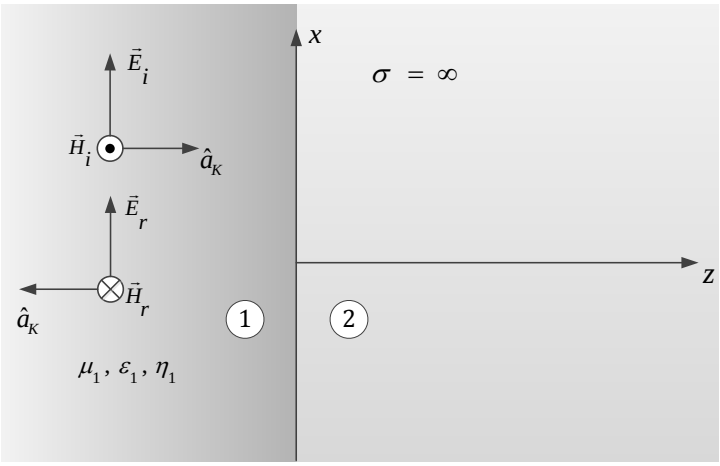

Figure 2.8: Normal incidence of a plane wave onto an interface separating a dielectric and a perfect conductor.

In the extreme case of a perfect conductor, $\kappa_2 \to \infty$, such that $r_\perp \to 1$–the wave is perfectly reflected from the interface. The situation is sketched in the Fig. 2.3.2. The electric and magnetic fields of the incident and reflected waves can then be represented as

$$\mathbf{E}_i(z,t) = \mathbf{e}_x \eta_1 H_i e^{i(k_1 z - \omega t)}, \tag{2.131}$$

$$\mathbf{H}_i(z,t) = \mathbf{e}_y H_i e^{i(k_1 z - \omega t)}. \tag{2.132}$$

and

$$\mathbf{E}_r(z,t) = \mathbf{e}_x \eta_1 H_i e^{-i(k_1 z + \omega t)}, \tag{2.133}$$

$$\mathbf{H}_r(z,t) = -\mathbf{e}_y H_i e^{-i(k_1 z + \omega t)}, \tag{2.134}$$

respectively. The total electric and magnetic fields in medium 1 can then be transformed to

$$\mathbf{E}_1 = \mathrm{Re}(\mathbf{E}_i + \mathbf{E}_r) = 2\mathbf{e}_x \eta_1 |H_i| \sin k_1 z \sin \omega t, \tag{2.135}$$

and

$$\mathbf{H}_1 = \mathrm{Re}(\mathbf{H}_i + \mathbf{H}_r) = 2\mathbf{e}_y |H_i| \cos k_1 z \cos \omega t. \tag{2.136}$$

These equations describe standing waves carrying no energy which conforms to our intuitive picture for reflection from a perfect conductor: The counterpropagating incident and reflected waves of equal amplitudes interfere to form a standing wave pattern in medium 1.

Exercise 2.11. *A right-hand circularly polarized wave, propagating in the positive z-direction is normally incident on a perfect conductor wall $z = 0$. Determine (a) the polarization of the reflected wave and (b) the induced current on the conducting wall.*

Transverse electric (TE) or s-polarization. – In the TE case, the electric field is normal to the incidence plane,

$$\boldsymbol{\mathcal{E}}_i = E_i \mathbf{e}_y, \tag{2.137}$$

and it is convenient to work with complex amplitudes of electric fields, expressing the the magnetic field amplitudes as

$$\boldsymbol{\mathcal{H}}_s = \frac{(\mathbf{e}_s \times \boldsymbol{\mathcal{E}}_s)}{\eta_s}; \qquad s = i, r, t. \tag{2.138}$$

Similarly to the p-polarization case, we can obtain the expressions

$$\begin{aligned} \boldsymbol{\mathcal{E}}_i &= E_i \mathbf{e}_y \\ \boldsymbol{\mathcal{H}}_i &= \frac{E_i}{\eta_0 k_0}(-k_{1z}\mathbf{e}_x + k_x \mathbf{e}_z), \end{aligned} \tag{2.139}$$

$$\begin{aligned} \boldsymbol{\mathcal{E}}_r &= E_r \mathbf{e}_y, \\ \boldsymbol{\mathcal{H}}_r &= \frac{E_r}{\eta_0 k_0}(k_{1z}\mathbf{e}_x + k_x \mathbf{e}_z), \end{aligned} \tag{2.140}$$

and

$$\begin{aligned} \boldsymbol{\mathcal{E}}_t &= E_t \mathbf{e}_y, \\ \boldsymbol{\mathcal{H}}_t &= \frac{E_t}{\eta_0 k_0}(-k_{2z}\mathbf{e}_x + k_x \mathbf{e}_z), \end{aligned} \tag{2.141}$$

for the complex amplitudes of incident, reflected, and transmitted fields, respectively. The continuity of tangential components of electric and magnetic fields across the interface leads to

$$E_i + E_r = E_t, \tag{2.142}$$

and

$$(-E_i + E_r)k_{1z} = -E_t k_{2z} \tag{2.143}$$

Solving the last pair of equations, we arrive at the complex reflectivity and transmittance of an s-polarized incident wave in the form

$$r_\mathrm{s} \equiv \frac{E_r}{E_i} = \frac{k_{1z} - k_{2z}}{k_{1z} + k_{2z}}, \tag{2.144}$$

and

$$t_\mathrm{s} \equiv \frac{E_t}{E_i} = \frac{2k_{1z}}{k_{1z} + k_{2z}}. \tag{2.145}$$

2.3.3 Brewster angle and surface plasmon polaritons

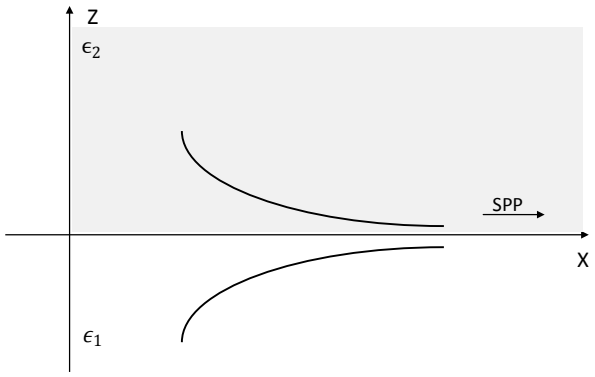

Figure 2.9: Surface electromagnetic wave (surface plasmon polariton) at a metal-dielectric interface. The electric and magnetic field decay fast away from the interface

Let us return to the general case of p-polarized wave reflection form the interface and study the behavior of reflectivity in more detail. We will assume both media to be transparent, for simplicity. It can be inferred from Eq. (2.126) that the reflectivity attains zero under the condition

$$\epsilon_2 k_{1z} = \epsilon_1 k_{2z}. \tag{2.146}$$

Solving Eq. (2.146), together with (2.113), we obtain expressions for the in-plane and normal components of the wave vectors as

$$k_x = \frac{\omega}{c}\sqrt{\frac{\epsilon_1\epsilon_2}{\epsilon_1+\epsilon_2}}, \tag{2.147}$$

and

$$k_{jz} = \frac{\omega}{c}\sqrt{\frac{\epsilon_j^2}{\epsilon_1+\epsilon_2}}, \qquad j = 1, 2. \tag{2.148}$$

The analysis of Eqs. (2.147) and (2.148) reveals two options. First, if both media permittivities are positive, $\epsilon_j > 0$, we may introduce real refractive indices, $n_j = \sqrt{\epsilon_j}$. It then follows at once from Eqs. (2.147) and (2.148) that there exists a special incidence angle θ_{B}, given by the expression

$$\tan\theta_{\mathrm{B}} = k_x/k_{1z} = n_2/n_1, \tag{2.149}$$

such that there is no p-polarized reflected wave. This special incidence angle is known as the Brewster angle. Alternatively, Eqs (2.147) and (2.148) describe a surface wave propagating along the interface, $k_x^2 > 0$ and exponentially decaying in the direction normal to the interface such that k_{jz} is purely imaginary (for transparent media), $k_{jz}^2 < 0$, Eqs. (2.147) and (2.148) imply that this is possible under the conditions,

$$\epsilon_1 + \epsilon_2 < 0, \tag{2.150}$$

and

$$\epsilon_1 \epsilon_2 < 0. \tag{2.151}$$

In other words, at least one of the permittivities must be negative. Usually, the wave is incident form a dielectric medium, $\epsilon_1 > 0$, implying that $\epsilon_2 < 0$. The latter condition can be realized for metals as we will see in Sec. 5.

These surface electromagnetic waves are known as surface plasmon polaritons (SPP). Using Eqs. (2.118), (2.120), and (2.148), the electromagnetic fields of SPPs on each side of the interface can be expressed as

$$\mathbf{H}(\mathbf{r},t) = \begin{cases} \mathbf{e}_y H_i e^{-|k_{2z}|z} e^{i(k_x x - \omega t)}, & z > 0; \\ \mathbf{e}_y H_i e^{|k_{1z}|z} e^{i(k_x x - \omega t)}, & z < 0, \end{cases} \tag{2.152}$$

and

$$\mathbf{E}(\mathbf{r},t) = \begin{cases} \frac{\eta_0 H_i}{k_0 \epsilon_2}(i|k_{2z}|\mathbf{e}_x - k_x \mathbf{e}_z) e^{-|k_{2z}|z} e^{i(k_x x - \omega t)}, & z > 0, \\ \frac{\eta_0 H_i}{k_0 \epsilon_1}(-i|k_{1z}|\mathbf{e}_x - k_x \mathbf{e}_z) e^{|k_{1z}|z} e^{i(k_x x - \omega t)}, & z < 0. \end{cases} \tag{2.153}$$

Thus, SPP fields propagate along the interface and exponentially decay away from the interface which is a characteristic signature of surface electromagnetic waves. In case the second medium is an ideal metal, its permittivity can be successfully modeled by the expression

$$\epsilon_2(\omega) = 1 - \frac{\omega_p^2}{\omega^2}, \tag{2.154}$$

where ω_p is the so-called plasma frequency. It can be seen from Eqs. (2.147) that in the short wavelength approximation, $k_x \to \infty$, the SPP frequency tends to a constant value, ω_∞ given by the expression

$$\omega_\infty = \frac{\omega_p}{\sqrt{1+\epsilon_1}}. \tag{2.155}$$

In this case, the SPP approaches its quasi-static limit termed a surface plasmon (SP).

Exercise 2.12. *Show that Eq. (2.155) can be derived in the quasi-static limit by solving Laplace's equation for the electrostatic potential and matching the appropriate boundary conditions.*

So far, we have assumed that the SPPs propagate on the interface of two transparent media. In reality, of course, all metals are lossy, albeit losses are usually small at optical frequencies. Realistic metals can then be properly described by complex dielectric permittivities to account for Joules' losses. Introducing a complex permittivity of medium 2 viz.,

$$\epsilon_2 = \epsilon_2' + i\epsilon_2'', \tag{2.156}$$

and assuming that under at optical frequencies of interest $|\epsilon_2''| \ll |\epsilon_2'|$, we can express the in-plane component of the SPP wave vector as

$$k_x = k_x' + ik_x'', \tag{2.157}$$

where

$$k_x' \simeq k_0 \sqrt{\frac{\epsilon_1 \epsilon_2'}{\epsilon_1 + \epsilon_2'}}, \tag{2.158}$$

and

$$k_x'' \simeq k_0 \sqrt{\frac{\epsilon_1 \epsilon_2'}{\epsilon_1 + \epsilon_2'}} \left[\frac{\epsilon_2'' \epsilon_1}{2\epsilon_2'(\epsilon_1 + \epsilon_2')} \right]. \tag{2.159}$$

Here the imaginary part specifies a characteristic inverse damping distance of the SPP,

$$L_{SPP} = 1/k_x''. \tag{2.160}$$

Exercise 2.13. *Derive Eqs. (2.158) and (2.159).*

It follows from Eq. (2.147) that a plane wave in the air with $\epsilon_1 = 1$ can never excite a plasmon because of the wave vector mismatch: the plasmon wave vector component along the interface is always greater than that of a plane wave in the air. One way to generate an SPP then will be to nano-engineer the surface by creating periodic imperfections such as grooves. The modified surface can serve as a diffraction grating by shifting the in-plane wave vector component of the incident wave to achieve phase matching. Introducing the lattice constant of the grooves a and assuming that the light wave is incident from air, we can write down the matching condition

$$k_{xSPP} = k_0 \sin\theta_i + 2\pi/a, \tag{2.161}$$

where θ_i is the incidence angle. This excitation scheme is sketched in the figure.

2.3.4 Total internal reflection

We saw in the previous section that a TM-polarized surface electromagnetic wave can be excited at an interface of a metal and transparent dielectric. In this section, we show that surface wave generation is also possible at an interface of two transparent media with refractive indices n_1 and n_2, when light is incident form a more optically dense medium, $n_1 > n_2$. This phenomenon is referred to as total internal reflection. It follows from Eq. (2.113) and the geometry of Fig. 2.3.1 that

$$k_{2z}^2 = k_0^2(n_2^2 - n_1^2 \sin^2\theta_1). \tag{2.162}$$

It can be readily inferred from Eq. (2.162) that the in-plane component of the wave vector in medium 2 becomes purely imaginary,

$$k_{2z} = i|k_{2z}| = ik_2 \sqrt{\tfrac{n_1^2}{n_2^2} \sin^2\theta_1 - 1}, \tag{2.163}$$

whenever the incidence angle exceeds the threshold,

$$\theta_{\rm c} = \sin^{-1}(n_2/n_1), \tag{2.164}$$

It then follows at once from Eqs. (2.126) and (2.163) that the for any wave incident at an angle grater than the critical angle given by Eq. (2.164), the reflectivity is unimodular, i. e.,

$$\overline{r}_{\rm p*} = \frac{\epsilon_2 k_{1z} - i\epsilon_1 |k_{2z}|}{\epsilon_2 k_{1z} + i\epsilon_1 |k_{2z}|}. \tag{2.165}$$

Alternatively, the reflectivity of a totally internally reflected wave can be expressed as

$$\boxed{\overline{r}_{\mathrm{p}*} = e^{-2i\phi_{\mathrm{p}*}}}, \tag{2.166}$$

where the phase can be expressed in terms of the incidence angle and refractive indices of the media as

$$\phi_{\mathrm{p}*} = \tan^{-1}\left(\frac{\epsilon_1|k_{2z}|}{\epsilon_2 k_{1z}}\right). \tag{2.167}$$

To better understand the behavior of the transmitted wave, we derive explicit expressions for its electric and magnetic fields. Using Eq. (2.163) in Eqs. (2.120), we can cast complex amplitudes of the transmitted magnetic and electric fields into

$$\mathbf{H}_t(\mathbf{r},t) = H_t\mathbf{e}_y e^{-|k_{2z}|z}e^{i(k_x x-\omega t)}, \tag{2.168}$$

and

$$\mathbf{E}_t(\mathbf{r},t) = \frac{\eta_0 H_t}{\epsilon_2 k_0}(i|k_{2z}|\mathbf{e}_x - k_x\mathbf{e}_z)e^{-|k_{2z}|z}e^{i(k_x x-\omega t)}. \tag{2.169}$$

We can conclude from Eqs. (2.168) and (2.169) that the transmitted wave fields exponentially decay into medium 2. Next, let us determine the magnitude and direction of the energy flow specified by the time-averaged Poynting vector. It follows from Eqs. (1.26) (2.168), and (2.169) after some algebra that

$$\langle\mathbf{S}_t(z)\rangle = \mathbf{e}_x\,\frac{4\epsilon_2 k_{1z}^2 k_x}{k_0(\epsilon_2^2 k_{1z}^2 + \epsilon_1^2|k_{2z}|^2)}\,I_i e^{-2|k_{2z}|z}, \tag{2.170}$$

where I_i is an optical intensity of the incident wave. It can be concluded from Eq. (2.170) that the power of the wave incident at an angle greater than the total internal reflection angle does not flow into the less optically dense medium. Rather, it propagates along the interface separating the two media, exponentially decaying in the direction normal to the interface. This is a signature of a surface wave. Such surface waves generated by total internal reflection are known as evanescent waves. The evanescent waves play a prominent role in generating surface plasmon polaritons in the laboratory. Indeed, one of the approaches to SPP generation employs evanescent waves. In practice, one uses a device referred to as a Kretschmann prism shown in the figure below. The refractive index of the prism makes it possible to match the in-plane wave vector components for a plane wave launched through the Kretschmann prism under the conditions of total internal reflection to that of the SPP. The launch angle is then determined by the matching condition,

$$k_{x\mathrm{pr}} = k_{x\mathrm{SPP}}, \tag{2.171}$$

implying that

$$n_{\mathrm{pr}}\sin\theta_{\mathrm{SPP}} = \sqrt{\frac{\epsilon_{\mathrm{d}}\epsilon_{\mathrm{m}}}{\epsilon_{\mathrm{d}}+\epsilon_{\mathrm{m}}}}, \tag{2.172}$$

where n_{pr} is the refractive index of the prism, typically it is equal to 1.5 for a glass prism, and ϵ_{d} and $\epsilon\mathrm{m}$ are the permittivities of the dielectric and metal on the two sides of the interface supporting the SPP. In the figure, the SPP is produced at the metal-air

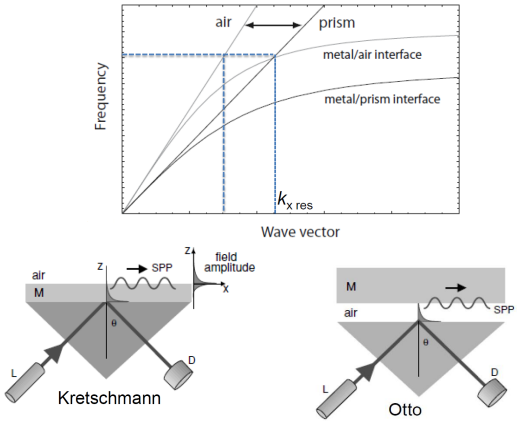

Figure 2.10: Illustrating SPP excitation with Kretschmann method. Reproduced from Novotny& Hecht, *Principles of Nanooptics*.

interface by an evanescent wave tunneling across the metal film from the glass prism.

Exercise 2.14. *Show that the reflectivity of a totally internally reflected TE-wave is given by the expression*

$$r_{s*} = e^{-2i\phi_{s*}}, \tag{2.173}$$

where

$$\phi_{s*} = \tan^{-1}(|k_{2z}|/k_{1z}). \tag{2.174}$$

Derive an expression for the transmitted energy flux.

2.4 Refraction and reflection from dielectric slab: Multi-wave interference

We will now examine a situation when two unbounded, homogeneous isotropic media–media 1 and 3–are separated by a slab of finite thickness d filled with a third medium, medium 3; for simplicity, we assume that the plane coincides with the xz-plane. The situation is illustrated in the figure below. Suppose further that a plane wave is incident from medium 1 onto the interface separating media 1 and 2 and limit ourselves to the instructive case of a p-polarized incident wave throughout this section. We will seek to determine the complex reflectivity and transmittance of the system. Next, we introduce the reflectivity and transmittance of each individual interface, r_{ij} and t_{ij}, $i, j = 1, 2, 3$, respectively, which are determined by Eqs. (2.126) and (2.127).

The incident, reflected, and transmitted magnetic field amplitudes can be expressed as

$$\mathbf{H}_s = H_s \mathbf{e}_y, \qquad s = i, r, t. \tag{2.175}$$

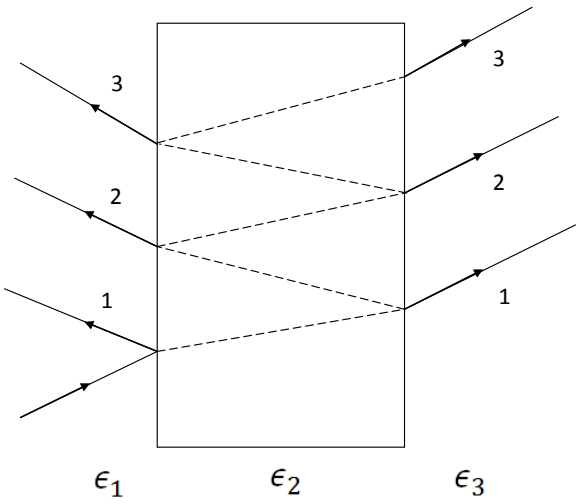

Figure 2.11: Illustrating the multi-wave reflection and transmission through a film.

We will then find the reflected magnetic field in terms of the incident field by adding up the contributions from reflected waves of all orders. Let us consider several lowest-order reflected waves, labeling the reflection order with the corresponding superscript assigned to H_r. The first-order reflected field is simply the field reflected from the first interface once. Thus,

$$\mathbf{H}_r^{(1)} = r_{12} H_i \mathbf{e}_y. \tag{2.176}$$

Next, the second-order reflected field is twice transmitted trough the first interface and once reflected from the second one, i. e.,

$$\mathbf{H}_r^{(2)} = t_{12} t_{21} r_{23} e^{i2k_{2z}d} H_i \mathbf{e}_y, \tag{2.177}$$

where we also included the accrued phase due to the optical path difference. By the same token, the third- and fourth-order reflected waves can be represented as

$$\mathbf{H}_r^{(3)} = t_{12} t_{21} r_{23}^2 r_{21} e^{i4k_{2z}d} H_i \mathbf{e}_y \tag{2.178}$$

and

$$\mathbf{H}_r^{(4)} = t_{12} t_{21} r_{23}^3 r_{21}^2 e^{i6k_{2z}d} H_i \mathbf{e}_y. \tag{2.179}$$

Summing up the contributions to all orders, we obtain

$$\mathbf{H}_r = \mathbf{e}_y H_i \left(r_{12} + r_{23} t_{12} t_{21} e^{i2k_{2z}d} \sum_{s=0}^{\infty} r_{21}^s r_{23}^s e^{i2sk_{2z}d} \right). \tag{2.180}$$

Observe that as follows from Eqs. (2.126) and (2.127),

$$r_{12} = -r_{21}, \quad \text{and} \quad t_{12} = t_{21}. \tag{2.181}$$

Hence, performing the summation on the right-hand side of Eq. (2.180) and employing Eq. (2.181), yields, after minor algebra, the expression

$$\mathbf{H}_r = \mathbf{e}_y H_i \frac{r_{12} + r_{23} e^{i2k_{2z}d}}{1 + r_{12} r_{23} e^{i2k_{2z}d}}. \tag{2.182}$$

Thus introducing the complex reflectivity,

$$\overline{r} \equiv E_r / E_i, \tag{2.183}$$

and using Eqs. (2.125), (2.182), we arrive at

$$\overline{r} = \frac{r_{12} + r_{23} e^{2ik_{2z}d}}{1 + r_{12} r_{23} e^{2ik_{2z}d}}. \tag{2.184}$$

Eq. (2.184) gives the reflectivity of the slab. The outlined method for reflectivity calculation using reflected wave summations of all orders is known as Airy technique.

The analysis of Eqs. (2.184) reveals two instructive particular cases which emerge whenever the reflectivity attains zero,

$$r_{12} + r_{23} e^{2ik_{2z}d} = 0. \tag{2.185}$$

First, we consider the reflectionless transmission of a homogeneous plane wave through a transparent film. This is a multi-wave analog of the Brewster regime except it can occur even for normal incidence. Indeed, as follows from Eq. (2.185) the reflectionless transmission is possible for normal incidence, $k_{2z} = k_2$, provided that

$$2k_2 d = \pi, \tag{2.186}$$

implying a constraint on the slab thickness,

$$d = \frac{\lambda}{4n_2}. \tag{2.187}$$

Eqs. (2.185) and (2.187) are compatible if the refractive index of the slab satisfies the condition

$$n_2 = \sqrt{n_1 n_3}. \tag{2.188}$$

The constraints (2.187) and (2.188) establish requirements for reflectionless transmission of a normally incident plane wave through a dielectric film. In practice, these conditions are taken advantage of in fabricating antireflection coatings of dielectric surfaces such as antireflection glass coating to protect against glare or improve night vision.

The second instance of no reflectivity corresponds to the generation of SPPs on both surfaces of the film. Under the circumstances, the waves multiply reflected from the film interfere constructively to transfer their energy into the SPPs. Thus all power of the incident wave is channeled into the surface waves, resulting in no reflection. In this case, the normal components of all wave vectors must be purely imaginary, a

signature of surface waves. In particular, the normal components of $\mathbf{k}$ in media 1 and 3 can be represented as

$$k_{1z} = -iq_1 = -i\sqrt{k_x^2 - k_1^2}, \tag{2.189}$$

and

$$k_{3z} = iq_3 = i\sqrt{k_x^2 - k_3^2}, \tag{2.190}$$

to ensure the exponential decay of the waves away from the interfaces. Note that these definitions imply that $q_{1,3} > 0$ since the positive root is taken on the right-hand sides of Eqs. (2.189) and (2.190). On the other hand, there exist both exponentially growing and decaying waves inside the slab, implying that

$$k_{2z} = iq_2 = \pm i\sqrt{k_x^2 - k_2^2}. \tag{2.191}$$

The SPP dispersion relation follows at once from Eqs. (2.126), (2.185) and Eqs. (2.189) through (2.191):

$$e^{-2q_2 d} = \left(\frac{\epsilon_1 q_2 + \epsilon_2 q_1}{\epsilon_1 q_2 - \epsilon_2 q_1}\right)\left(\frac{\epsilon_3 q_2 + \epsilon_2 q_3}{\epsilon_3 q_2 - \epsilon_2 q_3}\right). \tag{2.192}$$

In general, Eq. (2.192) describes a rather complicated dispersion relation. To gain a better insight into the SPPs in the film, let us consider a particular case when media 1 and 3 are the same such that $\epsilon_1 = \epsilon_3$ and $q_1 = q_3$. It can then be inferred from Eq. (2.192) after a minor algebra that two families of SPPs exist in this case with the dispersion relations governed by the equations

$$\tanh\left(\frac{q_2 d}{2}\right) = -\frac{\epsilon_1 q_2}{\epsilon_2 q_1}, \tag{2.193}$$

and

$$\tanh\left(\frac{q_2 d}{2}\right) = -\frac{\epsilon_2 q_1}{\epsilon_1 q_2}. \tag{2.194}$$

Exercise 2.15. *Derive Eqs. (2.193)and (2.194).*
It follows at once from Eqs. (2.193) and (2.194) that as the film thickness increases without limit, $d \to \infty$, both dispersion relations reduce to

$$\epsilon_1 q_2 = -\epsilon_2 q_1. \tag{2.195}$$

Since in this case, $q_2 < 0$, one of the permittivities ought to be negative, $\epsilon_2 < 0$, say. Comparison of Eq. (2.195) with (2.146) leads to the conclusion that the SPPs on both sides of a very thick film are uncoupled and have the same dispersion relation as the SPP at the interface of two unbounded media.

In the other extreme of very thin films, $d \to 0$, particularly simple results can be obtained under the condition

$$\tfrac{1}{2} q_2 d \ll 1. \tag{2.196}$$

In other words, the characteristic penetration depth in medium 2, $\delta \simeq |q_2|^{-1}$ is much smaller than half the film thickness. In physical terms, this condition implies strong

coupling between SPPs propagating on both sides of the film. Eqs. (2.193) and (2.196) then yield an approximate expression

$$q_1 \simeq -\frac{2\epsilon_1}{\epsilon_2 d}, \tag{2.197}$$

for the normal component of the wave vector in medium 1. Further, the in-plane component of the wave vector is given by

$$k_x \simeq \sqrt{k_0^2\epsilon_1 + \frac{4\epsilon_1^2}{\epsilon_2^2 d^2}}, \tag{2.198}$$

and the other normal component of the wave vector is

$$q_2 \simeq \pm\sqrt{k_0^2(\epsilon_1 - \epsilon_2) + \frac{4\epsilon_1^2}{\epsilon_2^2 d^2}}. \tag{2.199}$$

In particular, we apply our results to a thin metal film sandwiched between insulator media (IMI). Such a thin-film IMI geometry implies the following conditions

$$0 < \epsilon_1 \ll |\epsilon_2|, \qquad \epsilon_2 < 0. \tag{2.200}$$

Eqs. (2.196) through (2.200) will be consistent for genuinely thin films $d \ll \lambda_0$, yielding

$$|q_2| \simeq \sqrt{k_0^2|\epsilon_2| + \frac{4\epsilon_1^2}{\epsilon_2^2 d^2}}. \tag{2.201}$$

such that the light penetration depth into the metal and dielectric are approximately given by

$$\delta_{\rm m} \simeq \frac{1}{|q_2|}, \qquad \delta_{\rm d} \simeq \frac{|\epsilon_2| d}{2\epsilon_1}. \tag{2.202}$$

This case would correspond to a 20 nm thin metal film, say, with $\epsilon_2 \sim -20$ illuminated from glass $\epsilon_1 \simeq 1.25$ by a light beam with $\lambda_0 \sim 500$ nm, for example. The SPP confinement is still rather tight $\delta_{\rm d} \sim 200$ nm, and $\delta_{\rm m} \sim 50$ nm.

Exercise 2.16. *Plot an explicit dispersion relation curve $\omega = \omega(k_x)$ given by Eq. (2.198). What happens in the static limit, $k_x \to \infty$? You may assume an ideal metal with $\epsilon(\omega) = 1 - \omega_p^2/\omega^2$.*

Exercise 2.17. *Use the Airy technique to show that the transmittance of the slab examined in this section is given by the expression*

$$\bar{t} = \frac{t_{12}t_{23}e^{ik_{2z}d}}{1 + r_{12}r_{23}e^{2ik_{2z}d}}. \tag{2.203}$$

Suppose a dielectric film made of a transparent material is placed in the air. Define the transmission coefficient of the film by the expression

$$\mathcal{T} \equiv \frac{|E_t|^2}{|E_i|^2}, \tag{2.204}$$

and show that $\mathcal{T}$ can be expressed as

$$\mathcal{T} = \frac{T^2}{(1-R)^2} \frac{1}{1 + F \sin^2 \delta}. \tag{2.205}$$

Here

$$\delta = \delta_r + \frac{2\pi n d}{\lambda} \cos \theta_t, \tag{2.206}$$

and we introduced the transmission and reflection coefficients for each interface of the slab, T and R, respectively, and the interferometer finesse F by the expression

$$F = \frac{4R}{(1-R)^2}. \tag{2.207}$$

The considered system serves as a basis for a Fabry-Perot interferometer used to pre-

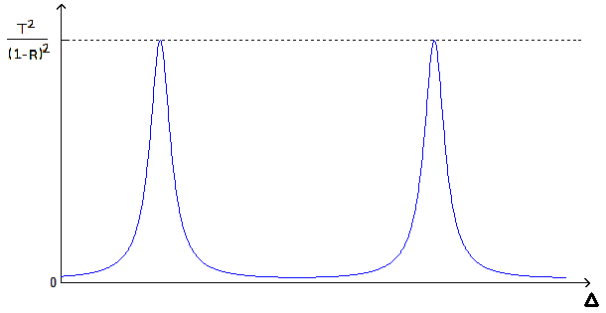

Figure 2.12: Fabry-Perot transmittance dependence on the detuning Δ.

cisely measure the wavelength of light. It can be inferred from Eq. (2.205) –(2.207) that for large enough reflectance, $R \simeq 1$, $\mathcal{T}$ has very sharp maxima at

$$\delta = \pi m, \qquad m = 0, 1, 2, \ldots. \tag{2.208}$$

In the ideal case, $\mathcal{T} = 1$ at the maxima and $\mathcal{T} = 1/F$ at the minima. Thus boosting the finesse, one can increase the contrast of the interferometer. The distance between the adjacent maxima can be determined from Eqs. (2.206) and (2.208) to be

$$d_{m+1} - d_m = \frac{\lambda}{2n \cos \theta}. \tag{2.209}$$

For sufficiently small angles, $\theta \simeq 0$, the latter reduces to

$$d_{m+1} - d_m \simeq \frac{\lambda}{2n}. \tag{2.210}$$

Eq. (2.210) can be used to infer the value of λ from the measurements of the maxima positions.

2.5 Classical theory of optical dispersion and absorption

2.5.1 Lorentz-Kramers expression for dielectric permittivity

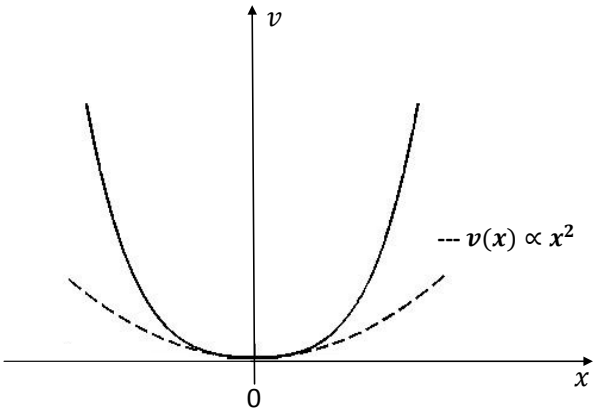

Figure 2.13: Schematic of a trapping Coulomb potential (solid) for an electron in an atom and its harmonic approximation (dashed) near the electron equilibrium position; x is a scalar displacement away from equilibrium.

As we saw in Sec. 2.2, atoms or molecules of realistic media do not respond instantaneously to an applied external electric field. The time lag between the applied electric field and induced polarization manifests itself as frequency dispersion when one examines the frequency behavior of medium response to a harmonic applied electric field,

$$\mathbf{E}(t) = \mathbf{E}_\omega e^{-i\omega t}. \tag{2.211}$$

To drive this point home, we develop a simple classical model of matter response to an external time-harmonic field. In this model atoms are treated as simple harmonic oscillators. A linear restoring force proportional to an electron displacement from its equilibrium position–in the classical sense, of course–is due to a harmonic interaction potential between an electron and the other electrons in an atom as well as the atomic nucleus. In reality each atomic electron is trapped by a complicated electrostatic potential which is strongly anharmonic. However, so long as the applied electric field is sufficiently weak such that the electron displacement from its equilibrium position is small compared to the characteristic atomic size, the electrostatic Coulomb potential in the vicinity of the electron equilibrium position can be well approximated by a harmonic one. The situation is schematically depicted in the figure.

Further, we assume that each atom has Z bound electrons. Assume also that there are f_s electrons per atom having the binding frequency ω_s which corresponds to a particular type of the trapping harmonic potential. The quantities $\{f_\mathrm{s}\}$ are referred to as the oscillator strengths.

Whenever an electron having the binding frequency ω_s is displaced by the displacement vector $\mathbf{r}_{\rm s}$ in response to the external electric field, it experiences three forces: the restoring force, $\mathbf{F}_{\rm r} = -m\omega_{\rm s}^2\mathbf{r}_{\rm s}$, the damping force, $\mathbf{F}_{\rm d} = -2m\gamma_s\dot{\mathbf{r}}_{\rm s}$–where $\gamma_{\rm s}$ is a phenomenological damping constant–and the force due to the external electric field, $\mathbf{F}_{\rm e} = -e\mathbf{E}_\omega e^{-i\omega t}$.

The equation of electron motion (second law of Newton) is then

$$m\ddot{\mathbf{r}}_{\rm s} = -m\omega_{\rm s}^2\mathbf{r}_{\rm s} - 2m\gamma_{\rm s}\dot{\mathbf{r}}_{\rm s} - e\mathbf{E}_\omega e^{-i\omega t}. \tag{2.212}$$

Here each "dot" stands for a time derivative. We seek a driven solution to Eq. (2.212) in the form,

$$\mathbf{r}_{\rm s}(t) = \mathbf{r}_{\rm s\omega} e^{-i\omega t}. \tag{2.213}$$

It follows from Eqs. (2.212) and (2.213) that the electron displacement amplitude is

$$\mathbf{r}_{\rm s\omega} = -\frac{e\mathbf{E}_\omega}{m(\omega_{\rm s}^2 - \omega^2 - 2i\omega\gamma_{\rm s})}, \tag{2.214}$$

implying that

$$\mathbf{r}_{\rm s}(t) = -\frac{e\mathbf{E}(t)}{m(\omega_{\rm s}^2 - \omega^2 - 2i\omega\gamma_{\rm s})}. \tag{2.215}$$

The induced individual dipole moment of the electron of this type will be $\mathbf{p}_{\rm s} = -e\mathbf{r}_{\rm s}$. Next, if there are N atoms per unit volume, the induced polarization is

$$\mathbf{P}(t) = N\sum_{\rm s} f_s\mathbf{p}_{\rm s}(t) = -Ne\sum_{\rm s} f_{\rm s}\mathbf{r}_{\rm s}(t) = \frac{Ne^2}{m}\sum_{\rm s}\frac{f_{\rm s}\mathbf{E}(t)}{(\omega_{\rm s}^2 - \omega^2 - 2i\omega\gamma_{\rm s})}. \tag{2.216}$$

Note that the oscillator strengths satisfy the so-called sum rule

$$\sum_{\rm s} f_{\rm s} = Z. \tag{2.217}$$

On comparing Eqs. (1.6), (2.36) and (2.216), we infer that

$$\epsilon(\omega) = 1 + \frac{Ne^2}{\epsilon_0 m}\sum_{\rm s} f_{\rm s}\mathcal{L}_s(\omega), \tag{2.218}$$

where we introduced a complex Lorentzian line-shape factor by the expression

$$\mathcal{L}_s(\omega) = \frac{1}{(\omega_{\rm s}^2 - \omega^2 - 2i\omega\gamma_{\rm s})}. \tag{2.219}$$

Eqs. (2.218) and (2.219) give a classical expression for the dielectric permittivity of materials as a function of frequency of the applied electric field. The real part describes dispersion while the imaginary part accounts for light absorption by medium atoms. The latter simply because we identified the imaginary part of ϵ with losses as the light propagates through the medium (c.f. Sec. 2.3). Clearly, the light wave loses its energy to the medium atoms which is a classical picture of light absorption.

Let us now explore what happens if the frequency of the applied electric field is close to a particular resonant frequency of the material. For the sake of clarity, let that be the lowest bound frequency of the dielectric, $\omega_0 \neq 0$, i.e, $\omega \approx \omega_0$. In this case, we can single out the resonant term in Eq. (2.218) implying that

$$\epsilon(\omega) = \epsilon_{\mathrm{NR}}(\omega) + \frac{Ne^2 f_0}{\epsilon_0 m} \frac{1}{(\omega_0^2 - \omega^2 - 2i\omega\gamma_0)}. \tag{2.220}$$

As typically $\gamma_s \ll \omega_s$, the contribution to the permittivity due to non-resonant terms, ϵ_{NR} is a purely real and only weakly frequency dependent. It can be expressed as

$$\epsilon_{\mathrm{NR}}(\omega) \simeq 1 + \sum_{s \neq 0} \frac{Ne^2 f_{\mathrm{s}}}{\epsilon_0 m(\omega_{\mathrm{s}}^2 - \omega^2)}. \tag{2.221}$$

Notice that close to resonance, we can approximate

$$-\omega^2 + \omega_0^2 - 2i\gamma_0\omega \simeq 2\omega(\omega_0 - \omega - i\gamma_0) \simeq 2\omega_0(\omega_0 - \omega - i\gamma_0). \tag{2.222}$$

It can be inferred from Eqs. (2.221) and (2.222) that the permittivity near optical resonance can be represented as

$$\epsilon(\omega) = \epsilon'(\omega) + i\epsilon''(\omega), \tag{2.223}$$

where

$$\epsilon'(\omega) = \epsilon_{\mathrm{NR}}(\omega) + \frac{Ne^2 f_0}{2\epsilon_0 m\omega_0} \left[\frac{(\omega - \omega_0)}{(\omega - \omega_0)^2 + \gamma_0^2}\right], \tag{2.224}$$

and

$$\epsilon''(\omega) = \frac{Ne^2 f_0}{2\epsilon_0 m\omega_0} \left[\frac{\gamma_0}{(\omega - \omega_0)^2 + \gamma_0^2}\right]. \tag{2.225}$$

The real and imaginary parts of the permittivity are sketched as functions of the frequency in Fig. 2.5.

As is seen in Fig. 2.5., the real part of the permittivity sufficiently far below and above the resonance frequency increases with the frequency. Such a behavior is known as normal dispersion. In the vicinity of resonance, however, ϵ' decreases with the frequency which is referred to as anomalous dispersion. Optical absorption is generally small far from resonance, but is seen to sharply increase as we approach the resonance frequency. Notice also that in regions of weak dispersion are nearly transparent, whereas strong dispersion is accompanied with pronounced absorption as well. This connection is not accidental. In fact, we show in the following chapters that there are fundamental quantitative relations, the Kramers-Kronig relations that link dispersive and absorptive properties of optical media.

The difference between realistic conductors and dielectrics can be attributed to the presence of free electrons in the former. Indeed, by looking into the low-frequency limit, we notice that for pure dielectrics the lowest bound frequency must be nonzero, while conductors can have a fraction of electrons, f_0, say, that have $\omega_0 = 0$; those

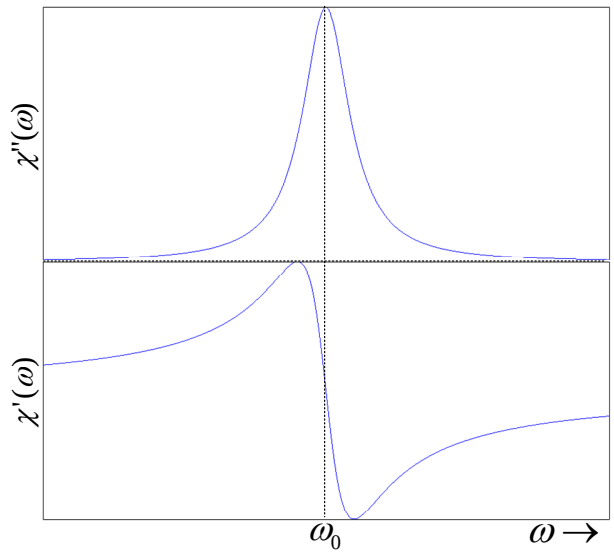

Figure 2.14: Imaginary (top) and real (bottom) parts of the electric permittivity as functions of frequency near resonance.

are essentially free electrons. Consequently, the dielectric permittivity of conductors is given by the expression

$$\epsilon_{\rm c}(\omega) = \epsilon_{\rm b}(\omega) + i\frac{Nf_0e^2}{\epsilon_0 m\omega(2\gamma_0 - i\omega)}, \tag{2.226}$$

where $\epsilon_{\rm b}$ is the overall contribution of the bound electrons with $\omega_s \neq 0$. Since free electrons can conduct currents, we can use Eq. (2.215) to determine the current density to be

$$\mathbf{J} = -Nef_0\dot{\mathbf{r}}_0 = \frac{Nf_0e^2}{m(2\gamma_0 - i\omega)}\mathbf{E}. \tag{2.227}$$

On comparing Eqs (2.37) and (2.227), we infer the expression for the conductivity,

$$\sigma(\omega) = \frac{Nf_0e^2}{m(2\gamma_0 - i\omega)}. \tag{2.228}$$

It is seen from Eq. (3.47) that in the dc limit $\omega \to 0$, we arrive at

$$\sigma \to \frac{Nf_0e^2}{2m\gamma_0} = \sigma_0, \tag{2.229}$$

the conductivity is real, describing dc currents. In view of Eq. (2.229), the expression for σ can be cast into the form

$$\sigma(\omega) = \frac{\sigma_0}{1 - i\omega\tau}, \tag{2.230}$$

where $\tau = 1/2\gamma_0$ is a characteristic time for current relaxation in conductors.

Next, comparing Eqs. (2.226) and (2.228), we can express the former as

$$\epsilon_{\rm c}(\omega) = \epsilon_{\rm b}(\omega) + i\frac{\sigma}{\epsilon_0\omega}. \tag{2.231}$$

Eq. (2.231) implies that losses in real conductors/metals come in two guises: absorption of electromagnetic waves by bound electrons–which is described by the imaginary part of ϵ_b–and ohmic losses due to generating electric currents as described by the second term on the right-hand side of Eq. (2.231).

Exercise 2.18. *Use the limiting case of Eq. (2.38) for isotropic media with no spatial dispersion and Eq. (2.231) to relate real and imaginary parts of permittivity and conductivity. Thus, you may argue that the distinction between conductors and dielectrics is rather artificial at optical frequencies.*

Next, we note that at the frequencies far exceeding the highest bound frequency, $\omega \gg \max(\omega_s)$, dielectrics and conductors respond to the applied electric field the same wave. In this limit, we can neglect all $\{\omega_s\}$ and $\{\gamma_s\}$ in the denominator of Eq. (2.218), leading to

$$\epsilon_{\rm c}(\omega) = 1 - \frac{\omega_p^2}{\omega^2}, \tag{2.232}$$

where we used Eq. (2.217) and introduced the plasma frequency

$$\omega_{\rm p} = \sqrt{\frac{NZe^2}{m}}. \tag{2.233}$$

Incidentally, Eq. (2.232) is a simplified form of the so-called Drude expression for a dielectric constant of a metal. The Drude model describes well noble metals; it follows from Eq. (2.232) that ϵ becomes negative for the frequencies above the plasma frequency.

Finally, we note that the polarization caused by a monochromatic applied electric field in an isotropic linear medium can be represented as

$$\mathbf{P}(\mathbf{r},\omega) = \epsilon_0\chi(\omega)\mathbf{E}(\mathbf{r},\omega), \tag{2.234}$$

where $\chi(\omega)$ is a linear susceptibility of the medium. In case of an optical pulse, consisting of many monochromatic components, the electric field of the pulse can be represented as a Fourier integral viz.,

$$\mathbf{E}(\mathbf{r},t) = \int_{-\infty}^{\infty}\frac{d\omega}{2\pi}\,\boldsymbol{\mathcal{E}}(\mathbf{r},\omega)e^{-i\omega t}, \tag{2.235}$$

where $\boldsymbol{\mathcal{E}}(\mathbf{r},\omega)$ is the spectral amplitude of the pulse. The polarization field induced by each spectral component of the pulse is given by

$$\boldsymbol{\mathcal{P}}(\mathbf{r},\omega) = \epsilon_0\chi(\omega)\boldsymbol{\mathcal{E}}(\mathbf{r},\omega). \tag{2.236}$$

It follows at once from Eqs. (2.235) and (2.236) that the overall polarization field induced by the pulse is given by a time convolution,

$$\mathbf{P}(\mathbf{r},t) = \epsilon_0\int_{-\infty}^{\infty}dt'\chi(t-t')\mathbf{E}(\mathbf{r},t'). \tag{2.237}$$

We will return to Eq. (2.237) in Chap. 4 where we will present a general theory of optical response of nonlocal noninstantaneous nonlinear media to electromagnetic pulses.

2.5.2 Classical theory of Faraday effect

Let us now consider the optical response of an isotropic dielectric to an applied static magnetic field $\mathbf{B}_0$. We will use the Lorentz-Kramers harmonic oscillator model of the medium elaborated in the previous subsection. We will assume that the external magnetic field is weak enough such that it can be treated as a small perturbation. The driven harmonic oscillator equation of motion of each electron can then be rewritten as

$$\ddot{\mathbf{r}}_{\rm s} + 2\gamma_{\rm s}\dot{\mathbf{r}}_{\rm s} + \omega_{\rm s}^2\mathbf{r}_{\rm s} = -\frac{e}{m}\mathbf{E}_\omega e^{-i\omega t} - \nu\frac{e}{m}[\dot{\mathbf{r}}_{\rm s} \times \mathbf{B}_0]. \tag{2.238}$$

Here we assume that the Lorentz force experienced by an electron due to the external magnetic field $\mathbf{B}_0$ is a small perturbation to the force exerted by the driving harmonic electric field. Instead of using an explicit small dimensionless parameter, we introduced a book-keeping parameter ν to aid keeping track of the same order terms in $\mathbf{B}_0$; we will let $\nu = 1$ at the end of our calculation. We can then represent the electron displacement as a perturbation series in the formal parameter ν as

$$\mathbf{r}_{\rm s} = \mathbf{r}_{\rm s}^{(0)} + \nu\mathbf{r}_{\rm s}^{(1)} + \nu^2\mathbf{r}_{\rm s}^{(2)} + \ldots \tag{2.239}$$

We will seek a driven solution to Eq.(2.238) in the form (2.213). On substituting Eq. (2.239) into (2.238), we can recover, to the first order in ν, the result of the previous subsection, i. e.,

$$\mathbf{r}_{{\rm s}\omega}^{(0)} = -\frac{e}{m}\mathcal{L}_s(\omega)\mathbf{E}_\omega. \tag{2.240}$$

To the first order in ν, we obtain from Eq. (2.238)

$$\ddot{\mathbf{r}}_{\rm s}^{(1)} + 2\gamma_{\rm s}\dot{\mathbf{r}}_{\rm s}^{(1)} + \omega_{\rm s}^2\mathbf{r}_{\rm s}^{(1)} = \frac{e}{m}[\dot{\mathbf{r}}_{\rm s}^{(0)} \times \mathbf{B}_0]. \tag{2.241}$$

Solving Eq. (2.241) in the steady-state regime, we arrive at the correction term as

$$\mathbf{r}_{{\rm s}\omega}^{(1)} = -\frac{ie^2\omega}{m^2}\mathcal{L}_s^2(\omega)[\mathbf{E}_\omega \times \mathbf{B}_0]. \tag{2.242}$$

Combining Eqs. (1.6) and (2.36, which furnish a macroscopic description of permittivity, with the classical microscopic picture of Eqs. (2.216) as well as with Eqs. (2.239) through (2.242), we finally obtain the following expression for the permittivity tensor,

$$\epsilon_{ij}(\omega) = \epsilon(\omega)\delta_{ij} + ig(\omega)\sum_p e_{ijp}B_{0p}. \tag{2.243}$$

Here

$$\epsilon(\omega) = 1 + \frac{Ne^2}{\epsilon_0 m}\sum_s f_s\mathcal{L}_s(\omega), \tag{2.244}$$

is a dielectric permittivity of an isotropic medium and

$$g(\omega) = \frac{Ne^3\omega}{\epsilon_0 m^2} \sum_s f_s \mathcal{L}_s^2(\omega), \tag{2.245}$$

is a Faraday coefficient which determines the rate of Faraday polarization rotation; it is related to the previously introduced Verdet constant, c. f., Sec. 2.2.3. Notice that Eq. (2.243) is identical to the expression (2.88) which we have introduced before on purely phenomenological grounds. Thus, the presented classical theory of Faraday's effect justifies the phenomenological approach of Sec. 2.3.3. Note also that the microscopic theory furnishes a classical expression for the rotation coefficient g as well.

Exercise 2.19. *Fill in missing steps in the derivation of Eq. (2.243).*

Exercise 2.20. *Extend the above discussion to determine the permittivity tensor correct to the second-order of perturbation theory. Show that the quadratic correction solely determines the rate of polarization rotation of a wave propagating orthogonally to the external magnetic field. This is known as Cotton-Mouton effect.*

Chapter 3

Pulses and beams in linear optics

3.1 Pulse propagation in dispersive media: non-resonant case

Let us consider propagation of electromagnetic waves in nonmagnetic media with frequency dispersion. The constitutive relation for the electric flux density in the space-frequency representation reads

$$\tilde{\boldsymbol{\mathcal{D}}}(\mathbf{r},\omega) = \epsilon_0 \epsilon(\omega) \tilde{\boldsymbol{\mathcal{E}}}(\mathbf{r},\omega), \tag{3.1}$$

where frequency dispersion enters through the dependence of the dielectric permittivity on the wave frequency. The corresponding wave equation takes the form

$$\nabla^2 \tilde{\boldsymbol{\mathcal{E}}} + \epsilon(\omega) \tfrac{\omega^2}{c^2} \tilde{\boldsymbol{\mathcal{E}}} = 0. \tag{3.2}$$

We seek a linearly polarized spatially homogeneous frequency-dependent wave propagating in the positive z-direction, i.e,

$$\tilde{\boldsymbol{\mathcal{E}}}(\mathbf{r},\omega) = \mathbf{e}_x \tilde{\mathcal{E}}(\omega, z) e^{ik_0 z}. \tag{3.3}$$

Here k_0 is a wave number associated with the carrier frequency ω_0, and a slowly-varying envelope is assumed such that

$$\partial_z \tilde{\mathcal{E}} \ll k_0 \tilde{\mathcal{E}}, \tag{3.4}$$

Eqs. (3.3) and (3.4) represent a spectral envelope amplitude of a slowly varying optical pulse. On substituting from Eqs. (3.3) and (3.4) into Eq. (3.2), we arrive at the paraxial wave equation in the space-frequency representation,

$$2ik_0 \partial_z \tilde{\mathcal{E}} + [k^2(\omega) - k_0^2] \tilde{\mathcal{E}} = 0, \tag{3.5}$$

where we introduced the frequency-dependent wave number viz.,

$$k^2(\omega) = \epsilon(\omega)\frac{\omega^2}{c^2}. \tag{3.6}$$

Suppose now the bandwidth of the pulse is small compared to the carrier frequency, i.e,

$$\Delta\omega = 2|\omega_{\max} - \omega_0| \ll \omega_0, \tag{3.7}$$

where ω_{max} is the frequency of the highest harmonic within the pulse associated with a finite amplitude. The combined approximations (3.4) and (3.7) constitute the slowly varying envelope approximation (SVEA) for optical pulses. The SVEA implies that

$$\tilde{\mathcal{E}}(\omega, z) \simeq \tilde{\mathcal{E}}(\omega - \omega_0, z) = \tilde{\mathcal{E}}(\omega', z), \tag{3.8}$$

that is the pulse envelope changes slowly over an optical cycle. To this level of accuracy, we can then expand the wave number in a Taylor series as

$$k(\omega) \simeq k_0 + \underbrace{k'(\omega_0)}_{k_1}(\omega - \omega_0) + \frac{1}{2!}\underbrace{k''(\omega_0)}_{k_2}(\omega - \omega_0)^2. \tag{3.9}$$

Assuming further that

$$k(\omega) + k_0 \simeq 2k_0,$$

we can cast Eq. (3.5) into the form

$$i\partial_z\tilde{\mathcal{E}} + k_1\omega'\tilde{\mathcal{E}} + \tfrac{1}{2}k_2\omega'^2\tilde{\mathcal{E}} = 0. \tag{3.10}$$

The overall electric field can then be factorized into a fast carrier wave and slowly varying pulse envelope as

$$\mathbf{E}(t, z) = \mathbf{e}_x \underbrace{e^{i(k_0 z - \omega_0 t)}}_{carrier\ wave}\underbrace{\int_{-\infty}^{+\infty} d\omega' e^{-i\omega' t}\tilde{\mathcal{E}}(\omega', z)}_{slow\ envelope}. \tag{3.11}$$

Introducing a Fourier transform of the pulse envelope spectrum by

$$\mathcal{E}(t, z) = \int_{-\infty}^{+\infty} d\omega' e^{-i\omega' t}\tilde{\mathcal{E}}(\omega'), \tag{3.12}$$

we can derive, using Fourier transform properties, a paraxial wave equation for the temporal envelope

$$2i(\partial_z\mathcal{E} + k_1\partial_t\mathcal{E}) - k_2\partial_{tt}^2\mathcal{E} = 0. \tag{3.13}$$

It is now convenient to transfer to a moving reference frame by introducing the coordinate transformation

$$\zeta = z; \qquad \tau = t - k_1 z, \tag{3.14}$$

One can then re-calculate the derivatives using the chain rules

$$\partial_t\mathcal{E} = \partial_\tau\mathcal{E}; \qquad \partial_{tt}^2\mathcal{E} = \partial_{\tau\tau}^2\mathcal{E}, \tag{3.15}$$

and

$$\partial_z \mathcal{E} = \partial_\zeta \mathcal{E} - k_1 \partial_\tau \mathcal{E}, \tag{3.16}$$

to arrive at the final form of the governing pulse propagation equation in linear dispersive media

$$2i\partial_\zeta \mathcal{E} - k_2 \partial^2_{\tau\tau} \mathcal{E} = 0. \tag{3.17}$$

To elucidate physical meaning of each term in Eq. (3.17), we observe that if one assumes that at the carrier frequency, $k_2(\omega_0) = 0$, we arrive at the greatly simplified equation

$$\partial_\zeta \mathcal{E} = 0, \tag{3.18}$$

with the solution

$$\mathcal{E}(t, z) = \mathcal{E}_0(t - z/v_g), \tag{3.19}$$

where $\mathcal{E}_0(t)$ is a pulse envelope in the source plane, and we introduced

$$k_1 \equiv v_g^{-1}. \tag{3.20}$$

It can be concluded from Eq. (3.19) that the pulse maintains its shape and its peak moves inside the medium with the speed v_g. This velocity is referred to as the **group velocity** of the pulse. To understand the role of k_2, it is sufficient to observe that Eq. (3.17) is a temporal analog of the paraxial wave equation governing beam diffraction in free space we have studied before. Hence the second derivative term in Eq. (3.17) describes pulse spreading in dispersive media. The **group velocity dispersion** coefficient k_2 then sets a spatial scale of the problem, the so-called dispersion length, $L_{dis} = t_p^2/k_2$, where t_p is a characteristic duration of the pulse in the source plane $z = 0$.

In the preceding development, we ignored spatial distribution of the pulse, which is justified in a plane wave geometry. Alternatively, pulse propagation in single-mode dispersive fibers can be of interest. In this case, the spatial distribution of the pulse is dictated by the fiber mode such that a more appropriate Ansatz for the field,

$$\tilde{\boldsymbol{\mathcal{E}}}(\mathbf{r}, \omega) = \mathbf{e}_x \tilde{\mathcal{E}}(\omega, z) \phi(\mathbf{r}_\perp, \omega)\, e^{i\beta_0 z}, \tag{3.21}$$

should be considered instead. Here β_0 is a carrier propagation constant in the fiber and $\phi(\mathbf{r}_\perp, \omega)$ is a fiber mode field distribution. Substituting from Eq. (3.21) into (3.2), separating spatial and temporal degrees of freedom and assuming the SVEA (3.4), we obtain the set of equations for the field amplitude

$$2i\beta_0 \partial_z \tilde{\mathcal{E}} + [\beta^2(\omega) - \beta_0^2]\tilde{\mathcal{E}} = 0, \tag{3.22}$$

and the fiber mode

$$\nabla^2_\perp \phi + [k^2(\omega) - \beta^2(\omega)]\phi = 0. \tag{3.23}$$

Next, assuming (3.7) and that the only allowed fiber mode is excited at the carrier frequency, we can approximate

$$\phi(\mathbf{r}_\perp, \omega) \simeq \phi(\mathbf{r}_\perp, \omega_0), \tag{3.24}$$

and replace $k(\omega)$ and $\beta(\omega)$ in the equation for the fiber mode by their values at the carrier frequency, i.e,

$$\nabla_\perp^2 \phi + [k^2(\omega_0) - \beta_0^2]\phi = 0. \tag{3.25}$$

The resulting eigenvalue equation, subject to the appropriate boundary conditions at the fiber boundaries, determines the spatial distribution of the fiber mode and the mode propagation constant. Further, expanding the frequency dependent propagation constant $\beta(\omega)$ in a Taylor series up to the second order

$$\beta(\omega) \simeq \beta_0 + \underbrace{\beta'(\omega_0)}_{\beta_1}(\omega - \omega_0) + \frac{1}{2!}\underbrace{\beta''(\omega_0)}_{\beta_2}(\omega - \omega_0)^2, \tag{3.26}$$

and following exactly the same procedure as before, we can arrive at the paraxial wave equation for pulse propagation in linear fibers as

$$2i\partial_\zeta \mathcal{E} - \beta_2 \partial_{\tau\tau}^2 \mathcal{E} = 0. \tag{3.27}$$

3.2 Resonant pulse propagation in linear absorbers

3.2.1 Resonant interaction of short pulses with linear media: Homogeneous line broadening

Let us now discuss a more general case of a near-resonant optical pulse, propagating in the medium in the positive z-direction. The displacement x of each Lorentz oscillator induced by the pulse is governed by the equation

$$\partial_t^2 x + 2\gamma \partial_t x + \omega_0^2 x = -eE/m, \tag{3.28}$$

where E is the electric field of the pulse in the scalar approximation. In the slowly-varying envelope approximation (SVEA), the pulse field and atomic dipole moments can be represented as

$$E(z,t) = \tfrac{1}{2}[\mathcal{E}(z,t)e^{i(kz-\omega t)} + c.c]; \qquad ex(z,t) = \tfrac{1}{2}[d_0\sigma(z,t)e^{i(kz-\omega t)} + c.c], \tag{3.29}$$

where ω is a carrier frequency of the pulse, and $d_0 = ex_0$ is a characteristic dipole moment amplitude. Further, $\mathcal{E}$ and σ are slowly varying envelope fields in the sense that

$$\partial_z \mathcal{E} \ll k\mathcal{E}, \qquad \partial_t \mathcal{E} \ll \omega\mathcal{E} \tag{3.30}$$

and

$$\partial_t \sigma \ll \omega\sigma. \tag{3.31}$$

On substituting from (3.29) into (3.28) and using (3.31), we obtain the equation

$$-\omega^2\sigma - 2i\omega\partial_t\sigma - 2i\gamma\omega\sigma + \omega_0^2\sigma = -e\mathcal{E}/mx_0. \tag{3.32}$$

Next, we have near resonance,

$$\omega_0^2 - \omega^2 \simeq 2\omega(\omega_0 - \omega) = 2\omega\Delta, \tag{3.33}$$

where Δ is a detuning of the carrier wave frequency ω from the atomic resonance frequency ω_0. On substituting from Eq. (3.33) into (3.32), we obtain, after some algebra, the SVEA equation for atomic dipole envelope evolution as

$$\partial_t \sigma = -(\gamma + i\Delta)\sigma + i\Omega, \tag{3.34}$$

where we introduced the field envelope in frequency units, $\Omega = -e\mathcal{E}/2m\omega x_0$.

Alternatively, Eq. (3.34) can be written in a real form by introducing the *in-phase* U and *quadrature* V components of the dipole moment viz.,

$$\sigma(t, z) = U(t, z) - iV(t, z), \tag{3.35}$$

such that provided $\Omega^* = \Omega$,

$$\partial_t U = -\gamma U + \Delta V, \tag{3.36}$$

and

$$\partial_t V = -\gamma V - \Delta U + \Omega. \tag{3.37}$$

Thus in the absence of pulse modulation, only the imaginary part of the dipole moment is directly coupled to the electric field amplitude, and it determines the pulse intensity evolution. For this reason, V is termed the absorptive part of σ. The real part U is referred to as dispersive part because it is coupled to the field only via the absorptive part. It will however govern pulse modulation dynamics, if any initial pulse modulation is present.

To better understand physical implications of Eq. (3.34), let us study a particular case of a cw electric field–which has induced the atomic dipole moments in the past–being suddenly switched off. In this case, $\Omega(t) = \theta(-t)\Omega_0(z)$, where $\theta(t)$ is a unit step function. It then follows that for $t > 0$, $\Omega = 0$ and, as follows from Eq. (3.34), each dipole moment exponentially decays with time according to

$$\sigma(t, z) = \sigma(0, z)\theta(t)e^{-\gamma t}e^{i\omega_0 t}. \tag{3.38}$$

This is called free-induction decay of an individual dipole moment. One can introduce a characteristic time $T_0 = 1/\gamma$ which is known as a dipole relaxation time.

A Fourier transform of σ can be defined as

$$\tilde{\sigma}(\omega, z) \equiv \int_{-\infty}^{\infty} dt\, \sigma(t, z)e^{-i\omega t}. \tag{3.39}$$

The spectral response, $S_0(\omega, z) \propto |\tilde{\sigma}(\omega, z)|^2$, obtained in a typical set of absorption measurements, is then given by

$$S_0(\omega, z) \propto \frac{|\sigma(0, z)|^2}{(\omega - \omega_0)^2 + \gamma^2} \tag{3.40}$$

The characteristic absorption spectral width is thus $\gamma = 1/T_0$ and is referred to as the width of *homogeneous broadening* as it is the same for each individual atom.

3.2.2 Inhomogeneous broadening

Consider the polarization of a macroscopic sample of atoms. Generally, in solid state samples, the resonant frequency ω_0 of atoms will vary from atom to atom due to local defects which perturb the atomic transition frequencies. As a result, the polarization is determined as an average over the resonant frequency fluctuations such that

$$P(t,z) = \tfrac{1}{2}[\mathcal{P}(t,z)e^{i(kz-\omega t)} + c.c], \tag{3.41}$$

where

$$\mathcal{P}(t,z) = Nd_0\langle\sigma(t,z,\omega_0)\rangle, \tag{3.42}$$

and the averaging is defined as

$$\langle\sigma(t,z,\omega_0)\rangle = \int_0^\infty d\omega_0\, f(\omega_0)\sigma(t,z,\omega_0). \tag{3.43}$$

Here the distribution function $f(\omega_0)$ is normalized to unity as

$$\int_0^\infty d\omega_0\, f(\omega_0) = 1.$$

In reality, the distribution function is often sharply peaked around some value of ω_0 which we denote by $\overline{\omega}_0$, say, i. e.,

$$f(\omega_0) \simeq f(\omega_0 - \overline{\omega}_0) = f(\Delta).$$

It then follows by changing the integration variable to Δ that for any average,

$$\int_0^\infty d\omega_0 f(\omega_0)(\ldots) = \int_{-\overline{\omega}_0}^\infty d\Delta\, f(\Delta)(\ldots) \simeq \int_{-\infty}^\infty d\Delta\, f(\Delta)(\ldots).$$

Thus,

$$\mathcal{P}(t,z) = Nd_0\int_{-\infty}^\infty d\Delta\, f(\Delta)\sigma(t,z,\Delta). \tag{3.44}$$

In gases or atomic vapors, Doppler's effect is at the origin of the frequency detuning distribution. To make this point clear, suppose a plane wave propagating in a laboratory frame has the form $e^{i(\mathbf{k}\cdot\mathbf{r}-\omega t)}$. In the reference frame moving with the atom at the velocity $\mathbf{v}$, the plane wave has the form $e^{i(\mathbf{k}\cdot\mathbf{r}'-\omega' t)}$, where $\mathbf{r}' = \mathbf{r} - \mathbf{v}t$ is a position of the atom at time t. It then follows that the wave form will be the same in the two frames–which it should as it is the same wave–if the frequencies ω' and ω in the moving and laboratory frames, respectively, are related as $\omega' = \omega - \mathbf{k}\cdot\mathbf{v}$. The frequency shift of the wave in a moving reference frame is known as the Doppler effect. For a plane wave propagating in the positive z-direction, the Doppler shifted frequency is

$$\omega' = \omega - kv_z. \tag{3.45}$$

Next, the pulse field and atomic dipole moment distributions in the moving reference frame are

$$E(z,t) = \tfrac{1}{2}[\mathcal{E}(z,t)e^{i[kz-(\omega-kv_z)t]}+c.c]; \qquad ex(z,t) = \tfrac{1}{2}[d_0\sigma(z,t)e^{i[kz-(\omega-kv_z)t]}+c.c], \tag{3.46}$$

and we dropped the prime over z to simplify the notation. The derivation along the lines outlined in the previous Lecture would yield the dipole evolution equation in the form

$$\partial_t \sigma = -(\gamma + i\Delta)\sigma + i\Omega, \tag{3.47}$$

where

$$\Delta = \omega_0 - \omega + kv_z. \tag{3.48}$$

Assuming that $\omega = \omega_0$–the light is tuned to the atomic transition at rest–we obtain the dependence of the detuning on the atom velocity,

$$\Delta = kv_z. \tag{3.49}$$

The atom velocities are distributed according to Maxwell's distribution such that for the z-component of velocity, we have

$$f(v_z) \propto \exp\left(-\frac{mv_z^2}{2k_BT}\right), \tag{3.50}$$

where k_B is the Boltzmann constant and T is the temperature. It then follows from Eqs. (3.49) and (3.50) that the detuning distribution is Maxwellian in this case,

$$f(\Delta) \propto \exp\left(-\frac{m\Delta^2}{2k^2k_BT}\right), \tag{3.51}$$

Let us now revisit the free-induction decay experiment and examine the polarization evolution,

$$\mathcal{P}(t,z) = Nd_0 \int_{-\infty}^{\infty} d\Delta\, f(\Delta)\sigma(t,z), \tag{3.52}$$

which can be rewritten in the free-induction decay as

$$P(t,z) \propto Nd_0 e^{-t/T_0} e^{i\omega_0 t} \int_{-\infty}^{\infty} d\Delta\, f(\Delta) e^{i\Delta t} + c.c. \tag{3.53}$$

Suppose, for simplicity, the detuning distribution is Lorentzian,

$$f(\Delta) \propto \frac{1}{\Delta^2 + 1/T_\Delta^2}, \tag{3.54}$$

where $1/T_\Delta$ characterizes the width of $g(\Delta)$. Using a Fourier transform table integral,

$$\mathcal{F}\left\{\frac{1}{\Delta^2 + 1/T_\Delta^2}\right\} \propto e^{-|t|/T_\Delta},$$

we obtain for $t > 0$,

$$P(t,z) \propto Nd_0 e^{-t/T_{eff}} e^{i\omega_0 t} + c.c. \tag{3.55}$$

Here

$$\frac{1}{T_{eff}} = \underbrace{\frac{1}{T_0}}_{homogeneous} + \underbrace{\frac{1}{T_\Delta}}_{inhomogeneous}. \tag{3.56}$$

The second term on the rhs describes *inhomogeneous broadening* which would occur in the spectral domain due to fluctuations of atomic detunings; its nature is atom specific (distribution of resonant frequencies, velocity distributions, etc.) The functional form of $g(\Delta)$ and the magnitude of a characteristic damping time T_Δ associated with inhomogeneous broadening depend on a specific broadening mechanism.

3.2.3 Maxwell-Lorentz pulse evolution equations and classical area theorem

We start by considering propagation of an optical pulse in a resonant medium. Assuming linear polarization, the electromagnetic field E of the pulse obeys the wave equation in the form

$$\partial_{zz}^2 E - c^{-2}\partial_{tt}^2 E = \mu_0 \partial_{tt}^2 P, \tag{3.57}$$

where the medium polarization P can be expressed as

$$P = -Ne\langle x \rangle. \tag{3.58}$$

In Eq. (3.58), the angle brackets denote averaging over detunings of the pulse from the resonance frequency ω_0.

In the slowly varying envelope approximation, we can use the representation (3.46) and assume that

$$\partial_z \mathcal{E} \ll k\mathcal{E}, \qquad \partial_t \mathcal{E} \ll \omega \mathcal{E} \tag{3.59}$$

and

$$\partial_t \sigma \ll \omega\sigma. \tag{3.60}$$

On substituting from Eq. (3.46) into (3.57) and using the SVEA (3.59), we can obtain the reduced wave equation for the slowly-varying field envelope as

$$\partial_z \Omega + c^{-1}\partial_t \Omega = i\kappa\langle\sigma\rangle. \tag{3.61}$$

which should be coupled with the derived dipole moment evolution equation (3.47). In Eq. (3.61), we introduced a coupling constant, $\kappa = \omega_{pe}^2/4c$, where $\omega_{pe} = (Ne^2/\epsilon_0 m)^{1/2}$ is the electron plasma frequency.

Exercise 3.1. *Derive Eq. (3.61).*

Transforming to the moving reference frame via $\tau = t - z/c$ and $\zeta = z$ just as we did in the derivation of nonresonant pulse propagation equation, we finally arrive at the coupled Maxwell-Lorentz propagation equations

$$\partial_\zeta \Omega = i\kappa\langle\sigma\rangle, \tag{3.62}$$

and

$$\partial_\tau \sigma = -(\gamma + i\Delta)\sigma + i\Omega. \tag{3.63}$$

To solve Eqs. (3.62) and (3.63) we use the familiar now Fourier transform technique. First, we introduce temporal Fourier transforms of the field and dipole moment as

$$\Omega(\tau, \zeta) = \int_{-\infty}^{\infty} d\omega\, \tilde{\Omega}(\omega, \zeta) e^{-i\omega\tau}, \tag{3.64}$$

and

$$\sigma(\tau,\zeta)=\int_{-\infty}^{\infty}d\omega\,\tilde{\sigma}(\omega,\zeta)e^{-i\omega\tau}, \tag{3.65}$$

Substituting those back into our evolution equations, we obtain the algebraic expression for $\tilde{\sigma}$ in the form

$$\tilde{\sigma}(\omega,\zeta)=\frac{i\tilde{\Omega}(\omega,\zeta)}{\gamma+i(\Delta-\omega)}. \tag{3.66}$$

It then follows from Eq. (3.66) and a Fourier transformed Eq. (3.62) that

$$\partial_{\zeta}\tilde{\Omega}=-\kappa\mathcal{R}\,\tilde{\Omega}, \tag{3.67}$$

where the spectral material response function is defined as

$$\mathcal{R}(\omega)=\left\langle\frac{1}{\gamma+i(\Delta-\omega)}\right\rangle. \tag{3.68}$$

Integrating Eq. (3.67) at once, we arrive at

$$\tilde{\Omega}(\omega,\zeta)=\tilde{\Omega}(\omega,0)\exp[-\kappa\mathcal{R}(\omega)\zeta]. \tag{3.69}$$

Hence the field envelope at any propagation distance can be expressed as

$$\mathcal{E}(\tau,\zeta)=\int_{-\infty}^{\infty}d\omega\,\tilde{\mathcal{E}}(\omega)\exp[-i\omega\tau-\kappa\mathcal{R}(\omega)\zeta], \tag{3.70}$$

where

$$\tilde{\mathcal{E}}(\omega)=\int_{-\infty}^{\infty}\frac{dt'}{2\pi}\,e^{i\omega t'}\mathcal{E}(t',0). \tag{3.71}$$

On combining Eqs. (3.70) and (3.71), we can express the answer in the original variables in the form

$$\mathcal{E}(t,z)=\int_{-\infty}^{\infty}\frac{dt'}{2\pi}\,\mathcal{E}(t',0)\int_{-\infty}^{\infty}d\omega\,e^{i\omega(t'-t)}\exp[i\omega z/c-\kappa\mathcal{R}(\omega)z]. \tag{3.72}$$

Exercise 3.2. *Fill in missing steps in the derivation of Eq. (3.72).*
Note that in the absence of inhomogeneous broadening (the so-called sharp line limit), $f(\Delta)=\delta(\Delta)$ and

$$\mathcal{R}_{hom}(\omega)=\frac{1}{(\gamma-i\omega)}. \tag{3.73}$$

The so-called classical area theorem follows directly from Eq. (3.72). Indeed, let us introduce the classical area, $\mathcal{A}$ as

$$A(z)=\int_{-\infty}^{\infty}dt\,\mathcal{E}(t,z). \tag{3.74}$$

Integrating Eq. (3.72) over time and using the integral representation of the delta function,

$$\delta(\omega)=\int_{-\infty}^{\infty}\frac{d\omega}{2\pi}e^{-i\omega t}, \tag{3.75}$$

we arrive at the area theorem

$$A(z) = A_0 \exp[-\kappa \mathcal{R}(0) z], \tag{3.76}$$

where $\mathcal{A}_0 = \mathcal{A}(0)$ is the initial area under the pulse profile. In general, the area theorem can be cast into the form

$$A(z) = A_0 e^{-\alpha z/2} e^{i\beta z/2}, \tag{3.77}$$

where we introduced a characteristic attenuation decrement α and the phase accumulation factor β by the expressions

$$\alpha = \left\langle \frac{2\kappa\gamma}{\gamma^2 + \Delta^2} \right\rangle, \tag{3.78}$$

and

$$\beta = \left\langle \frac{2\kappa\Delta}{\gamma^2 + \Delta^2} \right\rangle. \tag{3.79}$$

Thus, regardless of the incident pulse shape, the area under the pulse will exponentially decay on pulse propagation in linear resonant absorbers as a consequence of medium absorption manifested, in general, through homogeneous and inhomogeneous broadening.

Exercise 3.3. *Derive Eqs. (3.76) and (3.77).*

Finally, we examine the case of very long pulses such that the characteristic pulse width T_p is much longer than the longer of homogeneous or inhomogeneous damping times,

$$T_p \gg \max(T_0, T_\Delta). \tag{3.80}$$

It then follows from Eq. (3.63) that the dipole moment can be adiabatically eliminated: It decays fast to its dynamic equilibrium value determined by the pulse amplitude. Mathematically, we can formally set $\partial_\tau \sigma \simeq 0$ in Eq. (3.63) and conclude that

$$\sigma \simeq \frac{i\Omega}{\gamma + i\Delta}, \tag{3.81}$$

On substituting back into Eq. (3.62) we arrive at the pulse evolution equation as

$$\partial_\zeta \mathcal{E} = -\kappa \left\langle \frac{1}{\gamma + i\Delta} \right\rangle \mathcal{E}. \tag{3.82}$$

The latter implies that

$$\mathcal{E}(t, z) = e^{-\alpha z/2} e^{i\beta z/2} \mathcal{E}_0(t - z/c), \tag{3.83}$$

where $\mathcal{E}_0(t)$ is a pulse profile in the source plane.

Exercise 3.4. *Derive Eq. (3.83).*

Equation (3.83) is Beer's absorption law, familiar from elementary optics treatment of absorbers. It states that sufficiently long pulses propagate in absorbers undistorted except that their amplitudes decay exponentially with the propagation distance; the typical damping distance is known as Beers' absorption length, $L_B = \alpha^{-1}$.

3.3 Paraxial wave equation and Gaussian beam optics

We consider evolution of a monochromatic electromagnetic field in free space. The electric and magnetic fields can be represented as

$$\mathbf{E}(\mathbf{r},t) = \boldsymbol{\mathcal{E}}(\mathbf{r},\omega)e^{-i\omega t}, \qquad \mathbf{H}(\mathbf{r},t) = \boldsymbol{\mathcal{H}}(\mathbf{r},\omega)e^{-i\omega t}. \tag{3.84}$$

Thus Maxwell's equations for the field envelopes read

$$\nabla \times \boldsymbol{\mathcal{E}} = i\mu_0\omega\boldsymbol{\mathcal{H}}, \tag{3.85}$$

$$\nabla \times \boldsymbol{\mathcal{H}} = -i\epsilon_0\omega\boldsymbol{\mathcal{E}}, \tag{3.86}$$

and

$$\nabla \cdot \boldsymbol{\mathcal{E}} = 0, \qquad \nabla \cdot \boldsymbol{\mathcal{H}} = 0. \tag{3.87}$$

Eliminating the magnetic field in favor of the electric in Eqs. (3.85) – (3.87), we arrive at the equation for the electric field envelope in the form

$$\nabla^2\boldsymbol{\mathcal{E}} + k^2\,\boldsymbol{\mathcal{E}} = 0, \tag{3.88}$$

where $k = \omega/c$.

We seek a plane polarized beam-like solution to (3.88):

$$\boldsymbol{\mathcal{E}} = \mathbf{e}_y\mathcal{E}(x,z)e^{ikz}. \tag{3.89}$$

Physically, the solution (3.89) represents a beam of light propagating in the z-direction with an homogeneous electric field in the y-direction and an inhomogeneous intensity distribution in the x-direction. It automatically satisfies the transversality conditions (3.87). Note that in the limiting case when $\mathcal{E} = const$, we have a plane wave. The beam is different in that its field amplitude should in some sense be a slowly varying function of coordinates. To make this requirement more quantitative we stipulate that for the intensity distribution to represent a beam, the complex envelope $\mathcal{E}$ change slowly at the wavelength scale, i. e.,

$$\partial_z\mathcal{E} \ll k\mathcal{E}, \tag{3.90}$$

The latter condition is referred to as a slowly-varying amplitude approximation (SVEA). On substituting from Eq. (3.89) and taking the SVEA into account, we arrive at the *paraxial wave equation* for the beam envelope in the form

$$2ik\partial_z\mathcal{E} + \partial^2_{xx}\mathcal{E} = 0. \tag{3.91}$$

Let us now study the evolution of the beam with a Gaussian field profile in the source plane $z = 0$,

$$\mathcal{E}(x,0) = \mathcal{E}_0 e^{-x^2/2w_0^2}, \tag{3.92}$$

where w_0 characterizes the width of the source intensity profile. We use a Fourier transform method to address the problem. Consider a Fourier decomposition of the beam amplitude in the transverse direction,

$$\mathcal{E}(x,z) = \int_{-\infty}^{+\infty} dq e^{iqx}\,\tilde{\mathcal{E}}(q,z), \tag{3.93}$$

where the Fourier (spectral) amplitude can be determined by the inverse transformation,

$$\tilde{\mathcal{E}}(q,z) = \int_{-\infty}^{+\infty} \frac{dx}{2\pi} e^{-iqx}\, \mathcal{E}(x,z). \tag{3.94}$$

In particular, for the Gaussian beam of (3.92), we can obtain

$$\tilde{\mathcal{E}}(q,0) = \mathcal{E}_0 \sqrt{\frac{w}{2\pi}} e^{-q^2 w_0^2/2}. \tag{3.95}$$

Here we used the following standard integral

$$\int_{-\infty}^{+\infty} dx e^{-ax^2+bx} = \sqrt{\frac{\pi}{a}} e^{b^2/4a}, \tag{3.96}$$

where a and b are arbitrary complex numbers.

Next, we use the properties of Fourier transforms to convert Eq. (3.91) to the k-space,

$$2ik\partial_z \tilde{\mathcal{E}} - q^2 \tilde{\mathcal{E}} = 0. \tag{3.97}$$

Solving the latter, we obtain

$$\tilde{\mathcal{E}}(q,z) = \tilde{\mathcal{E}}(q,0) \exp\left(-\frac{iq^2 z}{2k}\right). \tag{3.98}$$

Combining Eqs. (3.95) and (3.98) and using the inverse Fourier transform (3.94), we obtain after some algebra the expression for the Gaussian beam envelope at any z,

$$\mathcal{E}(x,z) = \frac{\mathcal{E}_0}{\sqrt{1+i\zeta}} \exp\left[-\frac{x^2}{2w_0^2(1+i\zeta)}\right]. \tag{3.99}$$

Here

$$\zeta = z/z_R, \qquad z_R = kw_0^2. \tag{3.100}$$

Exercise 3.5. *Derive Eq. (3.99).*

To discuss the solution (3.99) it is convenient to represent it in the form where the complex phase and real amplitude are expressed explicitly as

$$\mathcal{E}(x,z) = \mathcal{E}_0 \sqrt{\frac{w_0}{w(z)}}\, e^{i\Phi(z)}\, \exp\left[\frac{ikx^2}{2R(z)}\right]\, \exp\left[-\frac{x^2}{2w^2(z)}\right]. \tag{3.101}$$

Exercise 3.6. *Derive Eq. (3.101).*
Here we introduced the beam width $w(z)$ as

$$w(z) = w_0 \sqrt{1 + z^2/z_R^2}, \tag{3.102}$$

the radius of the wavefront curvature $R(z)$,

$$R(z) = z(1 + z_R^2/z^2), \tag{3.103}$$

and the accrued phase $\Phi(z)$,

$$\Phi(z) = -\tfrac{1}{2}\,\arctan(z/z_R). \tag{3.104}$$

Notice first that although the intensity of a Gaussian beam steadily decreases upon diffraction in free space, the beam profile remains Gaussian in any transverse plane $z = const$. Further, the diffraction length z_R sets the characteristic spatial scale for the problem. It is equal to the distance over which the beam width doubles from its minimal value w_0 at the source. The plane where the beam width is the smallest is called the beam waist and the diffraction length is often referred to as the Rayleigh range.

Consider now the wavefront $\Psi(x, z)$ of the beam which is defined as a surface of constant phase. It follows from Eq . (3.101) that

$$\Psi(x, z) = \Phi(z) + \frac{kx^2}{2R(z)} = const \tag{3.105}$$

We observe that near the waist of the beam, $z \ll z_R$, the radius of the curvature is very large, $R \simeq z_R^2/z$, implying that in the limit $z \to 0$, $R \to \infty$, and the wavefront is flat. In the opposite limit, $z \to +\infty$, the accrued phase is $\Phi = -\pi/4$. This is the so-called Gouy phase shift of a Gaussian beam. Finally for large but finite propagation distances, $z \ll z_R$ such that $R(z) \simeq z$, the wavefront is parabolic

$$z \propto x^2/\lambda, \tag{3.106}$$

with the curvature decreasing in the inverse proportion to the propagation distance. The curvature attains its maximum at the Rayleigh range.

Finally, we mention that a natural generalization of the paraxial equation to two transverse dimensions is

$$2ik\partial_z\mathcal{E} + \nabla_\perp^2\mathcal{E} = 0, \tag{3.107}$$

where $\nabla_\perp^2$ is a Laplacian operator in the transverse plane defined as

$$\nabla_\perp^2 \equiv \partial_{xx}^2 + \partial_{yy}^2. \tag{3.108}$$

3.4 Plane wave decomposition of beams: Angular spectrum

Let us now approach beam propagation in free space from a different perspective. To this end, we consider any linearly polarized electromagnetic field–which, for simplicity, is assumed to be uniform in the polarization direction–as a linear superposition of plane waves in the form

$$\boldsymbol{\mathcal{E}}(x, z) = \mathbf{e}_y \int_{-\infty}^{+\infty}\int_{-\infty}^{+\infty} dk_x dk_z\, \tilde{\mathcal{A}}(k_x, k_z) e^{i(k_x x + k_z z)}. \tag{3.109}$$

The electromagnetic field is supposed to propagate in free space into the half space $z > 0$. The representation of the field by Eq. (3.109) is known as the angular spectrum: The field is composed of plane waves propagating at different angles to the z-axis.

Substituting from Eq. (3.109) into the wave equation, we obtain the equation for the spectral amplitude $\mathcal{A}$ as

$$\tilde{\mathcal{A}}(k_x, k_z)(-k_x^2 - k_z^2 + k^2) = 0. \tag{3.110}$$

It follows at once from Eq. (4.184) that $\mathcal{A}$ is constrained to lie on the circle in the k-space, i.e,

$$\tilde{\mathcal{A}}(k_x, k_z) = \mathcal{A}(k_x)\delta(k_x^2 + k_z^2 - k^2). \tag{3.111}$$

The circle in the k-space determines the dispersion relation for the wave vector components,

$$k_x^2 + k_z^2 = k^2 \implies k_z = \sqrt{k^2 - k_x^2}. \tag{3.112}$$

It can then be inferred from Eq. (3.112) that

$$k_z = \begin{cases} \sqrt{k^2 - k_x^2}, & k_x < k \\ \pm i\sqrt{k_x^2 - k^2}, & k_x > k \end{cases} \tag{3.113}$$

Combining Eqs. (3.109) and (3.113), we arrive at the angular spectrum representation of **any** linearly polarized $(1+1)$D electromagnetic field in the half-space $z > 0$

$$\boldsymbol{\mathcal{E}}(x,z) = \mathbf{e}_y \underbrace{\int_{k_x<k} dk_x\, \mathcal{A}(k_x) e^{i(k_x x + \sqrt{k^2-k_x^2}\, z)}}_{homogeneous\ waves} + \mathbf{e}_y \underbrace{\int_{k_x>k} dk_x\, \mathcal{A}(k_x) e^{ikx} e^{-\sqrt{k_x^2-k^2}\, z}}_{evanescent\ waves}. \tag{3.114}$$

The first and second terms provide contributions of homogeneous and evanescent plane waves; the latter exponentially decay away from the source plane $z = 0$. Notice incidentally that we chose " $+$ " sign to have the evanescent waves decay into $z > 0$ as the exponentially growing solution does not obviously make any sense.

Next, the evanescent waves quickly damp out as the field propagates sufficiently far from the source and their contribution is negligible outside of the source vicinity. Thus, we have

$$\boldsymbol{\mathcal{E}}(x,z) = \mathbf{e}_y \int_{k_x<k} dk_x\, \mathcal{A}(k_x) e^{i(k_x x + \sqrt{k^2-k_x^2}\, z)}. \tag{3.115}$$

Let us now specialize to the beam case whereupon all the plane waves making up the field propagate close to the z-axis such that $k_x \ll k$. It then follows upon a Taylor series expansion in Eq. (3.113) that

$$\sqrt{k^2 - k_x^2} \simeq k - \frac{k_x^2}{2k},$$

Therefore we can rewrite our plane wave decomposition as

$$\boldsymbol{\mathcal{E}}(x,z) \simeq \mathbf{e}_y e^{ikz} \int_{-\infty}^{+\infty} dk_x\, \mathcal{A}(k_x)\, e^{ik_x x}\, \exp\left(-\frac{ik_x^2 z}{2k}\right). \tag{3.116}$$

On comparing Eqs. (3.116) and

$$\boldsymbol{\mathcal{E}}(x,z) = \mathbf{e}_y \mathcal{E}(x,z) e^{ikz}, \tag{3.117}$$

we conclude that we can represent electric fields of optical beams as

$$\mathcal{E}(x,z) = \int_{-\infty}^{+\infty} dk_x\, \mathcal{A}(k_x)\, e^{ik_x x}\, \exp\left(-\frac{ik_x^2 z}{2k}\right). \tag{3.118}$$

It then follows from the Fourier transform definition that

$$\mathcal{E}(x,z) = \int_{-\infty}^{+\infty} dk_x\, \tilde{\mathcal{E}}(k_x,0)\, \exp\left(-\frac{ik_x^2 z}{2k}\right)\, e^{ik_x x}. \tag{3.119}$$

Hence,

$$\tilde{\mathcal{E}}(k_x,z) = \tilde{\mathcal{E}}(k_x,0)\, \exp\left(-\frac{ik_x^2 z}{2k}\right), \tag{3.120}$$

which coincides with Eq. (3.98). Thus our angular spectrum representation treatment is equivalent to the paraxial equation approach. While the latter is usually more convenient to solve practical problems and is straightforwardly generalized to nonlinear situations, the former brings up more insight into the physics of beam propagation in free space.

Finally, applying the convolution theorem of Fourier transforms to Eq. (3.120) and using Eq. (3.96) we can derive the Fresnel representation for any $(1+1)$D beam evolution in free space:

$$\mathcal{E}(x,z) = \sqrt{\frac{k}{2\pi i z}} \int_{-\infty}^{+\infty} dx'\, \mathcal{E}(x',0) \exp\left[\frac{ik(x-x')^2}{2z}\right]. \tag{3.121}$$

Exercise 3.7. *Derive Eq. (3.121).*
A natural generalization of the latter to two transverse dimensions is

$$\mathcal{E}(\boldsymbol{\rho},z) = \left(\frac{k}{2\pi i z}\right) \int d\boldsymbol{\rho}\, \mathcal{E}(\boldsymbol{\rho}',0) \exp\left[\frac{ik(\boldsymbol{\rho}-\boldsymbol{\rho}')^2}{2z}\right], \tag{3.122}$$

where $\boldsymbol{\rho} = x\mathbf{e}_x + y\mathbf{e}_y$ is a radius vector in the transverse plane of the beam.

Chapter 4

Nonlinear optics

4.1 Introduction. Qualitative description of nonlinear optical processes

Whenever an external electric field is applied to matter, it induces or reorients dipole moments of atoms or molecules of the matter, resulting in a nonzero average dipole moment per unit volume or polarization of the material. If the applied electric field is not too large, the polarization is proportional to the field strength, i.e,

$$P = \epsilon_0 \chi^{(1)} E, \tag{4.1}$$

where $\chi^{(1)}$ is the usual susceptibility of linear optics. In writing Eq. (4.1) we ignored, for simplicity, the vector nature of both the applied field and the resulting polarization.

As the magnitude of the field increases though, the simple linear relation (4.1) no longer holds. However, typical electric fields generated by all but most powerful modern lasers are in the range of 10^6 to 10^7 V/cm, whereas the electrons bound to atoms or molecules experience far greater fields of the order of 10^9 to 10^{10} V/cm. Consequently, one can assume the induced electron displacements in laser fields to be rather small; the latter circumstance justifies using a power series representation for the induced polarizations as

$$P = \epsilon_0 (\chi^{(1)} E + \chi^{(2)} E^2 + \chi^{(3)} E^3 + \ldots), \tag{4.2}$$

where $\chi^{(2)}$ and $\chi^{(3)}$ are referred to as second- and third-order susceptibilities, respectively.

To estimate orders of magnitude of the nonlinear susceptibilities, we consider nonlinearity of electronic origin. In this case, the nonlinear polarization depends on the displacements of the electrons from the nuclei. One could expect that the second-order contribution to the polarization would definitely be of the same order as the first one if the electrons are displaced a distance as large as the atomic size, which is roughly of the order of the Bohr radius, $a_0 = \hbar^2/me^2 \simeq 5 \times 10^{-9}$ cm. The corresponding electric field would be comparable with the field binding electrons to a nucleus,

$E_{at} = e/4\pi\epsilon_0 a_0^2 \simeq 5 \times 10^{11}$ V/m. As the linear susceptibility is of the order of unity, $\chi^{(1)} \sim 1$, it follows that the second-order susceptibility can be estimated as

$$\chi^{(2)} \sim E_{at}^{-1} \sim 10^{-12}, \text{ m/V}. \tag{4.3}$$

By the same token, a typical value of the third-order susceptibility for condensed-matter systems would be

$$\chi^{(3)} \sim 10^{-21} \text{ to } 10^{-22}, \text{ m}^2/\text{V}^2. \tag{4.4}$$

It can be readily inferred from Eqs. (4.3) and (4.4) that (a) one needs very large fields indeed to probe nonlinear response of dielectric materials and (b) for most laser field strengths encountered in practice, each higher-order contribution to the polarization field P is much smaller than the corresponding lower-order one, enabling us to take into account only the lowest order nonvanishing contribution to P in a given nonlinear medium.

In the following subsection, we are going to discuss nonlinear optical susceptibilities semi-quantitatively. A note of caution is due before we proceed any further: The just introduced expansion (4.2) fails in the vicinity of any internal atomic resonance of the medium, where nonlinear saturation effects start playing a role. Hence, a more subtle quantum theory has to be developed to describe such resonant light-matter interactions. Hereafter, we assume that frequencies of all electric fields involved are far away from any material resonance.

We now qualitatively examine second-order processes, starting with the second harmonic generation (SHG). To this end, consider a monochromatic input field,

$$E(t) = \tfrac{1}{2}(\mathcal{E}e^{-i\omega t} + c.c),$$

The second-order polarization associated with the field is

$$P^{(2)}(t) = \epsilon_0\chi^{(2)}E^2(t) = \tfrac{1}{2}\epsilon_0\chi^{(2)}|\mathcal{E}|^2 + \tfrac{1}{4}(\epsilon_0\chi^{(2)}\mathcal{E}^2e^{-i2\omega t} + c.c).$$

The first process describes generation of a dc field, **optical rectification** while the second is **second harmonic generation**. It is schematically illustrated in the block-diagram below.

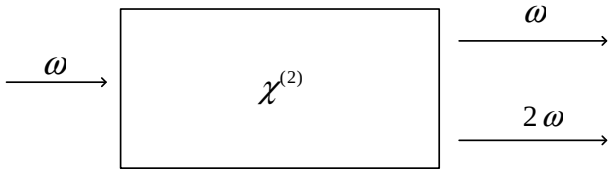

Figure 4.1: Illustrating the second harmonic generation.

In the SHG process an input wave of frequency ω generates an output at double frequency in a nonlinear medium. **Sum-** and **difference-frequency generation** are

more general processes taking place if two different input frequencies ω_1 and ω_2 are present. The input field is then

$$E(t) = \frac{1}{2}(\mathcal{E}_1 e^{-i\omega_1 t} + \mathcal{E}_2 e^{-i\omega_2 t} + c.c).$$

The generated output polarization takes the form

$$P^{(2)}(t) = \frac{1}{2}\sum_s \mathcal{P}(\omega_s) e^{-i\omega_s t} + c.c, \tag{4.5}$$

where the summation is over all possible combinations s of two frequency components and

$$\mathcal{P}_{SHG}(2\omega_j) = \frac{1}{2}\epsilon_0 \chi^{(2)} \mathcal{E}_j^2,$$
$$\mathcal{P}_{SFG}(\omega_1 + \omega_2) = \epsilon_0 \chi^{(2)} \mathcal{E}_1 \mathcal{E}_2,$$
$$\mathcal{P}_{DFG}(\omega_1 - \omega_2) = \epsilon_0 \chi^{(2)} \mathcal{E}_1 \mathcal{E}_2^*,$$
$$\mathcal{P}_{OR}(0) = \epsilon_0 \chi^{(2)} (|\mathcal{E}_1|^2 + |\mathcal{E}_2|^2).$$

While the first and last terms describe SHG and OR, the second and third correspond

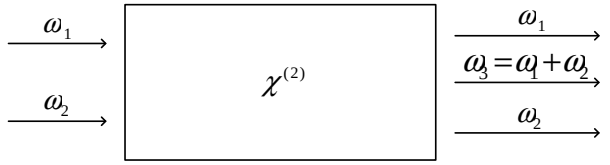

Figure 4.2: Schematic illustration of the sum-frequency generation process.

to new processes of sum- and difference frequency generation, to be abbreviated as (SFG) and (DFG), respectively. The block diagrams of the processes are displayed in Figs. 4.2 and 4.3.

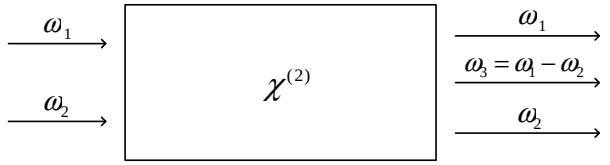

Figure 4.3: Schematic illustration of the difference-frequency generation process.

The fundamental difference between the two processes can be seen from the energy-level in Figs. 4.4 and 4.5.

In the SFG process two input photons at frequencies ω_1 and ω_2 annihilate giving rise to one photon at the sum frequency, $\omega_3 = \omega_1 + \omega_2$. In the DFG process, however, annihilation of a pump photon at frequency ω_1 and generation of a difference frequency photon $\omega_3 = \omega_1 - \omega_2$–sometimes referred to as signal–go hand in hand with generation

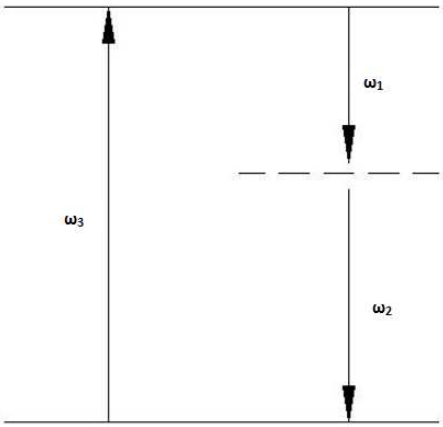

Figure 4.4: Energy-level description of sum-frequency generation.

of an idler photon at frequency ω_2, say. Thus the DFG production is accompanied by the amplification of one of input fields at the expense of the other. For this reason, DFG is often referred to as optical parametric amplification. SHG, SFG and DFG are collectively known as three-wave mixing processes.

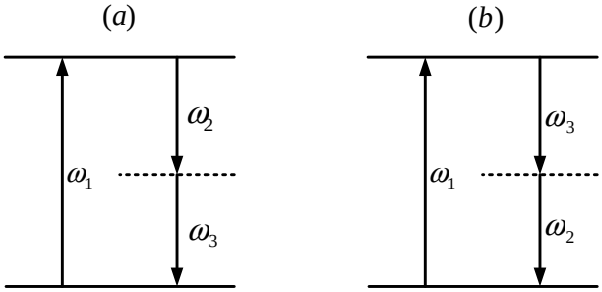

Figure 4.5: Energy-level diagram of difference-frequency generation.

Next, we briefly consider another three-wave mixing process, **stimulated Raman scattering** (SRS) which can be quantitatively described quantum-mechanically. In the SRS a pump photon of frequency ω gets blue-(Stokes mode) or red-shifted (anti-Stokes mode) such that $\omega_S = \omega - \omega_v$ and $\omega_A = \omega + \omega_v$ exciting some medium degrees of freedom on the way. As it was first studied in molecules where SRS causes medium vibrations, we used the subscript "v" to indicate the frequency ω_v of generated molecular vibrations. The process can be described by energy-level diagrams in Fig. 4.6.

Further, we consider the third-order processes, associated with $\chi^{(3)}$. As there are plethora of those–all falling into a general category of four-wave mixing–we will limit ourselves in this course to only third harmonic generation (THG) and self-focusing

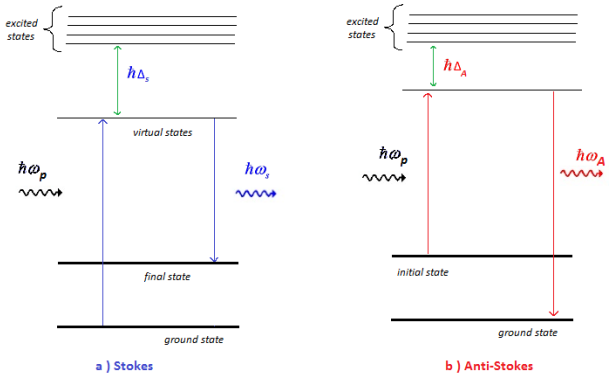

Figure 4.6: Illustrating stimulated Raman scattering; the subscripts "s" and "as" stand for the Stokes and anti-Stokes modes, respectively.

(SF), both excited by a monochromatic input field,

$$E(t) = \tfrac{1}{2}(\mathcal{E}e^{-i\omega t} + c.c),$$

The third-order polarization,

$$P^{(3)}(t) = \epsilon_0 \chi^{(3)} E^3(t)$$

The application of the trigonometric identity, $\cos^3 \omega t = \frac{1}{4}\cos 3\omega t + \frac{3}{4}\cos \omega t$ results in

$$P^{(3)}(t) = \tfrac{1}{2}[\mathcal{P}(3\omega)e^{-i3\omega t} + \mathcal{P}(\omega)e^{-i\omega t} + c.c.],$$

where the THG polarization field is

$$\mathcal{P}_{THG}(3\omega) = \tfrac{1}{2}\epsilon_0 \chi^{(3)} \mathcal{E}^3,$$

and the SF polarization field takes the form

$$\mathcal{P}_{SF}(\omega) = \tfrac{3\epsilon_0}{2}\chi^{(3)}|\mathcal{E}|^2\mathcal{E}.$$

The THG process is a third-order analog of the THG process; the THG block diagram is as follows The SF process is so called because the input field modifies the refractive

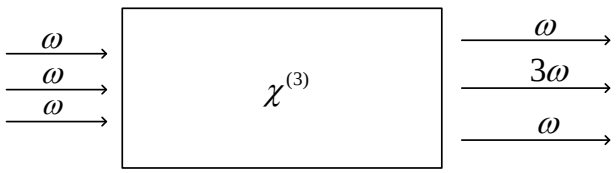

Figure 4.7: Illustrating the third harmonic generation.

index of the medium to

$$n = n_0 + n_2|\mathcal{E}|^2,$$

leading to self-lensing of a light beam. The self-induced "medium lens" is a positive one if $n_2 > 0$ and a negative one otherwise. Thus, either self-focusing or self-defocusing ensues. Another third-order process that, in general, accompanies SF is **two-photon absorption** (TPA). In the TPA process, two photons can be absorbed from a light wave by a medium atom, promoting the latter to an excited state which cannot be related to the ground state by a dipole transition. The situation is illustrated in Fig. 4.8.

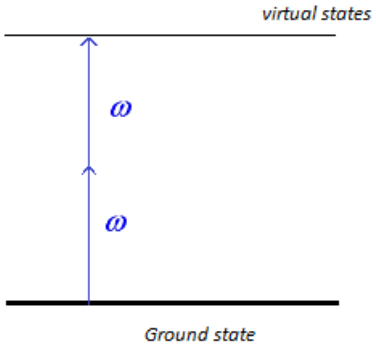

Figure 4.8: Illustrating two-photon absorption.

4.2 Nonlinear processes generated by arbitrary fields: Spatial and temporal dispersion

In general, the input field can have an arbitrary space-time dependence. Suppose, however, that the medium is stationary and homogeneous. This is a fairly general assumption which holds for most situations of practical interest. Under these conditions, the most general form of linear response is as follows

$$\mathbf{P}^{(1)}(\mathbf{r},t) = \epsilon_0 \int d\mathbf{r}' \int_{-\infty}^{\infty} dt' \boldsymbol{\chi}^{(1)}(\mathbf{r}-\mathbf{r}', t-t') \dot{:} \mathbf{E}(\mathbf{r}', t'), \tag{4.6}$$

where we have assumed that the polarization is invariant with respect to translations in space and shifts in time, thanks to stationarity and homogeneity of the medium. By the same token, the second-order nonlinear polarization can be represented as

$$\mathbf{P}^{(2)}(\mathbf{r},t) = \epsilon_0 \int d\mathbf{r}_1 \int d\mathbf{r}_2 \int_{-\infty}^{\infty} dt_1 \int_{-\infty}^{\infty} dt_2$$

$$\times \boldsymbol{\chi}^{(2)}(\mathbf{r}-\mathbf{r}_1, \mathbf{r}-\mathbf{r}_2; t-t_1, t-t_2) \dot{:} \mathbf{E}(\mathbf{r}_1, t_1)\mathbf{E}(\mathbf{r}_2, t_2), \tag{4.7}$$

The expressions for higher-order nonlinear polarization fields can be expressed in a similar fashion.

To proceed further, we will assume the medium response to be spatially local; this is a reasonably good approximation for a vast majority of optical media which we will rely on hereafter. In these conditions, the susceptibility tensors can be simplified to

$$\boldsymbol{\chi}^{(1)}(\mathbf{r}-\mathbf{r}',t-t') = \delta(\mathbf{r}-\mathbf{r}')\boldsymbol{\chi}_t^{(1)}(t-t'), \tag{4.8}$$

and

$$\boldsymbol{\chi}^{(2)}(\mathbf{r}-\mathbf{r}_1,\mathbf{r}-\mathbf{r}_2;t-t_1,t-t_2) = \delta(\mathbf{r}-\mathbf{r}_1)\delta(\mathbf{r}-\mathbf{r}_2)\boldsymbol{\chi}_t^{(2)}(t-t_1,t-t_2). \tag{4.9}$$

The corresponding contributions to the polarization field are greatly simplified as well:

$$\mathbf{P}^{(1)}(\mathbf{r},t) = \epsilon_0 \int_{-\infty}^{\infty} dt' \boldsymbol{\chi}^{(1)}(t-t') \dot{:} \mathbf{E}(\mathbf{r},t'), \tag{4.10}$$

$$\mathbf{P}^{(2)}(\mathbf{r},t) = \epsilon_0 \int_{-\infty}^{\infty} dt_1 \int_{-\infty}^{\infty} dt_2 \boldsymbol{\chi}^{(2)}(t-t_1,t-t_2) \dot{:} \mathbf{E}(\mathbf{r},t_1)\mathbf{E}(\mathbf{r},t_2). \tag{4.11}$$

In equations (4.10) and (4.11) we dropped, for brevity, the subscript "t" for the temporal parts of the linear and nonlinear susceptibilities.

The manifest translational invariance of susceptibilities prompts the introduction of Fourier transforms

$$\tilde{\boldsymbol{\chi}}^{(1)}(\omega) = \int_{-\infty}^{\infty} dt \boldsymbol{\chi}^{(1)}(t) e^{i\omega t}, \tag{4.12}$$

and

$$\tilde{\boldsymbol{\chi}}^{(2)}(\omega_1,\omega_2) = \prod_{s=1}^{2} \int_{-\infty}^{\infty} dt_s \boldsymbol{\chi}^{(2)}(t_1,t_2) e^{i\sum_{s=1}^{2}\omega_s t_s}. \tag{4.13}$$

An obvious generalization to the nth order is

$$\tilde{\boldsymbol{\chi}}^{(n)}(\omega_1,\dots\omega_n) = \prod_{s=1}^{n} \int_{-\infty}^{\infty} dt_s \boldsymbol{\chi}^{(n)}(t_1,\dots t_n) e^{i\sum_{s=1}^{n}\omega_s t_s}. \tag{4.14}$$

Using Eqs. (4.10) – (4.13), we can obtain in the component form

$$\tilde{P}_i^{(1)}(\mathbf{r},\omega) = \epsilon_0 \sum_j \tilde{\chi}_{ij}^{(1)}(\omega)\tilde{E}_j(\mathbf{r},\omega), \tag{4.15}$$

and

$$\tilde{P}_i^{(2)}(\mathbf{r},\omega_3) = \epsilon_0 \sum_{jk} \int_{-\infty}^{\infty} \frac{d\omega_1}{2\pi} \tilde{\chi}_{ijk}^{(2)}(-\omega_3,\omega_1,\omega_2)\tilde{E}_j(\mathbf{r},\omega_1)\tilde{E}_k(\mathbf{r},\omega_2), \tag{4.16}$$

where $\omega_3 = \omega_1 + \omega_2$.

Exercise. 4.1 *Derive Eq. (4.16).*

Generalizing Eq. (4.16) to any order n, we can write down

$$\tilde{P}^{(n)}_{j_n}(\mathbf{r},\omega_n) = \epsilon_0 \sum_{j_1\dots j_{n-1}} \prod_{s=1}^{n-1} \int_{-\infty}^{\infty} \frac{d\omega_s}{2\pi} \tilde{\chi}^{(n)}_{j_n j_1 j_2 \dots j_{n-1}}(-\omega_n,\omega_1,\omega_2,\dots\omega_{n-1}) \times \tilde{E}_{j_1}(\mathbf{r},\omega_1)\dots\tilde{E}_{j_{n-1}}(\mathbf{r},\omega_{n-1}), \tag{4.17}$$

with $\omega_n = \sum_{s=1}^{n-1}\omega_s$. In particular, the third-order polarization contribution is

$$\tilde{P}^{(3)}_i(\mathbf{r},\omega_4) = \epsilon_0 \sum_{jkl} \prod_{s=1}^{2} \int_{-\infty}^{\infty} \frac{d\omega_s}{2\pi} \tilde{\chi}^{(3)}_{ijkl}(-\omega_4,\omega_1,\omega_2,\omega_3)\tilde{E}_j(\mathbf{r},\omega_1)\tilde{E}_k(\mathbf{r},\omega_2)\tilde{E}_l(\mathbf{r},\omega_3), \tag{4.18}$$

where $\omega_4 = \omega_1 + \omega_2 + \omega_3$.

4.3 Formal properties of nonlinear optical susceptibilities

We now list generic properties of optical susceptibilities which follow from their definitions.

- *Intrinsic permutational symmetry*:

$$\tilde{\chi}^{(n)}_{jj_1\dots j_n}(-\omega,\omega_1\dots\omega_n) = P_t\cdot\tilde{\chi}^{(n)}_{jj_1\dots j_n}(-\omega,\omega_1\dots\omega_n). \tag{4.19}$$

where $\omega = \sum_{s=1}^{n}\omega_s$, and $P_t\cdot(\dots)$ stands for a permutation of the n index pairs $(j_1,\omega_1)\dots(j_n,\omega_n)$ with the exclusion of the pair $(j,-\sum_s\omega_s)$. This property follows at once from the definition of nonlinear optical susceptibilities (4.17): Indeed the indices $(j_1\dots j_n)$ are dummy ones, and hence the polarization field does not change upon interchanging any pair of them as long as we simultaneously exchange the corresponding frequencies.

Example: $\tilde{\chi}^{(2)}_{ijk}(-\omega,\omega_1,\omega_2) = \tilde{\chi}^{(2)}_{ikj}(-\omega,\omega_2,\omega_1)$.

- *Reality of χ in the time-domain*:

The reality of $\boldsymbol{\chi}^{(n)}$ in time domain implies the following relation in the Fourier domain

$$\tilde{\chi}^{(n)*}_{jj_1\dots j_n}(-\omega,\omega_1,\dots,\omega_n) = \tilde{\chi}^{(n)}_{jj_1\dots j_n}(\omega,-\omega_1,\dots,-\omega_n), \tag{4.20}$$

where $*$ denotes, as usual, complex conjugation.

Example: $\tilde{\chi}^{(2)*}_{ijk}(-\omega,\omega_1,\omega_2) = \tilde{\chi}^{(2)}_{ijk}(\omega,-\omega_1,-\omega_2)$.

Exercise 4.2. *Derive Eq. (4.20).*

- *Causality*:

For the response of a physical medium to be causal, the polarization field must be equal to zero at any instant before the electric field is applied, which implies, in accord with Eq.(4.17) that

$$\chi^{(n)}_{jj_1\ldots j_n}(t-\tau_1,\ldots t-\tau_n)=0, \qquad \text{for any} \quad \tau_s > t. \tag{4.21}$$

Let us now exhibit very tangible constraints on the functional form of the real and imaginary parts of the susceptibility functions in the Fourier domain, stemming from causality.

We begin by considering the linear susceptibility. It follows from Eq. (4.21) that a causal linear response function must obey

$$\boldsymbol{\chi}^{(1)}(\tau)=\boldsymbol{\chi}^{(1)}(\tau)\theta(\tau), \tag{4.22}$$

where $\theta(\tau)$ is a Heaviside step function defined as

$$\theta(\tau)=\begin{cases} 1 & \tau \geq 0, \\ 0 & \tau < 0. \end{cases} \tag{4.23}$$

On introducing Fourier transforms of $\boldsymbol{\chi}$ and θ by the expressions

$$\tilde{\boldsymbol{\chi}}^{(1)}(\omega)=\int_{-\infty}^{\infty} d\tau\, \boldsymbol{\chi}^{(1)}(\tau)e^{i\omega\tau}, \tag{4.24}$$

and

$$\tilde{\theta}(\omega)=\int_{-\infty}^{\infty} d\tau\, \theta(\tau)e^{i\omega\tau}, \tag{4.25}$$

we conclude from Eq. (4.22) that

$$\tilde{\boldsymbol{\chi}}^{(1)}(\omega)=\int_{-\infty}^{\infty}\frac{d\omega'}{2\pi}\tilde{\boldsymbol{\chi}}^{(1)}(\omega')\tilde{\theta}(\omega-\omega'). \tag{4.26}$$

Recall further that

$$\tilde{\theta}(\omega-\omega')=\mathcal{P}\left[\frac{1}{i(\omega-\omega')}\right]+\pi\delta(\omega-\omega'), \tag{4.27}$$

where $\mathcal{P}$ stands for a principal value, excluding the singularity in the denominator. It follows from Eqs. (4.26) and (4.27), after simple algebra, that

$$\tilde{\boldsymbol{\chi}}^{(1)}(\omega)=\frac{1}{\pi i}\mathcal{P}\int_{-\infty}^{\infty} d\omega'\,\frac{\tilde{\boldsymbol{\chi}}^{(1)}(\omega')}{\omega-\omega'}. \tag{4.28}$$

Eq. (4.28) implies that real and imaginary parts of the linear susceptibility tensor are related vie the following *Kramers-Kronig* relations

$$\mathrm{Re}\,\tilde{\boldsymbol{\chi}}^{(1)}(\omega)=\frac{1}{\pi}\mathcal{P}\int_{-\infty}^{\infty} d\omega'\,\frac{\mathrm{Im}\,\tilde{\boldsymbol{\chi}}^{(1)}(\omega')}{\omega-\omega'}, \tag{4.29}$$

and

$$\mathrm{Im}\,\tilde{\boldsymbol{\chi}}^{(1)}(\omega) = -\frac{1}{\pi}\mathcal{P}\int_{-\infty}^{\infty} d\omega'\,\frac{\mathrm{Re}\,\tilde{\boldsymbol{\chi}}^{(1)}(\omega')}{\omega-\omega'}. \tag{4.30}$$

Relations (4.29) and (4.30) not only impose a constraint on the functional form of the real and imaginary parts of the linear susceptibility tensor, but they also enable one to reconstruct the real part – describing dispersion – from the imaginary one, which is much easier to measure as it relates to absorption in the medium.

Kramers-Kronig relations can also be derived for some second-order susceptibilities. In particular, starting from the causality condition

$$\boldsymbol{\chi}^{(2)}(\tau_1,\tau_2) = \boldsymbol{\chi}^{(2)}(\tau_1,\tau_2)\theta(\tau_1)\theta(\tau_2), \tag{4.31}$$

and following the same line of argument as above, we obtain

$$\tilde{\boldsymbol{\chi}}^{(2)}(-\omega_3,\omega_1,\omega_2) = \frac{1}{\pi i}\mathcal{P}\int_{-\infty}^{\infty} d\omega_1'\,\frac{\tilde{\boldsymbol{\chi}}^{(2)}(-\omega_3',\omega_1',\omega_2)}{\omega_1-\omega_1'}. \tag{4.32}$$

Here $\omega_3 = \omega_1+\omega_2$ and $\omega_3' = \omega_1'+\omega_2$. This process is referred to as a sum-frequency generation. By the same token, the Kramers-Kronig relations for a difference-frequency generation are

$$\tilde{\boldsymbol{\chi}}^{(2)}(-\omega_3,\omega_1,-\omega_2) = \frac{1}{\pi i}\mathcal{P}\int_{-\infty}^{\infty} d\omega_2'\,\frac{\tilde{\boldsymbol{\chi}}^{(2)}(-\omega_3',\omega_1,-\omega_2')}{\omega_2-\omega_2'}, \tag{4.33}$$

where in this case, $\omega_3 = \omega_1-\omega_2$ and $\omega_3' = \omega_1-\omega_2'$.

Exercise 4.3. *Derive Eqs. (4.32) and (4.33) .*

Exercise 4.4.* *Consider a degenerate case of the sum-frequency generation, $\omega_1 = \omega_2 = \omega$, and derive the following Kramers-Kronig relations*

$$\tilde{\boldsymbol{\chi}}^{(2)}(-2\omega,\omega,\omega) = \frac{1}{\pi i}\mathcal{P}\int_{-\infty}^{\infty} d\omega'\,\frac{\tilde{\boldsymbol{\chi}}^{(2)}(-2\omega',\omega',\omega')}{\omega-\omega'}. \tag{4.34}$$

This case corresponds to an important second-order nonlinear process we will study in detail later on – it is referred to as the second-harmonic generation.

Unfortunately, no general Kramers-Kronig relations can be derived for higher-order nonlinear susceptibilities. Moreover, there are nonlinear processes for which no Kramers-Kronig relations exist, one of the most prominent cases being the self-focusing/self-defocusing process – specified by $\chi^{(3)}(-\omega,\omega,-\omega,\omega)$ – which is the most common nonlinear process in isotropic media with inversion symmetry.

The symmetry properties of nonlinear susceptibilities we have studied so far hold quite generally. In addition, there are other symmetry properties of $\boldsymbol{\chi}$ which depend on the symmetries of underlying physical systems. First, consider the multitude of orthogonal transformations – such as rotations, translations and inversions – that leave the medium unchanged. It follows that the corresponding susceptibility tensor of any rank must be invariant with respect to such transformations, implying for any n

$$\chi^{(n)}_{ii_1\ldots i_n} = \sum_{jj_1\ldots j_n} \mathcal{T}_{ij}\mathcal{T}_{i_1j_1}\ldots\mathcal{T}_{i_nj_n}\,\chi^{(n)}_{jj_1\ldots j_n}, \tag{4.35}$$

where the summation over the dummy indices is implied as usual. For instance,

$$\chi^{(1)}_{ij} = \sum_{kl} \mathcal{T}_{ik}\mathcal{T}_{jl}\,\chi^{(1)}_{kl}, \tag{4.36}$$

or

$$\chi^{(2)}_{ijk} = \sum_{lsm} \mathcal{T}_{is}\mathcal{T}_{jl}\mathcal{T}_{km}\,\chi^{(2)}_{slm}, \tag{4.37}$$

and so on.

Exercise 4.5. *A rotation with respect to the z-axis can be described by the matrix*

$$T_{ij} = \begin{pmatrix} \cos\theta & -\sin\theta & 0 \\ \sin\theta & \cos\theta & 0 \\ 0 & 0 & 1 \end{pmatrix}$$

Assume the medium is invariant with respect to rotations by $\theta = \pi/2$. Determine the constraints on the components of $\boldsymbol{\chi}^{(1)}$ imposed in this case.

One of the most important orthogonal transformations is *inversion* such that for an every point in the medium $\mathbf{r} \to -\mathbf{r}$ implying $\mathcal{T}_{ij} = -\delta_{ij}$. It follows at once from Eq. (4.35) that if the medium is symmetric with respect to inversions – i.e., if it has an inversion center – then for any susceptibility tensor of *odd* rank , or for an *even* $n = 2k$, we obtain

$$\chi^{(2k)}_{ii_1\ldots i_{2k}} = -\chi^{(2k)}_{ii_1\ldots i_{2k}} = 0. \tag{4.38}$$

In particular, in media with the inversion centers the lowest-order nonlinear response is cubic, described by $\chi^{(3)}_{ijkl}$. Such inversion symmetric media are referred to as *centrosymmetric*. Most gases and liquids as well as many solids possess such properties.

Another important constraint is imposed by requiring that media be lossless. In lossless media, equations of motions are symmetric with respect to time reversal – there are no losses and the microscopic evolution can in principle be reversed. Under such conditions,

$$\boldsymbol{\chi}^{(n)}(\tau_1 \ldots \tau_n) = \boldsymbol{\chi}^{(n)}(-\tau_1 \ldots -\tau_n). \tag{4.39}$$

It can then be readily inferred from Eq. (4.14) that

$$\tilde{\chi}^{(n)}_{jj_1\ldots j_n}(-\omega, \omega_1, \ldots \omega_n) = \chi^{(n)*}_{jj_1\ldots j_n}(-\omega, \omega_1, \ldots \omega_n), \tag{4.40}$$

that is a Fourier image of $\boldsymbol{\chi}$ is real.

Exercise 4.6. *Derive Eq. (4.40).*

Exercise 4.7. *Show that in lossless media ϵ_{ij} must be symmetric.*

Moreover, in lossless nonlinear media, there is an *overall permutation symmetry* of the susceptibility tensor, similar to that expressed in Eq. (4.19), except the pair $(j, -\sum_s \omega_s)$ is included.

$$\text{Example: } \tilde{\chi}^{(3)}_{ijkl}(-\omega_4, \omega_1, \omega_2, \omega_3) = \tilde{\chi}^{(3)}_{jlik}(\omega_1, \omega_3, -\omega_4, \omega_2).$$

Finally, if all frequencies involved in the interaction are *well below* the lowest resonant frequency of the medium, there exists a permutation symmetry of the Cartesian indices alone, known as the *Kleinmann symmetry*.

Example: $\tilde{\chi}^{(2)}_{ijk}(-\omega_3,\omega_1,\omega_2)=\tilde{\chi}^{(2)}_{jki}(-\omega_3,\omega_1,\omega_2)=\tilde{\chi}^{(2)}_{kij}(-\omega_3,\omega_1,\omega_2)$.

We stress though that Kleinman's symmetry is only an approximation valid far from any internal resonances where dispersive properties of nonlinear media are negligible such that one can virtually neglect frequency dependence of the nonlinear susceptibilities. The Kleinman symmetry breaks down, for instance, if there is an absorption band sandwiched between a pair of frequencies involved with a nonlinear interaction. In the latter case, dispersive properties of the medium would be important at those frequencies near the absorption band.

4.4 Nonlinear wave equation approach: Classical coupled-wave equations

We now proceed to deriving general nonlinear wave equations governing second-order nonlinear processes. To this end, we recall the Maxwell equations in charge- and current-free environment,

$$\nabla\cdot\mathbf{D}=0; \qquad \nabla\cdot\mathbf{B}=0, \tag{4.41}$$

$$\nabla\times\mathbf{H}=\partial_t\mathbf{D}, \qquad \nabla\times\mathbf{E}=-\partial_t\mathbf{B}. \tag{4.42}$$

In the optical frequency range, natural materials are nonmagnetic, allowing us close the set of Eqs. (4.41) and (4.42) with the constitutive relations

$$\mathbf{B}=\mu_0\mathbf{H}; \qquad \mathbf{D}=\epsilon_0\mathbf{E}+\mathbf{P}=\mathbf{D}_L+\mathbf{P}_{NL}, \tag{4.43}$$

where we found it convenient to decompose the polarization field $\mathbf{P}$ into linear and nonlinear components as

$$\mathbf{P}=\mathbf{P}_L+\mathbf{P}_{NL}. \tag{4.44}$$

$\mathbf{D}_L=\epsilon_0\mathbf{E}+\mathbf{P}_L$ in Eq. (4.43) refers to the linear electric flux density. Using Eq. (4.43) in Eqs. (4.41) and (4.42) and eliminating $\mathbf{H}$ from Maxwell's equations in favor of $\mathbf{E}$, we arrive at the set of continuity and wave equations

$$\nabla\cdot(\mathbf{D}_L+\mathbf{P}_{NL})=0, \tag{4.45}$$

and

$$\nabla\times(\nabla\times\mathbf{E})=-\mu_0\partial^2_{tt}\mathbf{E}-\mu_0\partial^2_{tt}\mathbf{P}. \tag{4.46}$$

We now assume a plane-wave geometry, that is all fields are harmonic and they depend only on one spatial coordinate z, say, along the wave propagation direction, which incidentally coincides with the optical axis of the system. Under these assumption, the relevant fields can be expressed as

$$\mathbf{E}(z,t)=\tilde{\mathbf{E}}(z,\omega_s)e^{-i\omega_s t}, \tag{4.47}$$

$$\mathbf{D}_L(z,t)=\tilde{\mathbf{D}}_L(z,\omega_s)e^{-i\omega_s t}, \tag{4.48}$$

and

$$\mathbf{P}_{NL}(z,t) = \tilde{\mathbf{P}}_{NL}(z,\omega_s)e^{-i\omega_s t}. \tag{4.49}$$

Here ω_s is the frequency of the wave we arbitrarily assign as a signal; hence the subscript "s". Henceforth, it will prove convenient to break all fields into longitudinal and transverse components as

$$\tilde{\mathbf{E}}(z,\omega_s) = \mathbf{e}_z\tilde{E}^{\parallel}(z,\omega_s) + \tilde{\mathbf{E}}^{\perp}(z,\omega_s), \tag{4.50}$$

and likewise,

$$\tilde{\mathbf{D}}_L(z,\omega_s) = \mathbf{e}_z\tilde{D}_L^{\parallel}(z,\omega_s) + \tilde{\mathbf{D}}^{\perp}(z,\omega_s), \tag{4.51}$$

and

$$\tilde{\mathbf{P}}_{NL}(z,\omega_s) = \mathbf{e}_z\tilde{\mathbf{P}}_{NL}^{\parallel}(z,\omega_s) + \tilde{\mathbf{P}}_{NL}^{\perp}(z,\omega_s). \tag{4.52}$$

It can be shown–see the exercise–that under the circumstances, $\nabla\times\nabla\times\tilde{\mathbf{E}}(z,\omega_s) = -\partial_{zz}^2\tilde{\mathbf{E}}^{\perp}(z,\omega_s)$.

Exercise 4.8. *By expressing the field in the cylindrical coordinates,* $\tilde{\mathbf{E}}(z,\omega_s) = \mathbf{e}_z\tilde{E}^{\parallel}(z,\omega_s) + \mathbf{e}_\rho\tilde{\mathbf{E}}_\rho(z,\omega_s) + \mathbf{e}_\phi\tilde{\mathbf{E}}_\phi(z,\omega_s)$*, show that* $\nabla\times\nabla\times\tilde{\mathbf{E}}(z,\omega_s) = -\partial_{zz}^2\tilde{\mathbf{E}}^{\perp}(z,\omega_s)$.

It then follows that Eqs. (4.45) and (4.46) can be cast into the form

$$\tilde{D}_L^{\parallel}(z,\omega_s) + \tilde{P}_{NL}^{\parallel}(z,\omega_s) = 0, \tag{4.53}$$

and

$$-\partial_{zz}^2\tilde{\mathbf{E}}^{\perp}(z,\omega_s) = \mu_0\omega_s^2[\tilde{\mathbf{D}}_L^{\perp}(z,\omega_s) + \tilde{\mathbf{P}}_{NL}^{\perp}(z,\omega_s)]. \tag{4.54}$$

Let us now assume that a generally anisotropic medium–anisotropy is needed for phase-matching in some cases–is uniaxial with the optical axis coinciding with the z-axis. The dielectric tensor of such a medium is known from Sec. 2.2.2. Using the results of this section, it is easy to see that

$$D_L^{\parallel} = \epsilon_{\parallel}(\omega_s)\tilde{E}^{\parallel}, \qquad \mathbf{D}_L^{\perp} = \epsilon_{\perp}(\omega_s)\tilde{\mathbf{E}}^{\perp}; \tag{4.55}$$

implying that

$$\epsilon_{\parallel}(\omega_s)\tilde{E}^{\parallel}(z,\omega_s) + \tilde{P}_{NL}^{\parallel}(z,\omega_s) = 0, \tag{4.56}$$

and

$$-\partial_{zz}^2\tilde{\mathbf{E}}^{\perp}(z,\omega_s) + \tfrac{\omega_s^2}{c^2}\epsilon_{\perp}(\omega_s)\tilde{\mathbf{E}}^{\perp}(z,\omega_s) + \mu_0\omega_s^2\tilde{\mathbf{P}}_{NL}^{\perp}(z,\omega_s) = 0. \tag{4.57}$$

It can be inferred from Eqs. (4.56) and (4.57) that while the longitudinal field component can be determined from a simple algebraic equation, following from Gauss's law, the transverse field component is governed by a wave equation. We will now focus on the transverse fields.

Hereafter, we will restrict ourselves to the case of linearly polarized waves in the plane transverse to the optical axis. As optical nonlinearities far from internal resonances of any natural media are fairly weak, it is reasonable to assume the fields profiles change very slowly – at the wavelength scale – in the plane, transverse to the

propagation direction. Hence, the electric field of a signal wave can be expressed as a slowly-varying envelope times a fast carrier plane wave,

$$\tilde{\mathbf{E}}^{\perp}(z,\omega_s) = \mathbf{e}(\omega_s)\mathcal{E}(z,\omega_s)e^{ik_s z}, \tag{4.58}$$

which induces the polarization field such that

$$\tilde{\mathbf{P}}^{\perp}_{NL}(z,\omega_s) = \mathbf{e}(\omega_s)\mathcal{P}_{NL}(z,\omega_s)e^{ik_s z}. \tag{4.59}$$

Here, the wave number satisfies the usual linear dispersion relation,

$$k^2(\omega_s) = \epsilon_{\perp}(\omega_s)\tfrac{\omega_s^2}{c^2}. \tag{4.60}$$

Substituting from Eqs. (4.58) – (4.60), and using the *slowly-varying envelope approximation* (SVEA),

$$\partial_z\mathcal{E} \ll k_s\mathcal{E}; \qquad\qquad \partial^2_{zz}\mathcal{E} \ll k_s^2\mathcal{E}, \tag{4.61}$$

we arrive at the nonlinear wave equation for the signal wave in the form

$$2ik_s\partial_z\mathcal{E} = -\mu_0\omega_s^2\mathcal{P}_{NL}. \tag{4.62}$$

Our treatment has been general so far. We will now specialize to the second-order processes. Recall that

$$\tilde{P}^{(2)}_i(z,\omega_s) = \epsilon_0 c^{(2)}(\omega_1,\omega_2)\sum_{jk}\tilde{\chi}^{(2)}_{ijk}(-\omega_s;\omega_1,\omega_2)\tilde{E}_j(z,\omega_1)\tilde{E}_k(z,\omega_2), \tag{4.63}$$

with $\omega_s = \omega_1 + \omega_2$ and the so-called degeneracy factor

$$c^{(2)}(\omega_1,\omega_2) = \begin{cases} 1, & \omega_s \neq 2\omega_1; \\ 1/2, & \omega_s = 2\omega_1. \end{cases} \tag{4.64}$$

Using Eqs. (4.63) and (4.59), we obtain for the slowly-varying second-order polarization field the expression

$$\begin{aligned} \mathcal{P}^{(2)}(z,\omega_s) \;\; = \;\; & \epsilon_0 c^{(2)}(\omega_1,\omega_2)\sum_{ijk}\tilde{\chi}^{(2)}_{ijk}(-\omega_s;\omega_1,\omega_2)e_i(\omega_s) \\ & \times e_j(\omega_1)e_k(\omega_2)\mathcal{E}(z,\omega_1)\mathcal{E}(z,\omega_2)e^{i\Delta k z}, \end{aligned} \tag{4.65}$$

where

$$\Delta k \equiv k(\omega_1) + k(\omega_2) - k(\omega_s). \tag{4.66}$$

Utilizing Eq. (4.65) and introducing

$$\chi^{(2)}_{eff}(-\omega_s;\omega_1,\omega_2) \equiv c^{(2)}(\omega_1,\omega_2)\sum_{ijk}\tilde{\chi}^{(2)}_{ijk}(-\omega_s;\omega_1,\omega_2)e_i(\omega_s)e_j(\omega_1)e_k(\omega_2), \tag{4.67}$$

we finally arrive at the set of coupled-wave equations governing the second-order nonlinear processes:

$$\partial_z\mathcal{E}_s = \tfrac{i\omega_s^2}{2k(\omega_s)c^2}\chi^{(2)}_{eff}(-\omega_s;\omega_1,\omega_2)\mathcal{E}_1\mathcal{E}_2 e^{i\Delta k z}. \tag{4.68}$$

Here we adopted the convention

$$\mathcal{E}_j(z,-\omega_j) = \mathcal{E}^*_j(z,\omega_j),$$

and introduced short-hand notations $\mathcal{E}_j \equiv \mathcal{E}(z,\omega_j)$, $j = s,1,2$.

4.5 Second-harmonic generation

4.5.1 Coupled wave equations and phase matching considerations

The process of second harmonic generation involves the interaction of two waves at frequency ω to produce a wave with the frequency 2ω. It is schematically illustrated in Fig. 1 below.

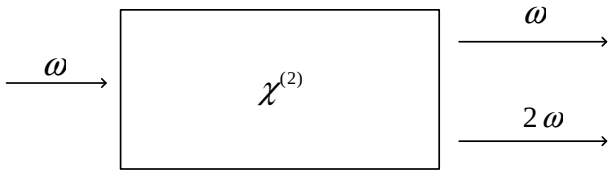

Figure 4.9: Illustrating the second harmonic generation.

The coupled wave equations governing the second harmonic generation (SHG) in lossless media can be obtained directly from the general coupled-mode equations derived in the previous Lecture by specializing to the case of two identical mixing frequencies. The resulting wave equations for the fundamental $\mathcal{E}_\omega$ and the second harmonic $\mathcal{E}_{2\omega}$ fields are

$$\partial_z \mathcal{E}_\omega = \tfrac{i\omega^2}{2k_\omega c^2}\chi^{(2)}_{eff}(-\omega, 2\omega, -\omega)\mathcal{E}_{2\omega}\mathcal{E}^*_\omega e^{-i\Delta kz}. \tag{4.69}$$

and

$$\partial_z \mathcal{E}_{2\omega} = \tfrac{i4\omega^2}{2k_{2\omega} c^2}\chi^{(2)}_{eff}(-2\omega, \omega, \omega)\, \mathcal{E}^2_\omega\, e^{i\Delta kz}, \tag{4.70}$$

where the wave number mismatch is now defined as

$$\Delta k = 2k_\omega - k_{2\omega}. \tag{4.71}$$

In Eqs. (4.69) – (4.71), we have introduced the notations

$$k_\omega = \frac{\omega n(\omega)}{c}, \qquad\qquad k_{2\omega} = \frac{2\omega n(2\omega)}{c}. \tag{4.72}$$

It follows from general properties of susceptibilities in the absence of losses that

$$\chi^{(2)}_{eff}(-\omega, 2\omega, -\omega) = 2\chi^{(2)}_{eff}(-2\omega, \omega, \omega) \equiv \chi^{(2)}_{eff}. \tag{4.73}$$

Using (4.73), we can transform the SHG coupled wave equations in the plane wave geometry to

$$\frac{d\mathcal{E}_\omega}{dz} = \frac{i\omega^2}{2k_\omega c^2}\chi^{(2)}_{eff}\, \mathcal{E}_{2\omega}\mathcal{E}^*_\omega e^{-i\Delta kz}. \tag{4.74}$$

and

$$\frac{d\mathcal{E}_{2\omega}}{dz} = \frac{i\omega^2}{k_{2\omega} c^2}\chi^{(2)}_{eff}\, \mathcal{E}^2_\omega\, e^{i\Delta kz}. \tag{4.75}$$

Let us now study the second harmonic generation in the undepleted pump approximation, which implies that the power of the fundamental wave is high enough and the efficiency of the second harmonic generation is low enough that we can neglect the power depletion of the fundamental wave. As the efficiency η_{SHG} of the second harmonic generation can be defined as the ratio of the second harmonic intensity at the output to the input intensity of the fundamental,

$$\eta_{SHG} \equiv \frac{I_{2\omega}(L)}{I_{\omega}(0)}, \tag{4.76}$$

we can define a quantitative criterion for the undepleted pump approximation to hold:

$$\eta_{SHG} \ll 1. \tag{4.77}$$

In the undepleted pump approximation, Eq. (4.75) can be integrated at once with the result

$$\mathcal{E}_{2\omega}(L) = \frac{i\omega^2}{k_{2\omega}c^2}\chi^{(2)}_{eff}\,\mathcal{E}^2_{\omega}\frac{e^{i\Delta kL}-1}{i\Delta k} = \frac{\omega^2 L\chi^{(2)}_{eff}}{k_{2\omega}c^2}\mathcal{E}^2_{\omega}e^{i\Delta kL/2}\frac{e^{i\Delta kL/2}-e^{-i\Delta kL/2}}{2i(\Delta kL/2)}, \tag{4.78}$$

where L is the length of the interaction region and $\mathcal{E}_{\omega} = const$. Further, equation (4.78) can be simplified as

$$\mathcal{E}_{2\omega}(L) = \frac{\omega^2 L\chi^{(2)}_{eff}\mathcal{E}^2_{\omega}}{k_{2\omega}c^2}e^{i\Delta kL/2}\frac{\sin(\Delta kL/2)}{\Delta kL/2}. \tag{4.79}$$

It can be readily inferred from Eq. (4.79) that the intensity of the second harmonic is given by

$$I_{2\omega}(L) = \frac{\omega^2 L^2\chi^{(2)2}_{eff}I^2_{\omega}}{2\epsilon_0 n_{2\omega}n^2_{\omega}c^3}\,\mathrm{sinc}^2\left(\frac{\Delta kL}{2}\right), \tag{4.80}$$

where we defined

$$\mathrm{sinc}(x) \equiv \frac{\sin x}{x}. \tag{4.81}$$

The analysis of Eq. (4.80) reveals that if the phases of the fundamental and second harmonic waves are matched, the intensity of the second harmonic is proportional to the square of the interaction length, $I_{2\omega}(L) \propto L^2$. Physically, it can be interpreted by observing that if all N polarized atomic dipoles in the interaction volume – whose total number is proportional to L – radiate in phase, their resulting fields interfere constructively; consequently the total intensity of the second harmonic is such that $I_{2\omega}(L) \propto N^2 \propto L^2$. On the other hand, if the phase matching condition (4.82) is not met, the efficiency of the second harmonic generation decreases dramatically, as is shown in Fig. 2.

Let us now discuss the efficiency of the SHG process. It follows from Eqs. (4.77) and (4.80) that under the best possible condition of the perfect *phase matching*

$$\Delta k = 0, \tag{4.82}$$

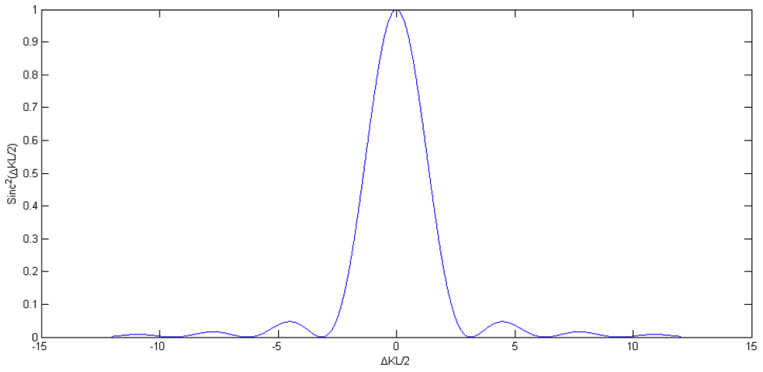

Figure 4.10: Second harmonic output as a function of the interaction length in the undepleted pump approximation

the undepleted pump approximation is valid provided

$$\eta_{SHG} = \frac{\omega^2 L^2 \chi_{eff}^{(2)2} I_\omega}{2\epsilon_0 n_{2\omega} n_\omega^2 c^3} \ll 1, \tag{4.83}$$

which can be physically interpreted as a limitation on the allowed interaction length for a (large) given power of the fundamental wave: the power depletion of the fundamental can no longer be neglected for sufficiently large interaction lengths. To estimate the efficiency of the SHG under typical experimental conditions, we can estimate the intensity of the fundamental as

$$I_\omega = \frac{P}{\pi w_0^2}, \tag{4.84}$$

where P is the laser power and w_0 is the spot size of the laser output beam, which we choose by stipulating that the corresponding diffraction length, $L_d \simeq k w_0^2$, be much greater that the interaction length,

$$L_d \gg L, \tag{4.85}$$

for the plane wave approximation to hold. Using typical values, for moderate-to-high power lasers $P \sim 1$ W, and $\chi_{eff}^2 \sim 5 \times 10^{-23}$ m^2/V^2, for $LiNbO_3$, say; with the other parameters being chosen as follows: $L \sim 1$ cm, $n_\omega \sim n_{2\omega} \sim 2$, $\lambda \sim 5 \times 10^{-5}$ cm, and the spot size $w_0 \sim 100$ μm, such that $L_d \sim 10$ cm, we obtain the order-of-magnitude estimate as $\eta_{SHG} \sim 10^{-3} \ll 1$. Clearly, the undepleted pump approximation is a good one even for relatively high power laser sources in the plane wave geometry. To increase the SHG conversion efficiency, it is advised that (a) pulsed lasers be employed to augment the input power and (b) source light beam be tightly focused into the interaction volume to significantly increase the intensity of the fundamental input wave. In general, the analysis of the SHG with such tightly focused laser beams requires a more careful consideration of diffraction effects. With this in mind, however, we could still make a rough order-of-magnitude estimate of the efficiency using Eq. (4.83) by taking

the spot size of a focused beam to be $w_0 \sim 10\ \mu$m, even though $L_d \ll L$. The resulting efficiency is of the order of 10%, which is already quite an improvement.

Due to the importance of phase matching, we briefly discuss the ways of realizing the condition (4.82), which, when translated in terms of the refractive indices, implies

$$n(2\omega) = n(\omega). \tag{4.86}$$

First, we note that the requirement (4.86) cannot be satisfied in an isotropic medium because of frequency dispersion: Typically, the refractive index of a nonlinear medium far below absorption resonances is a monotonically increasing function of frequency, a phenomenon referred to as normal dispersion. Thus isotropic media are in general not phase matchable.

Phase matching can be realized in anisotropic media, which is referred to as **birefringence phase matching**. As we previously mentioned, the distribution of the ordinary wave vectors is spherically symmetric–which is graphically illustrated in Fig. 3–where we assumed, for simplicity, the wave vector lies in the xz-plane–and one can introduce the corresponding frequency-dependent refractive index $n_o(\omega)$ by the expression

$$n_o(\omega) \equiv \frac{k_o c}{\omega} = \sqrt{\epsilon_\perp(\omega)}. \tag{4.87}$$

The extraordinary wave vector, on the other hand, does depend on the propagation direction, and the associated extraordinary refractive index is given by

$$n_e(\theta, \omega) \equiv \frac{k_e c}{\omega} = \left(\frac{\sin^2\theta}{\epsilon_\perp(\omega)} + \frac{\cos^2\theta}{\epsilon_\parallel(\omega)} \right)^{-1/2}. \tag{4.88}$$

The surface $n_e(\theta, \omega) = const$ is, in general, an ellipsoid, but it reduces to an ellipse if we restrict the extraordinary wave vector to lie in the $xz-$ plane, see Fig. 3.

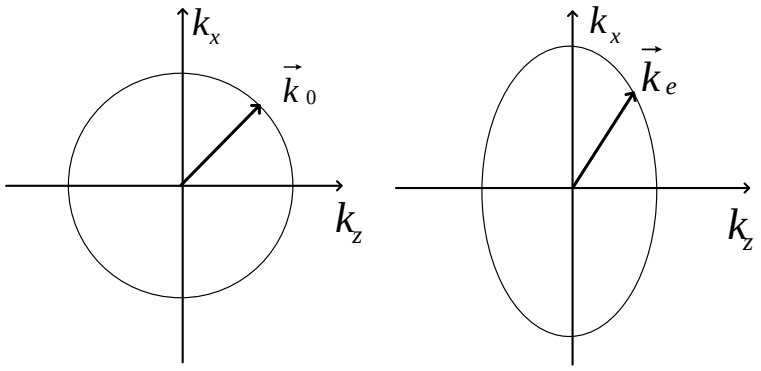

Figure 4.11: Graphical representation of the wave vectors of ordinary (left) and extraordinary (right) waves in a uniaxial crystal.

Assume now that the fundamental is an ordinary wave and the second harmonic is an extraordinary one. It can then be inferred from Fig. 4 that provided the extraordinary

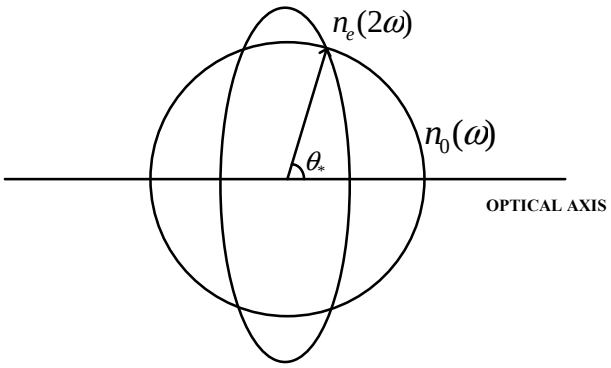

Figure 4.12: Illustrating phase matching for the SHG in uniaxial crystals.

refractive index for the SH along the crystal axis is smaller than the ordinary refractive index of the fundamental, which can be mathematically expressed by the inequality

$$\epsilon_{\parallel}(2\omega) < \epsilon_{\perp}(\omega), \tag{4.89}$$

the phase matching is possible at the angle θ_* which can be determined from Eqs. (4.86), (4.87) and (4.88) to be

$$\tan\theta_* = \sqrt{\frac{\frac{1}{\epsilon_{\parallel}(2\omega)} - \frac{1}{\epsilon_{\perp}(\omega)}}{\frac{1}{\epsilon_{\perp}(\omega)} - \frac{1}{\epsilon_{\perp}(2\omega)}}}. \tag{4.90}$$

Unfortunately, whenever the angle between the ordinary and extraordinary wave vectors is other than $90^{\rm deg}$, a spatial walkoff accrues on propagation of the two waves as a consequence of directional mismatch between the Poynting vector and propagation direction of an extraordinary wave. The walkoff reduces spatial overlap between the polarization modes, thereby drastically reducing the SHG efficiency. Fortunately, some nonlinear crystals, such as lithium niobate, have a pronounced dependence of their birefringence on the temperature. Thus, one can achieve phase matching by keeping the angle between the modes fixed at $90^{\rm deg}$ and varying the temperature of the crystal. This is called **temperature phase matching**.

In the situations when neither birefringence nor temperature phase matching is possible, the most powerful phase matching technique is used, the so-called **quasi-phase-matching**. The technique involves periodically polling $\chi^{(2)}$ samples to modulate the second-order susceptibility. The latter can then be expanded in a Fourier series

$$\chi^{(2)}(z) = \sum_{m=-\infty}^{\infty} \chi_m^{(2)} e^{i2\pi m z/\Lambda},$$

where Λ is a spatial period of the structure. The phase mismatch is then modified to $\Delta k_{eff} = \Delta k - 2\pi m/\Lambda$. As $\chi_m^{(2)}$ decreases with m, reducing the SH intensity, it is preferable to work with $m = 1$ harmonic and choose the period Λ to phase match the

interaction, i.e.,

$$\Lambda = 2\pi/\Delta k.$$

If Δk is so large, $\Delta k \sim k$ that it is impossible to attain perfect phase matching, quasi-phase-matching allows to extend, at least, the effective interaction length to

$$L_{eff} = L(1 + 2\pi/\Lambda\Delta k),$$

where the smallest available Λ should be used.

4.5.2 Second-harmonic generation: Beyond the undepleted pump approximation

In this section, we describe the second harmonic generation process under general conditions. To this end, we rewrite the governing coupled wave equations in the form

$$\frac{d\mathcal{E}_\omega}{dz} = \frac{i\omega^2}{2k_\omega c^2}\chi^{(2)}_{eff}\,\mathcal{E}_{2\omega}\mathcal{E}^*_\omega e^{-i\Delta kz}, \tag{4.91}$$

$$\frac{d\mathcal{E}_{2\omega}}{dz} = \frac{i\omega^2}{k_{2\omega} c^2}\chi^{(2)}_{eff}\,\mathcal{E}^2_\omega\, e^{i\Delta kz}. \tag{4.92}$$

Let us now introduce the total optical intensity of the fundamental and second harmonic waves as

$$I = I_1 + I_2. \tag{4.93}$$

It is convenient to transform to dimensionless real amplitudes $\mathcal{A}$ and phases ϕ, related to the complex amplitudes of the fundamental and second harmonic waves by the expressions

$$\mathcal{E}_\omega = \sqrt{\frac{I}{n_\omega \epsilon_0 c}}\mathcal{A}_\omega e^{i\phi_\omega}, \tag{4.94}$$

and

$$\mathcal{E}_{2\omega} = \sqrt{\frac{I}{n_{2\omega} \epsilon_0 c}}\mathcal{A}_{2\omega} e^{i\phi_{2\omega}}. \tag{4.95}$$

Using the definitions (4.94) and (4.95), one can derive from Eqs. (4.91) and (4.92) the equations for the real amplitudes as

$$\frac{d\mathcal{A}_\omega}{dz} = \frac{\mathcal{A}_\omega \mathcal{A}_{2\omega}}{l}\sin\theta, \tag{4.96}$$

$$\frac{d\mathcal{A}_{2\omega}}{dz} = -\frac{\mathcal{A}^2_\omega}{l}\sin\theta, \tag{4.97}$$

where

$$\theta = 2\phi_\omega - \phi_{2\omega} + \Delta kz, \tag{4.98}$$

and we have introduced the characteristic spatial period l of the power exchange between the fundamental and second harmonic by the expression

$$\frac{1}{l} = \frac{\omega\chi^{(2)}_{eff}}{2c}\sqrt{\frac{I}{n^2_\omega n_{2\omega}\epsilon_0 c}}. \tag{4.99}$$

Similarly, the equations for the phases take the form

$$\frac{d\phi_\omega}{dz} = \frac{\mathcal{A}_{2\omega}}{l}\cos\theta, \tag{4.100}$$

$$\frac{d\phi_{2\omega}}{dz} = \frac{\mathcal{A}_\omega^2}{l\mathcal{A}_{2\omega}}\cos\theta. \tag{4.101}$$

Introducing $\zeta = z/l$, we can cast our equations into the following dimensionless form

$$\frac{d\mathcal{A}_\omega}{d\zeta} = \mathcal{A}_\omega\mathcal{A}_{2\omega}\sin\theta, \tag{4.102}$$

$$\frac{d\mathcal{A}_{2\omega}}{d\zeta} = -\mathcal{A}_\omega^2\sin\theta, \tag{4.103}$$

$$\frac{d\phi_\omega}{d\zeta} = \mathcal{A}_{2\omega}\cos\theta, \tag{4.104}$$

$$\frac{d\phi_{2\omega}}{d\zeta} = \frac{\mathcal{A}_\omega^2}{\mathcal{A}_{2\omega}}\cos\theta. \tag{4.105}$$

It can be inferred at once from Eqs. (4.104) and (4.105) as well as from Eq. (4.98) that θ obeys the equation

$$\frac{d\theta}{d\zeta} = \Delta s + \left(2\mathcal{A}_{2\omega} - \frac{\mathcal{A}_\omega^2}{\mathcal{A}_{2\omega}}\right)\cos\theta, \tag{4.106}$$

where we have introduced the quantity

$$\Delta s = \Delta k l. \tag{4.107}$$

We can easily see from Eqs. (4.102) and (4.103) that the set possesses the integral of motion

$$\mathcal{A}_\omega^2 + \mathcal{A}_{2\omega}^2 = 1, \tag{4.108}$$

which implies the power conservation in the SHG process in a lossless medium. It then follows from Eqs. (4.102) and (4.103) that

$$\mathcal{A}_{2\omega} = \frac{1}{\sin\theta}\frac{d}{d\zeta}\ln\mathcal{A}_\omega, \tag{4.109}$$

and

$$\frac{\mathcal{A}_\omega^2}{\mathcal{A}_{2\omega}} = -\frac{1}{\sin\theta}\frac{d}{d\zeta}\ln\mathcal{A}_{2\omega}. \tag{4.110}$$

Substituting from the last two equations into Eq. (4.98), we obtain the equation for the phase difference in the form

$$\frac{d\theta}{d\zeta} = \Delta s + \cot\theta\frac{d}{d\zeta}\ln(\mathcal{A}_\omega^2\mathcal{A}_{2\omega}). \tag{4.111}$$

Hereafter we focus on the perfect phase matching situation, $\Delta s = 0$. In this case, we can transform Eq. (4.111), with the aid of Eq. (4.103) to

$$\frac{d \ln \cos\theta}{d\zeta} = -\frac{d}{d\zeta} \ln(\mathcal{A}_\omega^2 \mathcal{A}_{2\omega}), \tag{4.112}$$

which can be integrated at once yielding the second integral of motion as

$$\mathcal{A}_\omega^2 \mathcal{A}_{2\omega} \cos\theta = \Gamma. \tag{4.113}$$

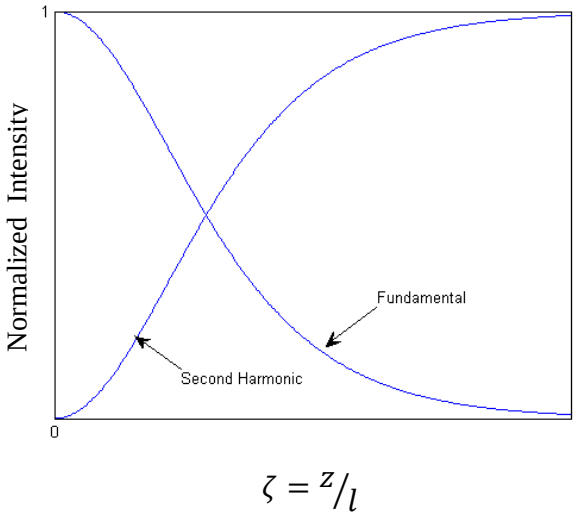

Figure 4.13: Intensity of the fundamental and second harmonic as functions of the interaction distance in the case of perfect phase matching.

Suppose now that $\Gamma = 0$ implying a fixed phase difference between the FW and SH, $\theta = -\pi/2$. It then follows that the equations of motion for the mode amplitudes simplify to

$$\frac{d\mathcal{A}_\omega}{d\zeta} = \mathcal{A}_\omega \mathcal{A}_{2\omega}, \tag{4.114}$$

$$\frac{d\mathcal{A}_{2\omega}}{d\zeta} = -\mathcal{A}_\omega^2, \tag{4.115}$$

Using Eq. (4.108), we can eliminate the fundamental from Eq. (4.115) resulting in

$$\frac{d\mathcal{A}_{2\omega}}{d\zeta} = -(1 - \mathcal{A}_{2\omega}^2), \tag{4.116}$$

which can be integrated at once yielding

$$\mathcal{A}_{2\omega} = \tanh\zeta; \qquad \mathcal{A}_\omega = \mathrm{sech}\zeta. \tag{4.117}$$

The intensities of the fundamental and second harmonic are displayed in the Fig. 5.

4.6 Sum-frequency generation

4.6.1 Coupled wave equations and their solution in the undepleted pump approximation

In this Lecture, we examine the sum-frequency generation (SFG), which involves mixing a signal wave at frequency ω_1 with a pump wave at frequency ω_2 to yield a harmonic oscillating at $\omega_3 = \omega_1 + \omega_2$, to be referred to as the sum-frequency (SF) wave. The SFG process is schematically illustrated in Fig. 1.

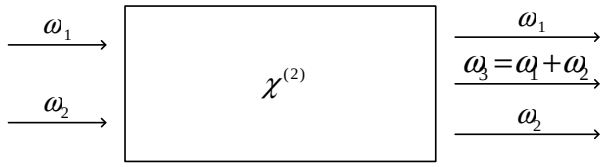

Figure 4.14: Schematic illustration of the sum-frequency generation process.

The wave equations governing the SFG can be readily obtained from the general coupled wave equations, yielding the following set

$$\partial_z \mathcal{E}_1 = \tfrac{i\omega_1^2}{2k_1c^2}\chi^{(2)}_{eff}(-\omega_1;\omega_3,-\omega_2)\mathcal{E}_3\mathcal{E}_2^* e^{-i\Delta kz}. \tag{4.118}$$

$$\partial_z \mathcal{E}_2 = \tfrac{i\omega_2^2}{2k_2c^2}\chi^{(2)}_{eff}(-\omega_2;\omega_3,-\omega_1)\mathcal{E}_3\mathcal{E}_1^* e^{-i\Delta kz}. \tag{4.119}$$

and

$$\partial_z \mathcal{E}_3 = \tfrac{i\omega_3^2}{2k_3c^2}\chi^{(2)}_{eff}(-\omega_3;\omega_1,\omega_2)\,\mathcal{E}_1\mathcal{E}_2\,e^{i\Delta kz}. \tag{4.120}$$

Here $\mathcal{E}_j = \mathcal{E}(z,\omega_j)$, $k_j = k(\omega_j)$; we also introduced the wave number mismatch Δk

$$\Delta k = k_1 + k_2 - k_3. \tag{4.121}$$

Exercise 4.9. *Using general symmetry properties of the second-order susceptibilities, show that*

$$\chi^{(2)}_{eff}(-\omega_2;\omega_3,-\omega_1) = \chi^{(2)*}_{eff}(-\omega_3;\omega_1,\omega_2), \tag{4.122}$$

and

$$\chi^{(2)}_{eff}(-\omega_1;\omega_3,-\omega_2) = \chi^{(2)*}_{eff}(-\omega_3;\omega_1,\omega_2). \tag{4.123}$$

The situation is further simplified if we neglect diffraction by focusing on a plane wave geometry. In these circumstances and taking account of the properties (4.122) and (4.123) to drop arguments of $\chi^{(2)}_{eff}$, we can reduce Eqs. (4.118) – (4.120) to the set of ODEs in the form

$$\frac{d\mathcal{E}_1}{dz} = \frac{i\omega_1^2}{2k_1c^2}\chi^{(2)*}_{eff}\mathcal{E}_3\mathcal{E}_2^* e^{-i\Delta kz}, \tag{4.124}$$

$$\frac{d\mathcal{E}_2}{dz} = \frac{i\omega_2^2}{2k_2c^2}\chi^{(2)*}_{eff}\mathcal{E}_3\mathcal{E}_1^* e^{-i\Delta kz}, \tag{4.125}$$

$$\frac{d\mathcal{E}_3}{dz} = \frac{i\omega_3^2}{2k_3c^2}\chi_{eff}^{(2)}\mathcal{E}_1\mathcal{E}_2 e^{i\Delta kz}. \tag{4.126}$$

Although Eqs. (4.124) – (4.126) can be solved in general, the solution is very complicated and not too instructive. Instead, we will study the SFG process in the so-called *undepleted pump approximation*, i.e, when the amplitude of the pump wave $\mathcal{E}_2$ is so much larger than those of the other waves that we can neglect the pump depletion – that is we will assume $\mathcal{E}_2 = const$ – which enables us to rewrite Eqs. (4.124) – (4.126) as

$$\frac{d\mathcal{E}_1}{dz} = \kappa_1\mathcal{E}_3 e^{-i\Delta kz}, \tag{4.127}$$

and

$$\frac{d\mathcal{E}_3}{dz} = \kappa_3\mathcal{E}_1 e^{i\Delta kz}. \tag{4.128}$$

Here we introduced the notations

$$\kappa_1 = \frac{i\omega_1^2\chi_{eff}^{(2)*}}{2k_1c^2}\mathcal{E}_2^*, \qquad \kappa_3 = \frac{i\omega_3^2\chi_{eff}^{(2)}}{2k_3c^2}\mathcal{E}_2. \tag{4.129}$$

Let us then assume perfect phase matching, $\Delta k = 0$. In this case, we can eliminate one of the fields from Eqs. (4.127) and (4.128) in favor of the other, reducing the set to a second-order ODE; for instance,

$$\frac{d^2\mathcal{E}_1}{dz^2} + \kappa_{eff}^2\mathcal{E}_1 = 0, \tag{4.130}$$

with

$$\kappa_{eff}^2 = -\kappa_1\kappa_3 = \frac{\omega_1^2\omega_3^2|\chi_{eff}^{(2)}|^2|\mathcal{E}_2|^2}{4k_1k_3c^4}. \tag{4.131}$$

A general solution to (4.130) is

$$\mathcal{E}_1 = C_1\cos\kappa_{eff}z + C_2\sin\kappa_{eff}z, \tag{4.132}$$

where C_1 and C_2 are arbitrary constants. It then follows from Eqs. (4.127), (4.128) and (4.132) that

$$\mathcal{E}_3 = -\frac{\kappa_{eff}C_1}{\kappa_1}\sin\kappa_{eff}z + \frac{\kappa_{eff}C_2}{\kappa_1}\cos\kappa_{eff}z. \tag{4.133}$$

Specifying the initial conditions, $\mathcal{E}_1(z=0) = \mathcal{E}_1(0)$ and $\mathcal{E}_3(z=0) = 0$ – there is no SF at the entrance to the medium – we obtain the expressions for the signal and the SF waves as

$$\mathcal{E}_1 = \mathcal{E}_1(0)\cos\kappa_{eff}z, \tag{4.134}$$

and

$$\mathcal{E}_3 = -\mathcal{E}_1(0)\frac{\kappa_{eff}}{\kappa_1}\sin\kappa_{eff}z, \tag{4.135}$$

In physical terms, the SFG in the undepleted pump approximation describes periodic power exchange between the signal and the SF waves. The periodic character of the

power exchange between the signal and the SF can be explained by observing that to create an SF photon, a signal photon has to be annihilated, $\omega_3 = \omega_1 + \omega_2$, such that the more the power residing with the SF, the less the power of the signal and vice versa.

Exercise 4.10. *Solve Eqs. (4.127) and (4.128) for $\Delta k \neq 0$ in the case when initially all power resides with ω_1 harmonic. Determine the SF intensity and show that its maximum reduces precipitously as Δk increases. Comment on the importance of phase matching for efficient SFG. Hint: look for solutions in the form*

$$\mathcal{E}_1 = \mathcal{A}_1 e^{-i\Delta k z/2}, \qquad \mathcal{E}_3 = \mathcal{A}_3 e^{i\Delta k z/2}, \tag{4.136}$$

and show that (4.127) and (4.128) reduce to homogeneous equations

$$\frac{d\mathcal{A}_1}{dz} = \frac{i\Delta k}{2}\mathcal{A}_1 + \kappa_1 \mathcal{A}_3, \tag{4.137}$$

and

$$\frac{d\mathcal{A}_3}{dz} = -\frac{i\Delta k}{2}\mathcal{A}_3 + \kappa_3 \mathcal{A}_1, \tag{4.138}$$

which can be solved by usual methods.

4.6.2 Manley-Rowe relations

Consider now the SFG in a lossless medium such that

$$\chi^{(2)}_{eff} = \chi^{(2)*}_{eff}. \tag{4.139}$$

The wave equations in the plane wave geometry, (4.124) – (4.126), can then be cast into the form

$$\frac{d\mathcal{E}_1}{dz} = \frac{i\omega_1^2}{2k_1 c^2}\chi^{(2)}_{eff}\mathcal{E}_3\mathcal{E}_2^* e^{-i\Delta k z}, \tag{4.140}$$

$$\frac{d\mathcal{E}_2}{dz} = \frac{i\omega_2^2}{2k_2 c^2}\chi^{(2)}_{eff}\mathcal{E}_3\mathcal{E}_1^* e^{-i\Delta k z}, \tag{4.141}$$

and

$$\frac{d\mathcal{E}_3}{dz} = \frac{i\omega_3^2}{2k_3 c^2}\chi^{(2)}_{eff}\mathcal{E}_1\mathcal{E}_2 e^{i\Delta k z}. \tag{4.142}$$

Let us now study relations among the energy fluxes associated with the mixing waves. To this end, we derive the following equations for the wave intensities

$$\frac{d|\mathcal{E}_1|^2}{dz} = \frac{\omega_1}{n_1 c}\chi^{(2)}_{eff}\mathrm{Im}(\mathcal{E}_1^*\mathcal{E}_2^*\mathcal{E}_3 e^{i\Delta k z}), \tag{4.143}$$

$$\frac{d|\mathcal{E}_2|^2}{dz} = \frac{\omega_2}{n_2 c}\chi^{(2)}_{eff}\mathrm{Im}(\mathcal{E}_1^*\mathcal{E}_2^*\mathcal{E}_3 e^{i\Delta k z}), \tag{4.144}$$

$$\frac{d|\mathcal{E}_3|^2}{dz} = -\frac{\omega_3}{n_3 c^2}\chi^{(2)}_{eff}\mathrm{Im}(\mathcal{E}_1^*\mathcal{E}_2^*\mathcal{E}_3 e^{i\Delta k z}), \tag{4.145}$$

where we introduced $k_j = n_j\omega_j/c$.

Further, we introduce the optical intensities of the signal, pump and the SF waves as

$$I_j = \frac{\epsilon_0 n_j c}{2}|\mathcal{E}_j|^2, \tag{4.146}$$

with $j = 1, 2, 3$. It can then be inferred from Eqs. (4.143) – (4.146) that

$$\frac{dI_1}{dz} = \frac{\epsilon_0 \omega_1}{2}\chi^{(2)}_{eff}\mathrm{Im}(\mathcal{E}_1\mathcal{E}_2\mathcal{E}_3^* e^{i\Delta kz}), \tag{4.147}$$

and

$$\frac{dI_2}{dz} = \frac{\epsilon_0 \omega_2}{2}\chi^{(2)}_{eff}\mathrm{Im}(\mathcal{E}_1\mathcal{E}_2\mathcal{E}_3^* e^{i\Delta kz}), \tag{4.148}$$

as well as

$$\frac{dI_3}{dz} = -\frac{\epsilon_0 \omega_3}{2}\chi^{(2)}_{eff}\mathrm{Im}(\mathcal{E}_1\mathcal{E}_2\mathcal{E}_3^* e^{i\Delta kz}). \tag{4.149}$$

It follows at once by adding Eqs. (4.147), (4.148) and (4.149) that

$$\sum_{j=1}^{3} I_j = const, \tag{4.150}$$

which is tantamount to energy conservation for the SFG in lossless media. We can also infer from Eqs. (4.147) – (4.149) that

$$\frac{d}{dz}\left(\frac{I_1}{\omega_1} - \frac{I_2}{\omega_2}\right) = 0, \tag{4.151}$$

$$\frac{d}{dz}\left(\frac{I_1}{\omega_1} + \frac{I_3}{\omega_3}\right) = 0, \tag{4.152}$$

and

$$\frac{d}{dz}\left(\frac{I_2}{\omega_2} + \frac{I_3}{\omega_3}\right) = 0. \tag{4.153}$$

The preceding differential laws are equivalent to the three new invariants for the SFG process, which are known as the Manley-Rowe relations; the latter take the form

$$\frac{I_1}{\omega_1} - \frac{I_2}{\omega_2} = \mathcal{M}_1 = const, \tag{4.154}$$

$$\frac{I_1}{\omega_1} + \frac{I_3}{\omega_3} = \mathcal{M}_2 = const, \tag{4.155}$$

$$\frac{I_2}{\omega_2} + \frac{I_3}{\omega_3} = \mathcal{M}_3 = const. \tag{4.156}$$

The physical interpretation of Eqs. (4.154) – (4.156) can be best furnished using the photon picture. To this end, one can introduce the photon number fluxes – the number of photons at frequency ω_j created or annihilated per second – by the expression, $N_j = I_j/\hbar\omega_j$. It then follows from Eq. (4.154) – (4.156) that the numbers of signal and idler photons generated per unit time in any SFG process must be separately equal to the number of pump photons destroyed per unit time. Summarizing, we can say that to generate one SF photon, a signal and a pump photon must be destroyed. The qualitative photon picture of the SFG is exhibited in the form of a simple three-photon diagram in Fig. 2.

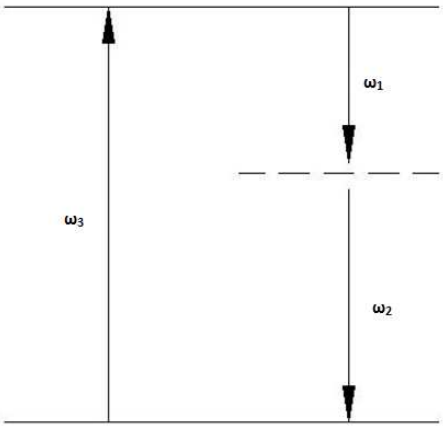

Figure 4.15: Illustrating Manley-Rowe relations with a photon diagram.

4.7 Difference-frequency generation (parametric down-conversion)

Let us now look into the difference-frequency generation (DFG), a second-order process of generating a difference frequency (DF) wave at frequency $\omega_3 = \omega_1 - \omega_2$ from the pump wave at frequency ω_1 and the idler wave at frequency ω_2 so named as its mere presence is required for realization of the process. The DF wave is often referred to as the signal. The DF generation is schematically illustrated in Fig. 1.

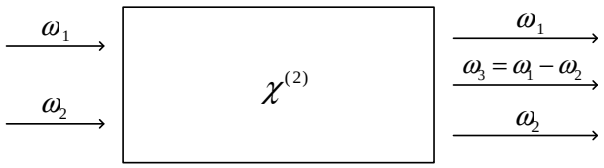

Figure 4.16: Schematic illustration of the difference-frequency generation process.

The paraxial wave equations governing DFG can be shown to take the form

$$\partial_z \mathcal{E}_1 = \tfrac{i\omega_1^2}{2k_1c^2}\chi^{(2)}_{eff}(-\omega_1;\omega_2,\omega_3)\mathcal{E}_2\mathcal{E}_3 e^{i\Delta kz}, \tag{4.157}$$

and

$$\partial_z \mathcal{E}_2 = \tfrac{i\omega_2^2}{2k_2c^2}\chi^{(2)}_{eff}(-\omega_2;\omega_1,-\omega_3)\mathcal{E}_1\mathcal{E}_3^* e^{-i\Delta kz}, \tag{4.158}$$

as well as

$$\partial_z \mathcal{E}_3 = \tfrac{i\omega_3^2}{2k_3c^2}\chi^{(2)}_{eff}(-\omega_3;\omega_1,-\omega_2)\,\mathcal{E}_1\mathcal{E}_2^*\, e^{-i\Delta kz}, \tag{4.159}$$

where the wave number mismatch is now defined as

$$\Delta k = k_1 - k_2 - k_3, \tag{4.160}$$

and the signal frequency is given by

$$\omega_3 = \omega_1 - \omega_2. \tag{4.161}$$

Using general symmetries of nonlinear susceptibilities it can be demonstrated that

$$\chi^{(2)}_{eff}(-\omega_3;\omega_1,-\omega_2) = \chi^{(2)*}_{eff}(-\omega_1;\omega_2,\omega_3) = \chi^{(2)}_{eff}(-\omega_2;\omega_1,-\omega_3). \tag{4.162}$$

It follows from Eqs. (4.157) – (4.159) and (4.162) that in the plane wave geometry, one can obtain the following set of DFG wave equations

$$\frac{d\mathcal{E}_1}{dz} = \frac{i\omega_1^2}{2k_1c^2}\chi^{(2)}_{eff}\mathcal{E}_2\mathcal{E}_3 e^{i\Delta kz}, \tag{4.163}$$

$$\frac{d\mathcal{E}_2}{dz} = \frac{i\omega_2^2}{2k_2c^2}\chi^{(2)*}_{eff}\mathcal{E}_1\mathcal{E}_3^* e^{-i\Delta kz}, \tag{4.164}$$

and

$$\frac{d\mathcal{E}_3}{dz} = \frac{i\omega_3^2}{2k_3c^2}\chi^{(2)*}_{eff}\mathcal{E}_1\mathcal{E}_2^* e^{-i\Delta kz}. \tag{4.165}$$

We will restrict ourselves to studying DFG in the undepleted pump approximation, $\mathcal{E}_1 = const$, implying that

$$\frac{d\mathcal{E}_2}{dz} = \zeta_2\mathcal{E}_3^* e^{-i\Delta kz}, \tag{4.166}$$

and

$$\frac{d\mathcal{E}_3}{dz} = \zeta_3\mathcal{E}_2^* e^{-i\Delta kz}. \tag{4.167}$$

Here we introduced the quantities

$$\zeta_j = \frac{i\omega_j^2}{2k_jc^2}\chi^{(2)*}_{eff}\mathcal{E}_1, \qquad\qquad j = 2,3. \tag{4.168}$$

Assuming, for simplicity, there is perfect phase matching, $\Delta k = 0$, we can reduce Eqs. (4.166) and (4.167) to

$$\frac{d^2\mathcal{E}_3}{dz^2} - \zeta^2_{eff}\mathcal{E}_3 = 0, \tag{4.169}$$

where

$$\zeta^2_{eff} = \frac{\omega_2^2\omega_3^2|\chi^{(2)}_{eff}|^2|\mathcal{E}_1|^2}{4k_2k_3c^4}. \tag{4.170}$$

A general solution to (4.169) is

$$\mathcal{E}_3(z) = D_1\cosh\zeta_{eff}z + D_2\sinh\zeta_{eff}z. \tag{4.171}$$

Stipulating that initially all power reside with the idler, $\mathcal{E}_3(z=0) = \mathcal{E}_3(0)$ and $\mathcal{E}_2(z=0) = 0$, yields the solution

$$\mathcal{E}_3(z) = \mathcal{E}_3(0)\cosh\zeta_{eff}z, \tag{4.172}$$

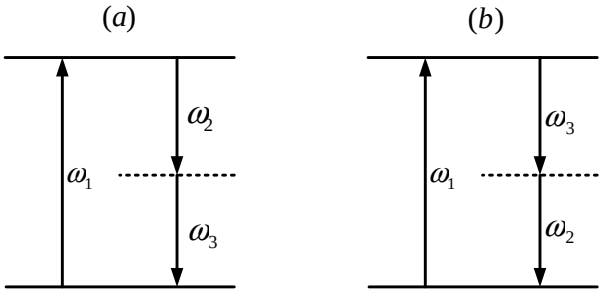

Figure 4.17: Schematic illustration of the difference-frequency generation process.

and

$$\mathcal{E}_2(z) = \frac{\zeta_{eff}\mathcal{E}_3^*(0)}{\zeta_3^*}\sinh\zeta_{eff}z. \tag{4.173}$$

It can be easily inferred from Eq. (4.172) and (4.173) that both the signal and the idler monotonically grow with the distance z. Such a behavior – which is in sharp contrast with the SFG – is graphically presented in the diagram in Fig. 2. To explain the diagram, it is sufficient to notice that in the DFG process, the signal and idler photons are created and annihilated in pairs, $\omega_1 = \omega_3 + \omega_2$. In other words, the greater the power of one wave – be it the signal or the idler – the greater the power of the other. The two possibilities are illustrated in Figs. 2(a) and 2(b), respectively.

We can show that the monotonic character of the signal and idler wave growth depends on the pump power level in case of finite mismatch $\Delta k \neq 0$. To this end, we transform Eqs. (4.166) and (4.167) to

$$\frac{d\mathcal{E}_2^*}{dz} = \zeta_2^*\mathcal{E}_3 e^{-i\Delta kz}. \tag{4.174}$$

$$\frac{d\mathcal{E}_3}{dz} = \zeta_3\mathcal{E}_2^* e^{-i\Delta kz}. \tag{4.175}$$

Introducing the new variables viz.,

$$\mathcal{E}_2^* = \overline{\mathcal{E}}_2 e^{i\Delta kz/2}, \qquad \mathcal{E}_3 = \overline{\mathcal{E}}_3 e^{-i\Delta kz/2}, \tag{4.176}$$

we arrive at the equations

$$\overline{\mathcal{E}}_2' + \tfrac{1}{2}i\Delta k\overline{\mathcal{E}}_2 = \zeta_2^*\overline{\mathcal{E}}_3, \tag{4.177}$$

and

$$\overline{\mathcal{E}}_3' - \tfrac{1}{2}i\Delta k\overline{\mathcal{E}}_2 = \zeta_3\overline{\mathcal{E}}_2. \tag{4.178}$$

Seeking solutions to Eqs. (4.177) and (4.178) in the form

$$\overline{\mathcal{E}}_2(z) = \overline{\mathcal{E}}_2^{(0)} e^{\Omega_{eff}z}; \qquad \overline{\mathcal{E}}_3(z) = \overline{\mathcal{E}}_3^{(0)} e^{\Omega_{eff}z}, \tag{4.179}$$

we obtain from the determinant condition, the expression for Ω_{eff}:

$$\Omega_{eff} = \sqrt{\zeta_{eff}^2 - (\Delta k/2)^2}. \tag{4.180}$$

The latter implies that in the presence of phase mismatch, there exists a power threshold for simultaneous amplification of the signal and idler modes,

$$I_{th} = \frac{2\epsilon_0 n_1 n_2 n_3 c^3}{\omega_2 \omega_3 |\chi^{(2)}_{eff}|^2} \left(\frac{\Delta k}{2}\right)^2. \tag{4.181}$$

Thus, for a given phase mismatch, the pump intensity must be greater than a certain critical value, $I_1 \geq I_{th}$, for parametric amplification to take place.

Next, general solutions for the idler and signal modes can be expressed above threshold as

$$\overline{\mathcal{E}}_2(z) = \mathcal{E}^*_2(0) \cosh \Omega_{eff} z + A \sinh \Omega_{eff} z, \tag{4.182}$$

and

$$\overline{\mathcal{E}}_3(z) = \mathcal{E}_3(0) \cosh \Omega_{eff} z + B \sinh \Omega_{eff} z. \tag{4.183}$$

Substituting from Eqs. (4.182) and (4.183) into Eqs. (4.177) and (4.178), we determine the coefficients A and B:

$$A = \frac{\zeta^*_2 \mathcal{E}_3(0) - \frac{1}{2}\Delta k \mathcal{E}^*_2(0)}{\Omega_{eff}}, \tag{4.184}$$

and

$$B = \frac{\zeta_3 \mathcal{E}^*_2(0) + \frac{1}{2}\Delta k \mathcal{E}_3(0)}{\Omega_{eff}}, \tag{4.185}$$

Finally, on substituting from Eqs. (4.184) and (4.185) into (4.182) and (4.183) we obtain, upon a slight rearrangement, the signal and idler fields in the form

$$\mathcal{E}_3(z) = \left[\mathcal{E}_3(0)\left(\cosh \Omega_{eff} z + \frac{i\Delta k}{2\Omega_{eff}} \sinh \Omega_{eff} z\right) + \frac{\zeta_3 \mathcal{E}^*_2(0)}{\Omega_{eff}} \sinh \Omega_{eff} z\right] e^{-i\Delta k z/2}, \tag{4.186}$$

and

$$\mathcal{E}_2(z) = \left[\mathcal{E}_2(0)\left(\cosh \Omega_{eff} z + \frac{i\Delta k}{2\Omega_{eff}} \sinh \Omega_{eff} z\right) + \frac{\zeta_2 \mathcal{E}^*_3(0)}{\Omega_{eff}} \sinh \Omega_{eff} z\right] e^{-i\Delta k z/2}. \tag{4.187}$$

Exercise 4.11. *Show that below threshold, the solutions can be obtained with the substitutions,*

$$\Omega_{eff} \to i\Omega_{eff}; \qquad \cosh i\Omega_{eff} z \to \cos \Omega_{eff} z, \qquad \sinh i\Omega_{eff} z \to i \sin \Omega_{eff} z,$$

yielding

$$\mathcal{E}_3(z) = \left[\mathcal{E}_3(0)\left(\cos \Omega_{eff} z + \frac{i\Delta k}{2\Omega_{eff}} \sin \Omega_{eff} z\right) + \frac{\zeta_3 \mathcal{E}^*_2(0)}{\Omega_{eff}} \sin \Omega_{eff} z\right] e^{-i\Delta k z/2},$$

and

$$\mathcal{E}_2(z) = \left[\mathcal{E}_2(0)\left(\cos \Omega_{eff} z + \frac{i\Delta k}{2\Omega_{eff}} \sin \Omega_{eff} z\right) + \frac{\zeta_2 \mathcal{E}^*_3(0)}{\Omega_{eff}} \sin \Omega_{eff} z\right] e^{-i\Delta k z/2}.$$

How can you reconcile the periodic power exchange between the signal and idler modes with the photon diagram of Fig. 2 demanding that signal and idler photons be created or annihilated in pairs?

The DFG process is also known as parametric down-conversion: A high-frequency pump photon generates a signal-idler photon pair at lower frequencies. It is the key process to generate a pair of entangled photons from a single pump photon in $\chi^{(2)}$ nonlinear media; the latter finds numerous applications in quantum optics.

Exercise 4.12. *Show that the Manley-Rowe relations for the DFG without the undepleted pump approximation take the form*

$$\frac{I_1}{\omega_1} + \frac{I_2}{\omega_2} = \mathcal{M}_1 = const,$$

$$\frac{I_1}{\omega_1} + \frac{I_3}{\omega_3} = \mathcal{M}_2 = const,$$

$$\frac{I_2}{\omega_2} - \frac{I_3}{\omega_3} = \mathcal{M}_3 = const.$$

and interpret your results using the photon diagram of Fig. 2.

4.8 Four-wave mixing: General considerations

In general, third-order nonlinear processes are much weaker than their second-order counterparts. For example, in solids the ratio of the third- to the second-order susceptibility is of the order of 10^{-9} m/V, implying that the fields as large as 10^3 MV/m are required to make the influence of the third-order nonlinearities felt in presence of the second-order ones. On the other hand, if the medium atoms do have the center of inversion, the third-order nonlinearity makes the dominant contribution to the nonlinear polarization. As most isotropic nonlinear media fall into this category, the third-order nonlinear interactions, involving mixing of four waves with, in general, different frequencies, are of the utmost importance both for our fundamental understanding of nonlinear optical processes and in potential applications. Quite generally, the third-order nonlinear processes are commonly referred to as *four-wave mixing*. We will study four-wave mixing in isotropic lossless media by deriving coupled wave equations describing the interaction of four quasi-monochromatic paraxial waves with different carrier frequencies. We will assume the beams to be linearly or circularly polarized. The electric field of a beam with the carrier frequency ω_s can be represented as

$$\tilde{\mathbf{E}}(z, \omega_s) = \mathbf{e}(\omega_s)\mathcal{E}(z, \omega_s)e^{ik_s z}. \tag{4.188}$$

Since a linearly –or circularly – polarized field maintains its state of polarization in an isotropic medium, the induced polarization field is then given by the expression

$$\tilde{\mathbf{P}}_{NL}(z, \omega_s) = \mathbf{e}(\omega_s)\mathcal{P}_{NL}(z, \omega_s)e^{ik_s z}, \tag{4.189}$$

where

$$k_s^2 = \epsilon(\omega_s)\tfrac{\omega_s^2}{c^2}. \tag{4.190}$$

The coupled nonlinear wave equations governing the field evolution can be expressed as

$$2ik_s\partial_z\mathcal{E}_s = -\mu_0\omega_s^2\mathcal{P}_{NL}. \tag{4.191}$$

Here we introduced the notation

$$\mathcal{E}_s \equiv \mathcal{E}(z,\omega_s). \tag{4.192}$$

Recall that the third-order polarization field can be expressed as

$$\begin{aligned}\tilde{P}_i^{(3)}(z,\omega_s) &= \epsilon_0 c^{(3)}(\omega_1,\omega_2,\omega_3)\sum_{jkl}\tilde{\chi}_{ijkl}^{(3)}(-\omega_s;\omega_1,\omega_2,\omega_3)\\ &\quad\times\tilde{E}_j(z,\omega_1)\tilde{E}_k(z,\omega_2)\tilde{E}_l(z,\omega_3),\end{aligned} \tag{4.193}$$

with $\omega_s = \omega_1+\omega_2+\omega_3$. Using Eqs. (4.193) and (4.189), we obtain for the slowly-varying third-order polarization field the expression

$$\begin{aligned}\mathcal{P}_i^{(3)}(z,\omega_s) &= \epsilon_0 c^{(3)}(\omega_1,\omega_2,\omega_3)\sum_{jkl}\tilde{\chi}_{ijkl}^{(3)}(-\omega_s;\omega_1,\omega_2,\omega_3)e_i(\omega_s)\\ &\quad\times e_j(\omega_1)e_k(\omega_2)e_l(\omega_3)\mathcal{E}(z,\omega_1)\mathcal{E}(z,\omega_2)\mathcal{E}(z,\omega_3)e^{i\Delta kz}\end{aligned} \tag{4.194}$$

where the phase mismatch is defined as

$$\Delta k \equiv k(\omega_1)+k(\omega_2)+k(\omega_3)-k(\omega_s). \tag{4.195}$$

Introducing the notation

$$\begin{aligned}\chi_{eff}^{(3)}(-\omega_s;\omega_1,\omega_2,\omega_3) &\equiv c^{(3)}(\omega_1,\omega_2,\omega_3)\sum_{ijkl}\tilde{\chi}_{ijkl}^{(3)}(-\omega_s;\omega_1,\omega_2,\omega_3)\\ &\quad\times\mathbf{e}_i(\omega_s)\mathbf{e}_j(\omega_1)\mathbf{e}_k(\omega_2)\mathbf{e}_l(\omega_3),\end{aligned} \tag{4.196}$$

we finally arrive at the paraxial wave equation governing the four-wave mixing processes

$$\partial_z\mathcal{E}_s = \tfrac{i\omega_s^2}{2k(\omega_s)c^2}\chi_{eff}^{(3)}(-\omega_s;\omega_1,\omega_2,\omega_3)\mathcal{E}_1\mathcal{E}_2\mathcal{E}_3e^{i\Delta kz}. \tag{4.197}$$

The family of third-order processes is very large; each particular process is specified by a choice of four mixing frequencies. In the following, we will only consider two commonly encountered processes: third-harmonic generation and self-focusing.

4.9 Third harmonic generation

Third harmonic generation (THG) is a process of producing a wave that oscillates at the frequency 3ω by mixing three waves, each having the same carrier frequency ω as is indicated in the diagram below.

The set of THG governing equations can be easily obtained from (4.197) to be

$$\partial_z\mathcal{E}_\omega = \tfrac{i\omega^2}{2k_\omega c^2}\chi_{eff}^{(3)}(-\omega;3\omega,-\omega,-\omega)\mathcal{E}_{3\omega}\mathcal{E}_\omega^{*2}e^{-i\Delta kz}. \tag{4.198}$$

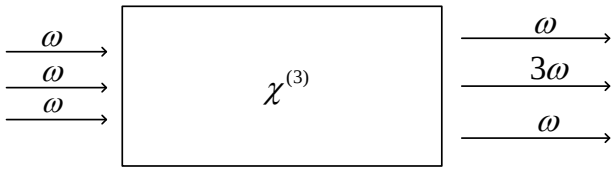

Figure 4.18: Illustrating the third harmonic generation.

and

$$\partial_z \mathcal{E}_{3\omega} = \frac{9i\omega^2}{2k_{3\omega}c^2}\chi^{(3)}_{eff}(-3\omega;\omega,\omega,\omega)\,\mathcal{E}^3_\omega\, e^{i\Delta kz}, \tag{4.199}$$

where the phase mismatch is given by

$$\Delta k = 3k(\omega) - k(3\omega). \tag{4.200}$$

The analysis reveals that the degeneracy factors associated with the corresponding mixing processes, $(3\omega = \omega + \omega + \omega)$ and $(\omega = 3\omega - \omega - \omega)$ are related as

$$c^{(3)}(3\omega,-\omega,-\omega) = 3c^{(3)}(\omega,\omega,\omega), \tag{4.201}$$

implying the relation between the effective susceptibilities as

$$\chi^{(3)}_{eff}(-\omega;3\omega,-\omega,-\omega) = 3\chi^{(3)}_{eff}(-3\omega;\omega,\omega,\omega) \equiv 3\chi^{(3)}_{eff} \tag{4.202}$$

Using Eq. (4.202) and assuming a plane wave geometry, we can transform the governing coupled wave equations, Eqs. (4.198) and (4.199), into the form

$$\frac{d\mathcal{E}_\omega}{dz} = \frac{3i\omega}{2n_\omega c}\chi^{(3)}_{eff}\,\mathcal{E}_{3\omega}\mathcal{E}^{*2}_\omega e^{-i\Delta kz}. \tag{4.203}$$

and

$$\frac{d\mathcal{E}_{3\omega}}{dz} = \frac{3i\omega}{2n_{3\omega}c}\chi^{(3)}_{eff}\,\mathcal{E}^3_\omega\, e^{i\Delta kz}. \tag{4.204}$$

The last equations are very similar to those describing second harmonic generation. Unfortunately, though, third harmonic generation is a rather weak process. Therefore relatively high optical intensities are required to generate THG in a crystal with a reasonable efficiency. To estimate the THG efficiency, we consider the THG process in the undepleted pump approximation, $\mathcal{E}_\omega = const$. Under these conditions, equations (4.203) and (4.204) can be easily integrated to give an expression for the third harmonic field in the form

$$\mathcal{E}_{3\omega}(L) = \frac{i3\omega}{2n_{3\omega}c}\chi^{(3)}_{eff}\mathcal{E}^3_\omega e^{i\Delta kL/2}\text{sinc}(\Delta kL/2). \tag{4.205}$$

In complete analogy with the SHG theory, we introduce the THG efficiency by the expression

$$\eta_{THG} = \frac{I_{3\omega}(L)}{I_\omega(0)}. \tag{4.206}$$

It follows from Eqs. (4.205) and (4.206), assuming perfect phase matching that in the undepleted pump approximation,

$$\eta_{THG} = 36\pi^2 \left(\frac{L}{\lambda}\right)^2 \frac{\chi_{eff}^{(3)2} I_\omega^2}{n_{3\omega} n_\omega^3 \epsilon_0^2 c^2}. \tag{4.207}$$

Even if we assume the fundamental field intensity is as large as a typical breakdown intensity in solids, $I \sim 100$ MW/cm^2 and take realistic values of the other parameters: $L \sim 1$ cm, $n_\omega \sim n_{3\omega} \sim 1.5$, $\lambda \sim 5 \times 10^{-5}$ cm, and $\chi_{eff}^{(3)} \sim 10^{-21}$ m^2/W^2, we arrive at an estimate

$$\eta_{THG} \sim 5 \times 10^{-7} \ll 1, \tag{4.208}$$

which is tiny for all practical purposes. Moreover, it is hard to achieve phase matching in crystals; all of which effectively precludes the laboratory THG realization in most solid media.

However, THG can be generated in gases, such as sodium or rubidium vapors, in the vicinity of an optical resonance where the magnitude of $\chi^{(3)}$ is significantly enhanced. Unfortunately, such an enhancement is, in general, accompanied by the increase in linear as well as nonlinear absorption that must also be reckoned with whenever third harmonic generation in gases is attempted. As linear absorption dominates at resonance, the best way to boost the THG efficiency is to tune the laser to a two-photon resonance as is indicated in Fig. 2(a).

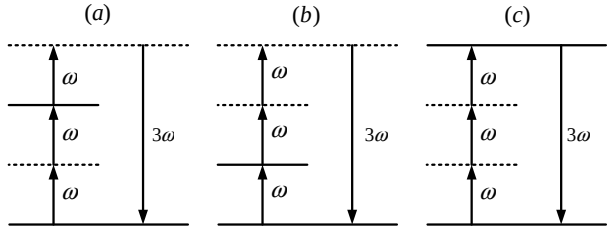

Figure 4.19: Illustrating the third-harmonic generation in gases under resonant excitation conditions. The laser is tuned to either two- or one- or else three-photon resonance in parts (a), (b) and (c), respectively.

4.10 Self-focusing, nonlinear absorption, and spatial solitons

Whenever a light beam propagates inside a nonlinear medium whose refractive index depends on the beam intensity, the light rays near the beam center, where the intensity is the highest, experience stronger refraction – assuming the nonlinear refractive index of the medium increases with the intensity – causing the rays to bend toward the center. As a result, the intensity increases toward the beam center on propagation in the medium. The light evolution looks as if the rays were focused by a positive lens

toward the beam center. Such a behavior is termed *self-focusing* of light in a nonlinear medium, and the medium with a positive nonlinear refractive index forming a focusing lens, self-focusing. As a consequence of self-focusing, the beam narrows and its peak intensity is enhanced with the propagation distance. On the other hand, every beam tends to spread due to diffraction which tends to decrease light intensity at the center. The two opposing trends are characterized by different spatial scales. We can easily estimate such scales – referred to as nonlinear and diffraction lengths, respectively – from elementary considerations. The characteristic diffraction length was defined before in the studies of Gaussian beam diffraction in free space:

$$L_D \simeq k w_0^2, \tag{4.209}$$

where $k = n_0\omega/c$, ω being the carrier frequency of the beam.

On the other hand, the intensity-dependent nonlinear refractive index modulates the optical phase of the beam electric field. This phenomenon is known as the *self-phase modulation*. Further, due to coupling of the intensity and phase dynamics of the field in nonlinear media, the change in the phase of the optical field induces modifications of the beam intensity profile. The influence of nonlinearity becomes important over distances such that the phase accretion is of the order of, at least, one radian, i. e.,

$$k\Delta n_{NL} L_{NL} \sim 1, \tag{4.210}$$

where the nonlinear change in the refractive index Δn_{NL} can be estimated using the peak intensity of the beam as

$$\Delta n_{NL} \sim \overline{n}_2 I_0. \tag{4.211}$$

Here I_0 is the peak intensity and $\overline{n}_2 > 0$ is a nonlinear refractive index coefficient to be discussed in greater detail below. It follows from Eqs. (4.210) and (4.211) that

$$L_{NL} \sim \frac{1}{k\overline{n}_2 I_0}. \tag{4.212}$$

The beam evolution scenario entirely depends on the relative sizes of the two characteristic lengths. In particular, if $L_D < L_{NL}$, diffraction dominates, and the beam spreads. However, if the diffraction and nonlinearity operate at the characteristic scales of the same order, exact balance of the two opposing trends is possible, leading to the formation of *spatial solitons*, i. e., the beams whose spatial profiles and widths do not change upon propagation in self-focusing nonlinear media. A soliton can be formed if the optical power of the beam is exactly equal to a certain critical power such that the nonlinearity can arrest diffraction-induced spreading. We can estimate the critical power necessary for soliton formation by imposing the balance condition

$$L_D \simeq L_{NL}. \tag{4.213}$$

It follows at once from Eqs. (4.209), (4.212) and (4.213) that the critical power, $P_{cr} = I_{cr}\pi w_0^2$ is given by

$$P_{cr} \simeq \frac{\lambda_0^2}{4\pi n_0 \overline{n}_2}, \tag{4.214}$$

where $\lambda_0 = 2\pi/k_0 = 2\pi c/\omega$.

Exercise 4.13. *The magnitude of the nonlinear refractive index for carbon disulfide (CS_2) is $\overline{n}_2 \simeq 3 \times 10^{-14}$ cm^2/W, the linear refractive index is equal to 1.63. Estimate the critical power for spatial soliton formation at $\lambda_0 \simeq 1$ μm. Compare your results with P_{cr} for silica glass for which $\overline{n}_2 \simeq 5 \times 10^{-16}$ cm^2/W, and $n_0 \simeq 1.4$.*

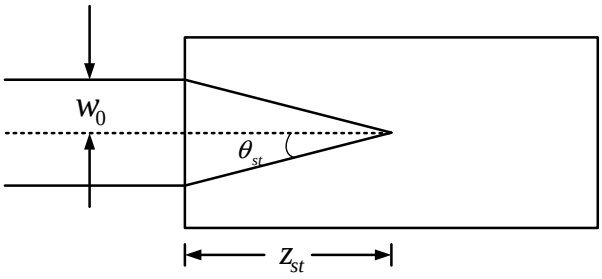

Figure 4.20: Illustrating the focal length in the self-focusing regime.

If the characteristic nonlinear length is smaller than the diffraction length, the nonlinearity prevails, causing self-focusing of the beam. One can estimate a characteristic self-focusing distance in the limit $L_{NL} \ll L_D$. In this case, diffraction is negligible, and geometrical optics approach would suffice for a rough estimate. According to Fermat's principle, any ray traveling from the wavefront up to the focusing point must traverse the same optical path, $\int dsn(s) = const$. As a result, we obtain for the paths exhibited in Fig. 3,

$$(n_0 + \delta n)z_f = \left(n_0 + \frac{\delta n}{2}\right)\sqrt{z_f^2 + w_0^2} \simeq n_0 z_f \left(1 + \frac{\delta n}{2n_0}\right)\left(1 + \frac{w_0^2}{2z_f^2}\right), \quad (4.215)$$

where we have assumed that the refractive index along the central ray is $n_0 + \delta n$, whereas the peripheral ray experiences the refractive index strength of roughly $n_0 + \delta n/2$. It then follows from (4.215) after simple algebra that the self-focusing distance is

$$z_f \simeq w_0\sqrt{\frac{n_0}{\delta n}} \simeq w_0\sqrt{\frac{n_0}{\overline{n}_2 I_0}}. \quad (4.216)$$

Finally, using the expressions for the beam power and the critical power as

$$P = I\pi w_0^2, \qquad P_{cr} = I_0\pi w_0^2, \quad (4.217)$$

we obtain the estimate

$$z_f \simeq \frac{L_D}{2}\sqrt{\frac{P_{cr}n_0}{P}}, \qquad P \gg P_{cr}. \quad (4.218)$$

Note that our approximate result (4.218) is consistent with our premise that diffraction is negligible, $z_f \ll L_D$ in the given power range. In reality, high-power optical beams, $P \gg P_{cr}$, will disintegrate into multiple filaments, each carrying approximately the

power of P_{cr}, long before the self-focusing distance is reached. The filamentation is caused by a transverse instability resulting from the growth of tiny imperfections of the beam wave front.

To quantitatively describe self-focusing, nonlinear absorption, and and soliton formation, we can derive the nonlinear wave equation corresponding to the self-action process by a fundamental wave of frequency ω. Mathematically, the corresponding susceptibility tensor is $\boldsymbol{\chi}^{(3)}(-\omega;\omega,-\omega,\omega)$. The resulting equation takes the form

$$\partial_z \mathcal{E}_\omega - \tfrac{i}{2k_\omega}\nabla_\perp^2 \mathcal{E}_\omega = \tfrac{i\omega^2}{2k_\omega c^2}\chi^{(3)}(\omega)|\mathcal{E}_\omega|^2\mathcal{E}_\omega, \tag{4.219}$$

where we have introduced the quantities

$$\chi^{(3)}(\omega) = \frac{3}{4}\chi^{(3)}_{eff}(-\omega;\omega,-\omega,\omega), \tag{4.220}$$

and

$$\chi^{(3)}_{eff}(-\omega;\omega,-\omega,\omega) \equiv \sum_{ijkl}\tilde{\chi}^{(3)}_{ijkl}(-\omega;\omega,-\omega,\omega)\mathbf{e}_i(\omega)\mathbf{e}_j(\omega)\mathbf{e}_k(\omega)\mathbf{e}_l(\omega). \tag{4.221}$$

Notice that there is no phase mismatch involved in the process of self-focusing, $\Delta k = k(\omega) + k(-\omega) + k(\omega) - k(\omega) = 0$, because $k(-\omega) = -k(\omega)$ in lossless media. Physically, this is the consequence of the fact that there is only one fundamental wave involved in the process which implies automatic conservation of the energy and momenta at the photon level.

Let us now focus on the situation when $L_{NL} \ll L_D$ such that diffraction effects can be neglected. Mathematically, the absence of diffraction effects implies that the second term on the l. h. s. of Eq. (4.219) can be dropped leading to

$$\partial_z \mathcal{E}_\omega = \tfrac{i\omega^2}{2k_\omega c^2}\chi^{(3)}(\omega)|\mathcal{E}_\omega|^2\mathcal{E}_\omega. \tag{4.222}$$

Recall that we assumed the medium to be transparent. We now lift that restriction by allowing for linear and nonlinear losses in the medium. In physical terms, linear losses lead to exponential decay of the field amplitude as we saw in Sec. 2. 2 with a decrement $\alpha/2$ determined by the imaginary part of the complex refractive index. Mathematically, linear losses can then be easily incorporated into Eq. (4.222) introducing the transformation

$$\mathcal{E}_\omega = \tilde{\mathcal{E}}_\omega\, e^{-\alpha(\omega)z/2}, \tag{4.223}$$

implying that

$$\partial_z \tilde{\mathcal{E}}_\omega = \tfrac{i\omega^2}{2k_\omega c^2}\chi^{(3)}(\omega)e^{-\alpha(\omega)z}\,|\tilde{\mathcal{E}}_\omega|^2\tilde{\mathcal{E}}_\omega. \tag{4.224}$$

Nonlinear losses are accounted for by assuming a complex $\chi^{(3)}$ such that

$$\chi^{(3)}(\omega) = \chi^{(3)}_r(\omega) + i\chi^{(3)}_i(\omega). \tag{4.225}$$

Next, introducing the amplitude and phase of $\mathcal{E}_\omega$ viz., $\mathcal{E}_\omega = |\mathcal{E}_\omega|e^{i\Phi_\omega}$, and separating real and imaginary parts in Eq. (4.224), we arrive at

$$\partial_z \Phi = \tfrac{3k_0\chi^{(3)}_r}{8n_0}|\tilde{\mathcal{E}}|^2 e^{-\alpha z}, \tag{4.226}$$

and

$$\partial_z|\tilde{\mathcal{E}}| = -\frac{3k_0\chi_i^{(3)}}{8n_0}|\tilde{\mathcal{E}}|^3 e^{-\alpha z}. \tag{4.227}$$

Here we dropped frequency subscripts, for notational simplicity, introduced $k_0 = \omega/c$, $k_\omega \simeq k_0 n_0$, where n_0 is the real part of the linear refractive index, and assumed linear losses to be sufficiently weak, $\alpha(\omega) \ll k_\omega$ which is a reasonably good assumption at optical frequencies far from any internal resonances of the medium. It is customary to introduce the optical intensity,

$$\tilde{I} = \frac{\epsilon_0 n_0 c}{2}|\tilde{\mathcal{E}}|^2. \tag{4.228}$$

It then follows that

$$\partial_z\Phi = k_0\overline{n}_2\tilde{I}e^{-\alpha z}, \tag{4.229}$$

and

$$\partial_z\tilde{I} = -\beta_2\tilde{I}^2 e^{-\alpha z}, \tag{4.230}$$

where we introduced the nonlinear refractive index $\overline{n}_2$ and the two-photon absorption (TPA) coefficient β_2 by the expressions

$$\overline{n}_2 = \frac{3\chi_r^{(3)}}{4\epsilon_0 n_0^2 c}, \tag{4.231}$$

and

$$\beta_2 = \frac{3k_0\chi_i^{(3)}}{2\epsilon_0 n_0^2 c}. \tag{4.232}$$

The two-photon coefficient is so called because the absorption rate on the r.h.s of Eq. (4.230) is proportional to the square of intensity, implying, in the photon picture, that two photons are absorbed in each elementary nonlinear absorption act as is depicted in Fig. 4.8. TPA processes play an important role in the optical excitation of semiconductor materials whenever the energy of a photon pair is greater than a semiconductor energy gap as is sketched in Fig. 4.21.

Integrating Eq. (4.230) with the initial condition, $I(\boldsymbol{\rho}, 0) = I_0(\boldsymbol{\rho})$ at the source, we obtain the beam intensity at any $z = const > 0$ as

$$I(\boldsymbol{\rho}, z) = \frac{I_0(\boldsymbol{\rho})e^{-\alpha z}}{1 + \beta_2 I_0(\boldsymbol{\rho})L_{\text{eff}}(z)}, \tag{4.233}$$

where the effective propagation length is defined as

$$L_{\text{eff}} = \frac{1}{\alpha}(1 - e^{-\alpha z}). \tag{4.234}$$

It can be inferred from Eq. (4.233) that the beam energy is monotonically decreasing on propagation in the medium.

The beam phase obeys the equation

$$\partial_z\Phi = \frac{k_0\overline{n}_2 I_0(\boldsymbol{\rho})e^{-\alpha z}}{1+\beta_2 I_0(\boldsymbol{\rho})L_{\text{eff}}(z)}. \tag{4.235}$$

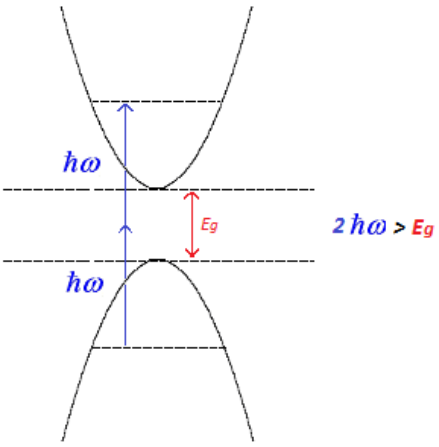

Figure 4.21: Illustrating two-photon absorption in direct-gap semiconductor materials. Photo-excitation is possible whenever $2\hbar\omega \geq E_g$, where E_g is the gap energy.

To gain a better qualitative understanding of beam phase behavior, let us restrict ourselves again to the transparent case, $\alpha = \beta_2 = 0$ and assume, for simplicity, the beam has a Gaussian intensity profile at the source,

$$I_0(\boldsymbol{\rho}) = I_0 \exp\left(-\frac{\rho^2}{2w_0^2}\right). \tag{4.236}$$

In most practical situations the nonlinear refractive index is quite small. Assuming further the medium sample thickness to be small as well–this is referred to as a thin sample approximation–the resulting nonlinear phase shift can be evaluated by expanding the Gaussian envelope in Eq. (4.236) in a Taylor series to the first order. On substituting the resulting expansion into Eq. (4.235) and integrating, we obtain the nonlinear shift

$$\Delta\Phi(\rho) \simeq -\frac{k_0\overline{n}_2 I_0\rho^2}{2w_0^2}\Delta L, \tag{4.237}$$

where ΔL is a medium sample thickness. On comparing this expression with a quadratic phase acquired by a diffracting Gaussian beam, we can conclude that the transparent nonlinear medium works as a thin lens, imparting a quadratic phase shift on a beam wavefront. The latter corresponds to a converging spherical wave for $\overline{n}_2 > 0$ causing self-focusing of the beam, or a diverging spherical wave in the self-defocusing case, $\overline{n}_2 < 0$. The self-focusing case is sketched in Fig. 4.22.

To explain the identification of $\overline{n}_2$ with a nonlinear refractive index, we shall consider the polarization field. To this end, we assume, for simplicity, a transparent medium and linear polarization of the beam – such that any polarization effects can be ignored – and introduce the scalar polarization field $\mathcal{P}_{tot} \equiv \mathcal{P}_i e_i$, by the expression

$$\mathcal{P}_{tot} = \epsilon_0\left(\chi^{(1)}\mathcal{E} + \frac{3}{4}\chi^{(3)}|\mathcal{E}|^2\mathcal{E}\right) = \epsilon_0\chi_{tot}\mathcal{E}, \tag{4.238}$$

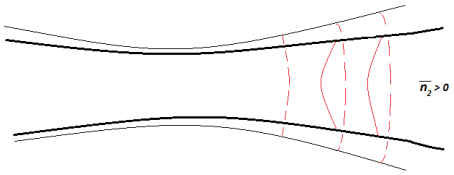

Figure 4.22: Self-phase modulation in self-focusing nonlinear media resulting in the extra beam focusing, the so-called nonlinear lens effect.

where the total susceptibility is given by

$$\chi_{tot} = \chi^{(1)} + \frac{3}{4}\chi^{(3)}|\mathcal{E}|^2. \tag{4.239}$$

We can then defines the total refractive index as

$$n^2 = 1 + \chi_{tot}, \tag{4.240}$$

and the nonlinear refractive index by the expression

$$n = n_0 + n_2|\mathcal{E}|^2. \tag{4.241}$$

It follows from Eq. (4.239) and (4.240) and the fact that the nonlinear refraction is always a small effect as compared with the linear one that

$$(n_0 + n_2|\mathcal{E}|^2)^2 \simeq n_0^2 + 2n_0 n_2|\mathcal{E}|^2. \tag{4.242}$$

On comparing Eqs. (4.239) and (4.242), we infer that

$$n_2 = \frac{3\chi^{(3)}}{8n_0}, \tag{4.243}$$

which provides a relation between the third-order susceptibility and the nonlinear refractive index.

The nonlinear refractive index associated with the optical intensity is introduced viz.,

$$n = n_0 + \overline{n}_2 I, \tag{4.244}$$

The nonlinear refractive index n_2 has the units of m^2/V^2 whereas the other one, $\overline{n}_2$, is measured in m^2/W^2. The two indices are related as

$$\overline{n}_2 = \frac{2}{\epsilon_0 n_0 c} n_2. \tag{4.245}$$

It follows from Eqs. (4.243), (4.244) and (4.245) that $\overline{n}_2$ is given by Eq. (4.231) with $\chi_r^{(3)} = \chi^{(3)}$ in the transparent case, and hence its identification with the nonlinear refractive index.

The nonlinear wave equation for self-focusing in a transparent medium can be rewritten as

$$i\partial_z\mathcal{E} + \tfrac{1}{2k}\nabla_\perp^2\mathcal{E} + \tfrac{kn_2}{n_0}|\mathcal{E}|^2\mathcal{E} = 0. \tag{4.246}$$

Equation (4.246) is referred to as the *nonlinear Schrödinger equation* (NLSE) because of its formal similarity with the Schrödinger equation in quantum mechanics. We can now introduce dimensionless variables, $Z = z/L_D$, $U = \mathcal{E}/\mathcal{E}_0$, $\mathbf{R}_\perp = \mathbf{r}_\perp/w_0$, $\mathcal{E}_0 = (2I_0/\epsilon_0 c n_0)^{1/2}$, and transform the NLSE to the dimensionless form

$$i\partial_Z U + \tfrac{1}{2}\nabla_\perp^2 U + \mathcal{N}^2|U|^2 U = 0. \tag{4.247}$$

Here we have introduced the only dimensionless parameter – the soliton parameter $\mathcal{N}$, governing the dynamics of the system. It is defined as follows

$$\mathcal{N}^2 \equiv \frac{L_D}{L_{NL}}, \tag{4.248}$$

where the diffraction and nonlinear lengths, L_D and L_{NL} are given by the expressions

$$L_D = k w_0^2, \qquad\qquad L_{NL} = \frac{1}{k\overline{n}_2 I_0}. \tag{4.249}$$

A numerical analysis of Eq. (4.247) confirms formation of a spatial soliton for the beam power such that $\mathcal{N} = 1$. However, the soliton turns out to be unstable with respect to small perturbations. Stable solitons can be formed in two-spatial dimensions, provided the saturation of nonlinear refractive index is allowed. Stable spatial solitons can be generated in Kerr-like nonlinear media in a planar waveguide geometry where trapping in one spatial dimension is realized by the nonlinear medium whereas the other spatial dimension is trapped by the waveguide. The dimensionless NLSE in the planar waveguide geometry takes the form

$$i\partial_Z U + \tfrac{1}{2}\partial_{XX}^2 U + \mathcal{N}^2|U|^2 U = 0. \tag{4.250}$$

The lowest order soliton corresponds to the exact balance between the nonlinearity and diffraction, $\mathcal{N} = 1$, and its spatial profile is given by

$$U(Z, X) = \text{sech}\, X\, e^{-iZ/2}. \tag{4.251}$$

Higher-order solitons also exist. They correspond to more intense beams, $\mathcal{N} > 1$. In such cases, the nonlinearity dominates at first, causing self-focusing of the beam. However, in $(1+1)$D geometry – indicating one transverse dimension plus one dimension along the waveguide unaffected by the waveguide trapping – the initial self-focusing can be slowed down and eventually reversed by increased diffraction of a more tightly focused beam. As a result, the periodic pattern of contraction and expansion of the soliton manifests itself, with the soliton returning to its initial shape and transverse size every half-period. Such solitons are called optical breathers. An example of a breather is displayed in Fig. 4(b) for $\mathcal{N} = 3$.

Exercise 4.14. *Show that the 1D NLSE is invariant with respect to the Galilean transformation,*

$$X' = X - vZ; \qquad Z' = Z,$$

for an arbitrary speed v. In other words, demonstrate that Eq. (4.250) has the same form in the "primed" variables, provided the fields in the two coordinate systems are related by a gauge transformation,

$$U(Z, X) = V(Z', X')e^{if(Z', X')}.$$

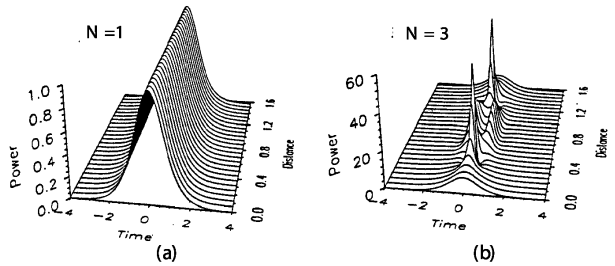

Figure 4.23: Intensity of the fundamental (a) and the third-order (b) soliton as function of the propagation distance.

Determine the phase f. Draw conclusions about the functional form of a moving soliton field.

4.11 Z-scan measurement of nonlinear refractive index

The so-called $z-$scan technique for nonlinear refractive index measurement is based on examining self-focusing (defocusing) of a Gaussian light beam transmitted through a thin nonlinear sample. If the sample is placed behind the beam focal plane, the self-

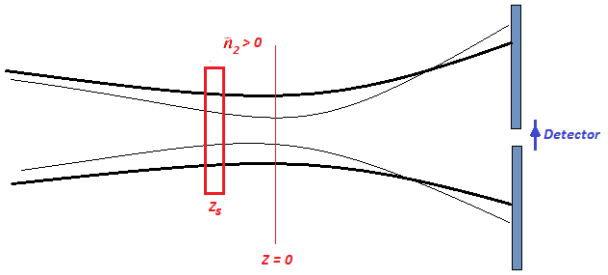

Figure 4.24: Schematic illustration of the z-scan experimental arrangement. The self-focusing sample is placed behind beam focus.

focusing medium causes additional focusing of the beam and hence a stronger beam divergence past the focal plane. Therefore, the fraction of the beam power passing through a detector pinhole on the axis reduces. Thus, the on-axis beam intensity at the detector decreases. The situation is depicted in Fig. 4.24. On the other hand, if the sample is placed in front of the focal plane, the additional focusing due to the nonlinear medium results in the increased power fraction captured by the on-axis detector and hence the on-axis intensity increase as is seen in Fig. 4.25. In practice, the on-axis intensity is always normalized to its magnitude in the absence of the sample, yielding a transmittance. The latter is greater than one for the in-front-of-the-focus sample position and less than one for the behind-the-focus position. The situation is reversed for a self-defocusing nonlinear sample.

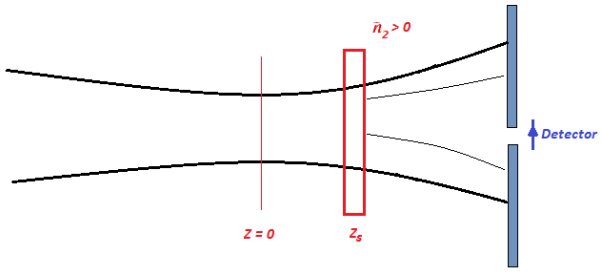

Figure 4.25: Schematic illustration of the z-scan experimental arrangement. The self-focusing sample is placed in front of the beam focus.

To develop a quantitative theory, let us recall Gaussian beam characteristics in free space. A straightforward generalization of the results of Sec.3.1. to two-dimensional beams yields the field profile in any transverse plane as

$$\mathcal{E}(\boldsymbol{\rho}, z) = \frac{\mathcal{E}_0}{(1+i\zeta)} \exp\left[-\frac{\rho^2}{2w_0^2(1+i\zeta)}\right], \tag{4.252}$$

where we introduced dimensionless variables in terms of the Rayleigh range z_R as

$$\zeta = z/z_R, \qquad z_R = kw_0^2. \tag{4.253}$$

The Gaussian beam field can be cast into the form

$$\mathcal{E}(\rho, z) = \mathcal{E}_0 \left[\frac{w_0}{w(z)}\right] e^{i\Phi(z)} \exp\left[\frac{ik\rho^2}{2R(z)}\right] \exp\left[-\frac{\rho^2}{2w^2(z)}\right]. \tag{4.254}$$

Here we introduced the beam width $w(z)$ as

$$w(z) = w_0\sqrt{1+z^2/z_R^2}, \tag{4.255}$$

the radius of the wavefront curvature $R(z)$,

$$R(z) = z(1+z_R^2/z^2), \tag{4.256}$$

and the accrued phase $\Phi(z)$,

$$\Phi(z) = -\arctan(z/z_R). \tag{4.257}$$

The freely propagating Gaussian beam intensity in the sample plane z_s can then be expressed as

$$I(\boldsymbol{\rho}, z_s) = \frac{I_0}{(1+z_s^2/z_R^2)} \exp\left[-\frac{\rho^2}{w_s^2}\right], \tag{4.258}$$

where $w_s \equiv w(z_s)$. It then follows from Eq. (4.229) that the phased picked up by a beam upon passing through a thin sample of length ΔL of a transparent nonlinear medium placed in the plane z_s is given by

$$\Delta\Phi_{NL}(\rho, \Delta L) = \frac{k_0\overline{n}_2 I_0 \Delta L}{(1+z_s^2/z_R^2)} \exp\left[-\frac{\rho^2}{w_s^2}\right], \tag{4.259}$$

where we assumed that $\Delta L \ll \min(z_s, z_R)$ (thin sample). The accrued nonlinear phase can be expressed through its value on the axis as

$$\Delta\Phi_{NL}(\rho, \Delta L) = \Delta\Phi_0 \exp\left[-\frac{\rho^2}{w_s^2}\right]. \tag{4.260}$$

The on-axis value can in turn be written in the form

$$\Delta\Phi_0 = \frac{\Delta\phi}{(1 + z_s^2/z_R^2)}, \tag{4.261}$$

where

$$\Delta\phi = k_0 \overline{n}_2 I_0 \Delta L. \tag{4.262}$$

is the on-axis phase shift for the sample placed in the focal plane, $z = 0$.

The Gaussian beam envelope emerging from the sample can then be written as

$$\mathcal{E}(\rho, z_s) = \mathcal{E}_s \exp\left[\frac{ik\rho^2}{2R_s}\right] \exp\left[-\frac{\rho^2}{2w_s^2}\right] \exp[i\Delta\Phi_{NL}(\rho, \Delta L)], \tag{4.263}$$

where $\Phi_s \equiv \Phi(z_s)$ and $R_s \equiv R(z_s)$ and we combined all factors independent on ρ into $\mathcal{E}_s$. Let us now expand the nonlinear phase shift term on the r.h.s. of Eq. (4.263) into a Taylor series and using Eqs. (4.260) though (4.262), we obtain

$$\exp[i\Delta\Phi_{NL}(\rho, \Delta L)] = \sum_{m=0}^{\infty} \frac{(i\Delta\Phi_0)^m}{m!} \exp\left[-\frac{m\rho^2}{w_s^2}\right]. \tag{4.264}$$

It follows from Eqs. (4.263) and (4.264) that the Gaussian beam envelope at the exit to the sample is then

$$\mathcal{E}(\rho, z_s) = \mathcal{E}_s \exp\left[\frac{ik\rho^2}{2R_s}\right] \sum_{m=0}^{\infty} \frac{(i\Delta\Phi_0)^m}{m!} \exp\left[-\frac{\rho^2}{2w_s^2}(1 + 2m)\right]. \tag{4.265}$$

Employing the Fourier transform technique discussed in Sec. 3.1, we can determine the beam envelope in the detector aperture plane, located a distance L_a away from the sample, in the form

$$\mathcal{E}(\rho, L_a) = \overline{\mathcal{E}}_s \sum_{m=0}^{\infty} \frac{(i\Delta\Phi_0)^m}{q_m m!} \exp\left(-\frac{\rho^2}{2q_m\sigma_m^2}\right), \tag{4.266}$$

where

$$\frac{1}{\sigma_m^2} = \frac{1 + 2m}{w_s^2} - \frac{ik}{R_s}, \tag{4.267}$$

and

$$q_m = 1 + \frac{L_a}{R_s} + \frac{i(1 + 2m)L_a}{z_R}. \tag{4.268}$$

Exercise. 4. 15. *Derive Eqs. (4.266) through (4.268).*
It follows from Eq. (4.266) that the beam envelope on the axis at the aperture location is then

$$\mathcal{E}(0, L_a) = \overline{\mathcal{E}}_s \sum_{m=0}^{\infty} \frac{(i\Delta\Phi_0)^m}{q_m m!}. \tag{4.269}$$

The actually measured quantity is the on-axis detector transmittance defined as

$$T(L_a, \Delta\phi) \equiv \frac{I(z_s + L_a, \rho = 0, \Delta\phi)}{I(z_s + L_a, \rho = 0, \Delta\phi = 0)}. \tag{4.270}$$

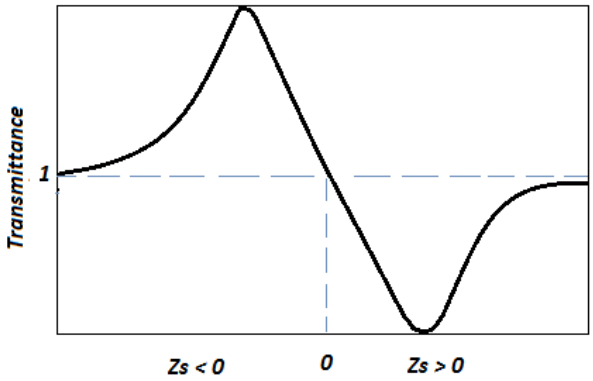

Figure 4.26: Typical transmittance curve in the z-scan experiment.

We assume that the detector aperture is placed in the far zone of the sample such that $L_a \gg z_R$ and the sample is placed sufficiently close to the focal plane of the beam, $z_s \ll z_R$ to ensure the beam divergence is not too large and there is enough power captured by the detector aperture to guarantee a reasonable signal-to-noise ratio. Next, the nonlinearity is typically small, implying the accumulated phase shifts $|\Delta\phi| \ll 1$. Therefore one can expand the r.h.s. of Eq. (4.269) in a Taylor series and keeping the lowest nontrivial contribution in Eq. (4.270), we arrive, after minor algebra, at the expression

$$T(x, \Delta\phi) \simeq 1 + \frac{4x\Delta\phi}{(x^2 + 9)(x^2 + 1)}, \tag{4.271}$$

where $x = z_s/z_R$. The analysis of Eq. (4.267) reveals that it has a maximum (peak) and a minimum (valley) as is sketched in Fig. 4.26. The difference between the two is given by

$$T_{\max} - T_{\min} \approx 0.406\,\Delta\phi. \tag{4.272}$$

By measuring the curve T as a function of x and determining the peak-value difference, one can determine the nonlinear phase shift on the beam axis and hence infer the nonlinear refractive index using Eq. (4.262). This is the essence of the $z-$scan technique.
Exercise. 4. 16. *Derive Eq. (4.271).*

The necessity to determine the whole T-curve to infer the peak-valley difference is a disadvantage of the traditional $z-$scan approach. In practice, an experimentalist has to translate a sample by translating a stage which entails some technical limitations.

Exercise 4. 17. *Assuming your a translation stage allows for a 20 cm travel, how tight a focus is required such that you could capture a typical $z-$scan signature (peak-to-valley) of the transmittance curve? What is a maximum sample thickness such that the thin sample approximation, $\Delta L \ll z_R$, is satisfied for a 632 nm laser beam?*

As an alternative, one can tightly focus a Gaussian beam and apply the so-called quadratic phase approximation (QPA) for the accumulated nonlinear phase shift

$$\exp[i\Delta\Phi_{NL}(\rho,\Delta L)] \simeq e^{i\Delta\Phi_0} e^{-i\Delta\Phi_0\rho^2/w_s^2}, \tag{4.273}$$

which is obtained by expanding **the exponent** in the last term on the r.h.s. of Eq. (4.263) into a Taylor series and keeping only quadratic term in ρ/w_s. The QPA can be justified by observing that it is very accurate near the beam axis, $\rho \ll w_s$. As one moves away from the axis, the QPA accuracy decreases. However, it is largely irrelevant as the diffraction pattern contribution from the beam tails is practically negligible due to a very fast (Gaussian) fall off of the field intensity towards the beam periphery. The QPA is expected to be particularly accurate for tightly focused Gaussian beams, typically employed in the z-scan measurements in most practical situations.

It then follows at once from Eqs (4.263) and (4.273) that

$$\mathcal{E}(\rho,z_s) = \mathcal{E}_s e^{i\Delta\Phi_0}\, \exp\left[\frac{ik\rho^2}{2R_{\rm eff}}\right]\, \exp\left[-\frac{\rho^2}{2w_s^2}\right], \tag{4.274}$$

where the effective radius of wavefront curvature $R_{\rm eff}$ is defined as

$$\frac{1}{R_{\rm eff}} = \frac{1}{R_s}\left(1 - \frac{2\Delta\Phi_0 z_R}{z_s}\right). \tag{4.275}$$

It can be inferred from Eq. (4.275) that for $\overline{n}_2 > 0$, $R_{\rm eff} > R_s$, resulting in partial diffraction suppression by self-focusing in the sample. Conversely, if $\overline{n}_2 < 0$, $R_{\rm eff} < R_s$ causing additional beam spreading due to self-defocusing in the sample. Thus, the sample works as a thin lens.

Having elucidated the thin sample effect on the beam in the QPA approximation in physical terms, we can proceed to study beam propagation from the sample to the aperture. The beam envelope at the aperture can be derived, given its expression at the sample exit (4.274). The resulting on-axis aperture transmittance takes the form

$$T_{\rm QPA}(\Delta\Phi_0) = \frac{1 + \frac{z_s^2}{z_R^2}\left(1 + \frac{z_R^2}{z_s L_a}\right)^2}{1 + \frac{z_s^2}{z_R^2}\left(1 - 2\Delta\Phi_0\frac{z_R}{z_s} + \frac{z_R^2}{z_s L_a}\right)^2}. \tag{4.276}$$

Eq. (4.276) can be easily inverted, yielding the expression for the nonlinear phase shift as

$$\Delta\Phi_0 = \frac{z_s}{2z_R}\left[1 + \frac{z_R^2}{z_s L_a} - \frac{z_R}{z_s}\sqrt{\frac{1 - T_{\rm QPA} + \frac{z_s^2}{z_R^2}\left(1 + \frac{z_R^2}{z_s L_a}\right)}{T_{\rm QPA}}}\right]. \tag{4.277}$$

Expressions (4.261), (4.262), and (4.277) make it possible to extract both the sign–determined by the sign of $\Delta\Phi_0$ in Eq. (4.277)–and magnitude of $\overline{n}_2$ from a **single** measurement of the relative transmittance in the Fresnel zone, a distance L_a away from the sample placed at the position z_s. There is no need for sample position scanning in this approach.

Let us discuss key restrictions on relevant distances under the QPA. First, the sample must be thin, implying that $\Delta L \ll z_s$. Second, the beam emerging from the sample must still be tightly focused for the QPA to hold well, leading to the restriction on the sample position relative to the beam Rayleigh range, $z_s \ll z_R$. Third, the beam should not have significantly diverged on arrival at the aperture to avoid substantial power loss, implying that $L_a \leq z_R$. Combining these criteria, we arrive at

$$\Delta L \ll z_s \ll L_a \leq z_R. \tag{4.278}$$

Note also that if Eq. (4.278) is met, $\Delta\Phi_0 \simeq \Delta\phi$, yielding

$$\Delta\phi = \frac{z_s}{2z_R}\left[1 + \frac{z_R^2}{z_s L_a} - \frac{z_R}{z_s}\sqrt{\frac{1 - T_{\mathrm{QPA}} + \frac{z_s^2}{z_R^2}\left(1 + \frac{z_R^2}{z_s L_a}\right)}{T_{\mathrm{QPA}}}}\right]. \tag{4.279}$$

It might be possible to adjust the measurement setup such that

$$\frac{z_R^2}{z_s L_a} \gg 1, \tag{4.280}$$

is fulfilled. Under the circumstances, Eq. (4.279) can be simplified to yield a particularly compact working formula

$$\Delta\phi \simeq \frac{z_R}{2L_a}\left(1 - \frac{L_a}{z_R}\sqrt{\frac{1 - T_{\mathrm{QPA}} + z_s/L_a}{T_{\mathrm{QPA}}}}\right). \tag{4.281}$$

Exercise 4.18. *Derive Eq. (4.277).*

4.12 Polarization dynamics of third-order processes

So far we have ignored tensor properties of nonlinear optical susceptibilities by considering linearly or circularly polarized light whose polarization properties do not change on propagation in isotropic media. Whenever elliptically polarized light is launched into such media, its state of polarization does in general change despite the isotropy of the medium. Thus, we shall be interested in polarization dynamics of light propagating in isotropic nonlinear media. If the isotropic medium possesses reflectional symmetry, the lowest order of the optical susceptibility tensor is the third. Remarkably, the mere isotropy and reflectional symmetry of the medium are sufficient to determine a general form of the third-order susceptibility tensor which we will do following a seminal work of Maker and Tehrune. In the next subsection, we examine tensor properties of the third-order susceptibility in the media with isotropic linear and nonlinear responses,

while we will then explore the influence of linear anisotropy of the nonlinear medium – whose nonlinear properties can still be assumed isotropic – on light polarization dynamics in such media.

We begin by observing that since there is no privileged direction in such a medium, the third-order susceptibility tensor cannot have an index – corresponding to a given Cartesian coordinate – repeat an odd number of times: In other words, $\chi^{(3)}_{ijjj} = 0$ for any $j = x, y, z$. To demonstrate this property, consider a polarization component, P_x, say. If $\chi^{(3)}_{xyyy} \neq 0$, it follows that $P_x = \epsilon_0 \chi^{(3)}_{xyyy} E_y E_y E_y \neq 0$. On the other hand, polarization along the $x-$axis in an isotropic medium should not be affected by reflections with respect to the $xz-$plane. The latter affect the y-component of the field, though, $E_y \to -E_y$. Consequently, $P_x = \epsilon_0 \chi^{(3)}_{xyyy} E_y E_y E_y = (-1)^3 \epsilon_0 \chi^{(3)}_{xyyy} E_y E_y E_y$, implying that $\chi^{(3)}_{xyyy} = 0$. By the same token, all the other tensor components containing three repeated indices can be shown to be zero.

Further, we conclude by inspection that there are four kinds of nonzero tensor elements which are mutually related by the symmetry relations as

$$\chi^{(3)}_{xxxx} = \chi^{(3)}_{yyyy} = \chi^{(3)}_{zzzz}, \tag{4.282}$$

$$\chi^{(3)}_{xxyy} = \chi^{(3)}_{xxzz} = \chi^{(3)}_{yyxx} = \chi^{(3)}_{yyzz} = \chi^{(3)}_{zzyy} = \chi^{(3)}_{zzxx}, \tag{4.283}$$

$$\chi^{(3)}_{xyxy} = \chi^{(3)}_{xzxz} = \chi^{(3)}_{yzyz} = \chi^{(3)}_{zxzx} = \chi^{(3)}_{zyzy} = \chi^{(3)}_{yxyx}, \tag{4.284}$$

$$\chi^{(3)}_{xyyx} = \chi^{(3)}_{yxxy} = \chi^{(3)}_{xzzx} = \chi^{(3)}_{zxxz} = \chi^{(3)}_{yzzy} = \chi^{(3)}_{zyyz}. \tag{4.285}$$

Moreover, as $\chi^{(3)}_{ijkl}$ must be invariant with respect to rotations, the diagonal and off-diagonal elements of the susceptibility tensor can be shown to satisfy the relations

$$\chi^{(3)}_{xxxx} = \chi^{(3)}_{xxyy} + \chi^{(3)}_{xyyx} + \chi^{(3)}_{xyxy}, \tag{4.286}$$

with similar ones for $\chi^{(3)}_{yyyy}$ and $\chi^{(3)}_{zzzz}$. We can then infer from Eqs. (4.282) – (4.285) as well as Eq. (4.286) that the third-order susceptibility tensor in isotropic media with inversion symmetry takes a general form

$$\chi^{(3)}_{ijkl} = \chi^{(3)}_{xxyy} \delta_{ij} \delta_{kl} + \chi^{(3)}_{xyxy} \delta_{ik} \delta_{jl} + \chi^{(3)}_{xyyx} \delta_{il} \delta_{jk}. \tag{4.287}$$

The expression (4.287) can be simplified even further for particular nonlinear processes if one recalls intrinsic symmetries of $\chi^{(3)}$ with respect to frequency permutations. We will focus here on the self-focusing (SF) process, $\omega_1 = \omega_2 = -\omega_3 = -\omega_4 = \omega$. The intrinsic permutation symmetry then implies

$$\chi^{(3)}_{ijkl}(-\omega, \omega, -\omega, \omega) = \chi^{(3)}_{ilkj}(-\omega, \omega, -\omega, \omega). \tag{4.288}$$

It follows at once that

$$\chi^{(3)}_{xxyy}(-\omega, \omega, -\omega, \omega) = \chi^{(3)}_{xyyx}(-\omega, \omega, -\omega, \omega). \tag{4.289}$$

We can then arrive at the final form for the third-order susceptibility for SF in isotropic media,

$$\begin{aligned}\chi^{(3)}_{ijkl}(-\omega,\omega,-\omega,\omega) &= \chi^{(3)}_{xxyy}(-\omega,\omega,-\omega,\omega)(\delta_{ij}\delta_{kl}+\delta_{il}\delta_{jk}) \\ &\quad + \chi^{(3)}_{xyxy}(-\omega,\omega,-\omega,\omega)\delta_{ik}\delta_{jl}. \end{aligned} \tag{4.290}$$

Exercise 4.19. *Use intrinsic permutation symmetries of $\chi^{(3)}_{ijkl}$ to determine a general form of the susceptibility tensor $\chi^{(3)}_{ijkl}(-3\omega,\omega,\omega,\omega)$ for the third harmonic generation in isotropic media.*

The third-order polarization field for self-focusing takes the form

$$\mathcal{P}_i(\omega) = \frac{3\epsilon_0}{4}\sum_{jkl}\chi^{(3)}_{ijkl}(-\omega,\omega,-\omega,\omega)\mathcal{E}_j(\omega)\mathcal{E}_k(-\omega)\mathcal{E}_l(\omega), \tag{4.291}$$

where

$$\mathcal{E}_k(-\omega) = \mathcal{E}^*_k(\omega). \tag{4.292}$$

Substituting from Eqs. (4.290) into (4.291) we obtain, after some algebra, the expression

$$\mathcal{P}_i = \frac{3\epsilon_0}{2}\,\chi^{(3)}_{xxyy}\mathcal{E}_i\sum_k \mathcal{E}_k\mathcal{E}^*_k + \frac{3\epsilon_0}{4}\,\chi^{(3)}_{xyxy}\mathcal{E}^*_i\sum_l \mathcal{E}_l\mathcal{E}_l. \tag{4.293}$$

The latter can be written in the vector form as

$$\boldsymbol{\mathcal{P}}_{NL} = \epsilon_0[A(\boldsymbol{\mathcal{E}}\cdot\boldsymbol{\mathcal{E}}^*)\boldsymbol{\mathcal{E}} + \tfrac{1}{2}B(\boldsymbol{\mathcal{E}}\cdot\boldsymbol{\mathcal{E}})\boldsymbol{\mathcal{E}}^*], \tag{4.294}$$

where we have introduced the notations of *Maker and Terhune (1965)*

$$A \equiv \frac{3}{2}\chi^{(3)}_{xxyy}, \qquad\qquad B \equiv \frac{3}{2}\chi^{(3)}_{xyxy}. \tag{4.295}$$

Equation (4.294) gives the most general form of the third-order polarization response to an applied field of any polarization for a self-focusing process in an isotropic non-chiral nonlinear medium.

To better understand the role of the two terms entering the expression (4.294), we consider an elliptically polarized wave, propagating in the positive z-direction, which can be conveniently represented as a linear superposition of the right- and left-handed circular polarizations as

$$\boldsymbol{\mathcal{E}} = \mathcal{E}_+\mathbf{e}_+ + \mathcal{E}_-\mathbf{e}_-, \tag{4.296}$$

where the unit vectors associated with the circular polarizations are defined as

$$\mathbf{e}_\pm = \frac{\mathbf{e}_x \pm i\mathbf{e}_y}{\sqrt{2}}; \qquad\qquad \mathbf{e}_- = \mathbf{e}^*_+. \tag{4.297}$$

It follows from (4.297) that

$$\mathbf{e}_\pm\cdot\mathbf{e}_\pm = 0, \qquad\qquad \mathbf{e}_\pm\cdot\mathbf{e}_\mp = 1. \tag{4.298}$$

The dot product of the two electric field vectors can then be expressed as

$$\boldsymbol{\mathcal{E}} \cdot \boldsymbol{\mathcal{E}} = 2\mathcal{E}_+\mathcal{E}_-, \qquad \boldsymbol{\mathcal{E}} \cdot \boldsymbol{\mathcal{E}}^* = |\mathcal{E}_+|^2 + |\mathcal{E}_-|^2. \tag{4.299}$$

Let us define the nonlinear polarization field in the circular polarization basis by the expression

$$\boldsymbol{\mathcal{P}}_{NL} = \mathcal{P}_{NL}^{(+)}\mathbf{e}_+ + \mathcal{P}_{NL}^{(-)}\mathbf{e}_-, \tag{4.300}$$

It can be inferred from (4.294), (4.299) and (4.300) that

$$\mathcal{P}_{NL}^{(\pm)} = \epsilon_0[A|\mathcal{E}_\pm|^2 + (A+B)|\mathcal{E}_\mp|^2]\mathcal{E}_\pm. \tag{4.301}$$

Further, we can represent the total polarization field as a linear superposition of the circular polarization components as

$$\boldsymbol{\mathcal{P}} = \mathcal{P}_+\mathbf{e}_+ + \mathcal{P}_-\mathbf{e}_-, \tag{4.302}$$

where $\mathcal{P}_+$ and $\mathcal{P}_-$ are effectively decoupled – there is an indirect coupling, though, via the nonlinear susceptibility – such that each polarization component is proportional to the corresponding electric field viz.,

$$\mathcal{P}_\pm = \epsilon_0 \left[\chi_L + \chi_{NL}^{(\pm)}\right] \mathcal{E}_\pm. \tag{4.303}$$

Here the nonlinear susceptibility of each component is given by

$$\chi_{NL}^{(\pm)} = A|\mathcal{E}_\pm|^2 + (A+B)|\mathcal{E}_\mp|^2. \tag{4.304}$$

The corresponding effective refractive index, including linear as well as nonlinear parts, can be defined as

$$n_\pm^2 = 1 + \chi_L + \chi_{NL}^{(\pm)}. \tag{4.305}$$

Since in practice, $\chi_{NL} \ll \chi_L$, we can make the approximation

$$n_\pm \simeq n_L + \frac{\chi_{NL}^{(\pm)}}{2n_L}. \tag{4.306}$$

The analysis of Eqs. (4.302) – (4.306) reveals that in the circular polarization basis, the nonlinear wave equation in isotropic media can be effectively decoupled into the two as

$$\frac{\partial^2 E_\pm}{\partial t^2} - \frac{n_\pm^2}{c^2}\frac{\partial^2 E_\pm}{\partial z^2} = 0, \tag{4.307}$$

where we have neglected any spatial dependence in the transverse directions. Equations (4.307) are satisfied by the plane wave solutions

$$E_\pm(z,t) = \mathcal{E}_\pm e^{i(k_\pm z - \omega t)}, \tag{4.308}$$

where

$$k_\pm = \frac{n_\pm \omega}{c}. \tag{4.309}$$

On substituting from Eq. (4.306) into (4.308), and using the identities

$$n_{\pm} = \overline{n} \pm \Delta n/2, \tag{4.310}$$

where

$$\overline{n} \equiv \frac{n_+ + n_-}{2}, \qquad \Delta n = n_+ - n_-; \tag{4.311}$$

we obtain the expression for the total field as

$$\mathbf{E}(z,t) = [\mathcal{E}_+ e^{i\Delta n\omega z/2c}\mathbf{e}_+ + \mathcal{E}_- e^{-i\Delta n\omega z/2c}\mathbf{e}_-]e^{i\omega(\overline{n}z/c-t)}. \tag{4.312}$$

Here we have introduced the average effective refractive index

$$\overline{n} = n_L + \frac{(2A+B)}{4n_L}(|\mathcal{E}_+|^2 + |\mathcal{E}_-|^2), \tag{4.313}$$

and the refractive index difference,

$$\Delta n = n_+ - n_- = \frac{B}{2n_L}(|\mathcal{E}_-|^2 - |\mathcal{E}_+|^2), \tag{4.314}$$

respectively. The electric field can be represented as

$$\mathbf{E}(z,t) = [\mathcal{E}_+\mathbf{e}_+(z) + \mathcal{E}_-\mathbf{e}_-(z)]e^{i\omega(\overline{n}z/c-t)}, \tag{4.315}$$

where the rotating circular polarization basis is

$$\mathbf{e}_{\pm}(z) = \frac{\mathbf{e}_x(z) \pm i\mathbf{e}_y(z)}{\sqrt{2}}, \tag{4.316}$$

with

$$\mathbf{e}_x(z) = \cos(\Delta n\omega z/2c)\mathbf{e}_x + \sin(\Delta n\omega z/2c)\mathbf{e}_y, \tag{4.317}$$

$$\mathbf{e}_y(z) = \cos(\Delta n\omega z/2c)\mathbf{e}_y - \sin(\Delta n\omega z/2c)\mathbf{e}_x. \tag{4.318}$$

Exercise 4.20. *Verify that the representation of the field in terms of rotating polarization vectors, given by Eqs. (4.315) – (4.318), does indeed correspond to our field of Eq. (4.312).*

Analyzing Eqs. (4.316) – (4.318), we can conclude that the electric field is elliptically polarized at any position z, according to Eq. (4.315); yet the polarization ellipse rotates in the $xy-$ plane at the rate proportional to the differences of refractive indices along the two principal axes. The latter is referred to as *birefringence*; it is the nonlinear birefringence of the medium that gives rise to polarization rotation even in isotropic optical media. Notice also that the rate of polarization rotation depends only on the coefficient B as is evidenced by Eqs. (4.314) and (4.317), (4.318). Hence the second term on the r.h.s. of Eq. (4.294) is wholly responsible for nonlinear birefringence effects. The first term on the r.h.s of (4.294) contributes to the overall phase accretion factor which is proportional to $\overline{n}$, but it does not affect polarization rotation.

Exercise 4.21. *In the fiber optical case, the nonlinear response of the medium is of electronic type such that $A = B$. Silica-glass optical fibers can serve as an important particular example. Linear birefringence of the fiber is typically introduced – either intentionally or inadvertently – at the fabrication stage. On account of linear birefringence, the most general field propagating in such a fiber can be represented as*

$$\mathbf{E} = \frac{1}{2}\left(\mathbf{e}_x\mathcal{E}_x e^{i\beta_x z} + \mathbf{e}_y\mathcal{E}_y e^{i\beta_y z}\right) e^{-i\omega t} + c.\, c,$$

where $\beta_{x,y}$ is the propagation constant of the corresponding linear polarization component; the field components are assumed to be polarized along the principal axes of the fiber. Show that the polarization field at the frequency ω is then given by

$$\mathbf{P}_{NL} = \frac{1}{2}\left(\mathbf{e}_x\mathcal{P}_x e^{i\beta_x z} + \mathbf{e}_y\mathcal{P}_y e^{i\beta_y z}\right) e^{-i\omega t} + c.\, c., \tag{4.319}$$

where

$$\mathcal{P}_x = \frac{3\epsilon_0}{4}\chi^{(3)}_{xxxx}\left[(|\mathcal{E}_x|^2 + \frac{2}{3}|\mathcal{E}_y|^2)\mathcal{E}_x + \frac{1}{3}\mathcal{E}_x^*\mathcal{E}_y^2 e^{-2i\Delta\beta z}\right], \tag{4.320}$$

$$\mathcal{P}_y = \frac{3\epsilon_0}{4}\chi^{(3)}_{xxxx}\left[(|\mathcal{E}_y|^2 + \frac{2}{3}|\mathcal{E}_x|^2)\mathcal{E}_x + \frac{1}{3}\mathcal{E}_y^*\mathcal{E}_x^2 e^{2i\Delta\beta z}\right]. \tag{4.321}$$

Here $\Delta\beta = \beta_x - \beta_y$.

4.13 Electro-optical Kerr effect

In this section, we study the electro-optical Kerr effect which manifests itself in the modification of a linear refractive index of an isotropic non-chiral media in presence of an electrostatic field. The effect becomes possible due to the second-order (Kerr) nonlinearity – which is the leading nonlinearity in such media – and hence the name, electro-optical Kerr effect. Classically, the corresponding polarization reads

$$\mathcal{P}_{NLi} = 3\epsilon_0 \sum_{jkl}\chi^{(3)}_{ijkl}(-\omega,\omega,0,0)\mathcal{E}_j(\omega)E_k(0)E_l(0). \tag{4.322}$$

Substituting from Eq. (4.287) into Eq. (4.322), we obtain

$$\begin{aligned}\mathcal{P}_{NLi} &= 3\epsilon_0\chi^{(3)}_{xxyy}\mathcal{E}_i(\omega)\sum_k E_k^2(0) + 3\epsilon_0\chi^{(3)}_{xyxy}E_i(0)\sum_j E_j(0)\mathcal{E}_j(\omega) \\ &\quad + 3\epsilon_0\chi^{(3)}_{xyyx}E_i(0)\sum_j \mathcal{E}_j(\omega)E_j(0).\end{aligned} \tag{4.323}$$

The intrinsic permutation symmetry, $\chi^{(3)}_{ijkl}(-\omega,\omega,0,0) = \chi^{(3)}_{ijlk}(-\omega,\omega,0,0)$, implies that

$$\chi^{(3)}_{xyxy} = \chi^{(3)}_{xyyx}, \tag{4.324}$$

Using Eq. (4.324), Eq. (4.323) can be written in the vector form as

$$\boldsymbol{\mathcal{P}}_{NL} = 3\epsilon_0[\chi^{(3)}_{xxyy}\,\boldsymbol{\mathcal{E}}(\mathbf{E}_0\cdot\mathbf{E}_0) + 2\chi^{(3)}_{xyxy}\,\mathbf{E}_0(\boldsymbol{\mathcal{E}}\cdot\mathbf{E}_0)], \tag{4.325}$$

where we have introduced the notations,

$$\boldsymbol{\mathcal{E}} \equiv \boldsymbol{\mathcal{E}}(\omega) \quad \text{and} \quad \mathbf{E}_0 \equiv \mathbf{E}(0). \tag{4.326}$$

Equation (4.325) represents the general form of the polarization associated with the electro-optical Kerr effect for the electrostatic and optical fields of any polarizations. Let us focus on the case of linear polarization of the dc field such that

$$\mathbf{E}_0 = E_0\mathbf{e}_x, \qquad \boldsymbol{\mathcal{E}} = \mathcal{E}_x\mathbf{e}_x + \mathcal{E}_y\mathbf{e}_y. \tag{4.327}$$

Under the circumstances, the polarization components take the form

$$\begin{aligned}\mathcal{P}_{NLx} &= 3\epsilon_0[\chi^{(3)}_{xxyy}\mathcal{E}_xE_0^2 + 2\chi^{(3)}_{xyxy}E_0^2\mathcal{E}_x] \\ &= 3\epsilon_0[(\chi^{(3)}_{xxyy} + 2\chi^{(3)}_{xyxy})]E_0^2\mathcal{E}_x = 3\epsilon_0\chi^{(3)}_{xxxx}E_0^2\mathcal{E}_x,\end{aligned} \tag{4.328}$$

and

$$\mathcal{P}_{NLy} = 3\epsilon_0\chi^{(3)}_{xxyy}E_0^2\mathcal{E}_y. \tag{4.329}$$

It can be inferred from Eqs. (4.328) and (4.329) that the components of the total polarization field can be represented as

$$\mathcal{P}_{x,y} = \epsilon_0\chi_{x,y}\mathcal{E}_{x,y}, \tag{4.330}$$

where the components of the effective susceptibility tensor are

$$\chi_x = \chi^{(1)} + 3\chi^{(3)}_{xxxx}E_0^2, \tag{4.331}$$

and

$$\chi_y = \chi^{(1)} + 3\chi^{(3)}_{xxyy}E_0^2. \tag{4.332}$$

The corresponding components of the total refractive index are given by

$$n_x \simeq n + \frac{3\chi^{(3)}_{xxxx}}{2n}E_0^2, \tag{4.333}$$

and

$$n_y \simeq n + \frac{3\chi^{(3)}_{xxyy}}{2n}E_0^2. \tag{4.334}$$

It follows from Eqs. (4.330) – (4.332) that in electro-optical Kerr effect with the dc field breaking the azimuthal symmetry, it is the Cartesian components of the optical field that are decoupled; each satisfies the wave equation – neglecting spatial dependence in the transverse plane – of the form

$$\frac{\partial^2E_{x,y}}{\partial t^2} - \frac{n_{x,y}^2}{c^2}\frac{\partial^2E_{x,y}}{\partial z^2} = 0, \tag{4.335}$$

The plane-wave solutions to Eq. (4.335) are

$$E_{x,y}(z,t) = \mathcal{E}_{x,y} e^{i(k_{x,y} z - \omega t)}, \tag{4.336}$$

where

$$k_{x,y} = \frac{n_{x,y}\omega}{c}. \tag{4.337}$$

The evolution of the optical field can then be represented as

$$\mathbf{E}(z,t) = \mathcal{E}_x[\mathbf{e}_x + \mathbf{e}_y \tan\theta e^{-i\Delta n\omega z/c}] e^{i\omega(n_x z/c - t)}, \tag{4.338}$$

where $\tan\theta = \mathcal{E}_y/\mathcal{E}_x$, and

$$\Delta n = \frac{3\chi^{(3)}_{xyxy} E_0^2}{n}. \tag{4.339}$$

The analysis of Eq. (4.338) reveals that the Kerr effect is present in two guises: the dc field breaks the symmetry of the isotropic medium turning the medium into a uniaxial one and it generates effective linear birefringence which manifests itself in the polarization rotation. The latter can be seen by observing, for instance, that if the wave is initially linearly polarized at 45° to the dc field, such that $\tan\theta = 1$, it can acquire a circular polarization provided, $e^{-i\Delta n\omega L/c} = \pm i$ at the exit to the medium, $z = L$. In general, the polarization rotation angle for the beam having traversed a distance L inside the medium is given by

$$\Delta\phi_L = \frac{\Delta n\omega L}{c} = \frac{3\omega}{nc}\chi^{(3)}_{xyxy} E_0^2 L. \tag{4.340}$$

In experimental work, the so-called *Kerr constant* K is often introduced via the relation

$$\Delta n = K\lambda E_0^2. \tag{4.341}$$

The Kerr constant is related to relevant components of the susceptibility tensor by the expression

$$K = \frac{3\chi^{(3)}_{xyxy}}{n\lambda}. \tag{4.342}$$

Exercise 4.22. *Determine the dc field strength needed to produce a circular polarization by a 10 cm long Kerr cell filled with carbon disulfide, CS_2. For carbon disulfide, $K = 3.6 \times 10^{-14}$ m/V^2.*

4.14 Spontaneous and stimulated Raman scattering: CW case

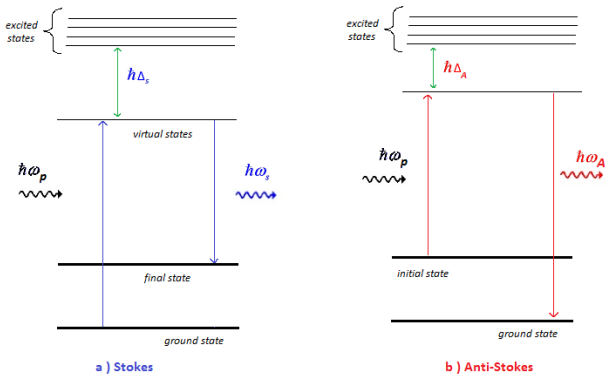

Figure 4.27: Illustrating a photon picture of Raman scattering.

Spontaneous Raman scattering is an inelastic scattering process of an electromagnetic wave off of individual molecules such that part of the electromagnetic wave energy is lost to the medium excitations. The excitations are typically come in the form of molecular vibrations or rotations. If a particular molecule was in the ground state with the energy E_g prior to an elementary scattering act, it can absorb a photon from the incident laser beam and re-emit a photon of a lower frequency. The energy difference is lost to exciting a vibrational or rotational phonon, a quantum of vibration or rotation. On the other hand, if the molecule was thermally excited to the state E_f– the probability of this event is determined by the Gibbs factor $e^{-(E_f-E_g)/kT}$–it can emit a photon of a greater frequency than the laser beam photon to return to its ground state. In the first instance, the generated photon is said to belong to the Stokes mode, and in the second–to anti-Stokes one. This photon picture of the scattering process is schematically illustrated in Fig. 5.1. We note that medium excitations in the Raman case are optical phonons.

Unfortunately, there is no simple classical picture of spontaneous Raman scattering that can adequately describe the process. We will only point out that the total scattered power P can be described in terms of the scattering cross-section σ, which has area units, through the expression

$$P = \sigma I_0, \tag{4.343}$$

where I_0 is the incident intensity of the laser beam. If we consider the scattered power dP flowing through an infinitesimal area dS on a sphere of radius R centered at the molecule, we can determine the power flux,

$$\frac{dP}{dS} = \frac{1}{R^2}\frac{dP}{d\Omega} = \frac{I_0}{R^2}\frac{d\sigma}{d\Omega}. \tag{4.344}$$

Here $d\Omega$ is an infinitesimal solid angle shown in Fig. 5.2 and we have introduced a differential cross-section $d\sigma/d\Omega$. In most experimental situations, there is a finite number

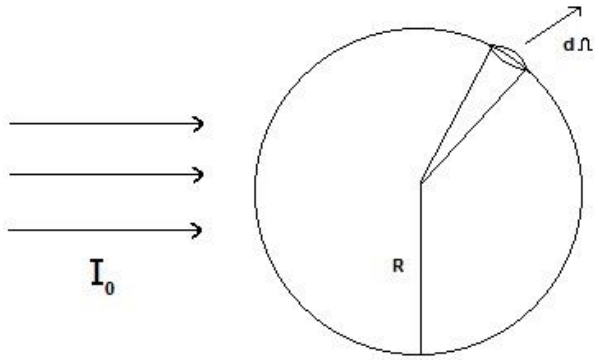

Figure 4.28: Illustrating the concept of scattering cross-section.

$N \geq 1$ of the medium molecules within the interaction region and the collection solid angle $\Delta\Omega$ is typically rather small such that the overall power scattered into $\Delta\Omega$ can be evaluated approximately as

$$P_\Delta = \int_{d\Omega} \frac{dP}{d\Omega} \simeq N I_0 \Delta\Omega \frac{d\sigma}{d\Omega}. \tag{4.345}$$

It follows at once from Eq. (4.345) that the scattered power can be calculated from the knowledge of the differential cross-section which is tabulated in the table below[1] for common gases and liquids, relative to its value for nitrogen.

Molecule	Raman shift (cm^{-1})	$\frac{d\sigma}{d\Omega} / \left.\frac{d\sigma}{d\Omega}\right\|_{N_2}$
N_2	2330	1
H_2	4156	3.2
O_2	1556	1.23
CO_2	1388	1.51
CO	2143	0.98
NO	1876	0.49
H_2O	3657	2.5
SO_2	1151	4.9
O_3	1103	3.0
CH_4	2917	7.3

The nitrogen differential cross-section at $\lambda_p = 488$ nm is

$$\left.\frac{d\sigma}{d\Omega}\right|_{N_2} = 5.5 \times 10^{-31}\ \text{cm}^2/\text{Sr}/\text{molecule}. \tag{4.346}$$

Note that as is customary in spectroscopy, Raman shifts are measured in cm^{-1}, i. e., in the inverse vacuum wavelengths in cm. One can convert these units to Raman shifts

[1]Source: S. A. Danchkin et.al., "Raman scattering parameters for gas molecules (survey)," *Journal of Applied Spectroscopy*, **35**, 1057-1066 (1981).

$\Delta\lambda$ in wavelength units of μm through

$$\Delta\lambda\,[\mu\text{m}] = 10^4/\text{shift}[\text{cm}^{-1}], \tag{4.347}$$

where 10^4 comes from the difference between nm and cm. The corresponding Raman frequency shift is then

$$\Delta\nu = c/\Delta\lambda. \tag{4.348}$$

It can be inferred from the table that due to tiny magnitudes of $d\sigma/d\Omega$ spontaneous Raman scattering is an extremely weak process with the scattered power being proportional to the incident intensity.

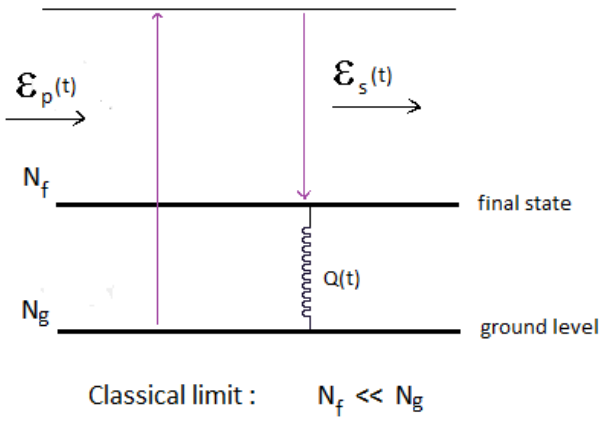

Figure 4.29: Classical picture of stimulated Raman scattering. The number of molecules N_f in the excited (final) state is negligible as compared to the number N_g of unexcited ones, $N_f \ll N_g$.

The scattering strength can be dramatically enhanced in presence of stimulating laser and Stokes/anti-Stokes beam. In this situation the scattering process is referred to as *stimulated* Raman scattering (SRS). SRS can be described entirely in classical terms in the weak molecular excitation limit. In this limit, the number of excited molecules N_f is much smaller than that N_g in the ground state. Hence we can neglect the level population dynamics and treat each molecule as a simple harmonic oscillator, weakly excited away from its ground state. The molecular excitation is due to a dipole moment induced by the external laser fields. The polarized molecule is assumed to vibrate or rotate around its center of mass which can be described as a "spring" deviation from its equilibrium position quantified by a generalized coordinate $\mathcal{Q}$, see Fig. 5.3.

The potential energy of a polarized molecule can be expressed as

$$W = -\tfrac{1}{2}pE, \tag{4.349}$$

where the induced dipole moment p can be expressed in terms of the molecular polarizability α,

$$p = \epsilon_0\alpha(\mathcal{Q})E. \tag{4.350}$$

For sufficiently small vibrations, the polarizability can be expanded into a Taylor series in terms of the generalized coordinate as

$$\alpha \simeq \alpha_0 + \left(\frac{d\mathcal{Q}}{d\alpha}\right)_0 \mathcal{Q}. \tag{4.351}$$

On combining Eqs. (4.350) and (4.351), we arrive at

$$p \simeq \epsilon_0 \left[\alpha_0 + \left(\frac{d\mathcal{Q}}{d\alpha}\right)_0 \mathcal{Q}\right] E. \tag{4.352}$$

The force can be determined as a gradient of the energy. It then follows from Eqs. (4.349) and (4.352) that

$$F_{\rm d} = -\nabla_{\mathcal{Q}} W = \frac{\epsilon_0}{2}\left(\frac{d\mathcal{Q}}{d\alpha}\right)_0 E^2, \tag{4.353}$$

Within the oscillator model framework, the vibrational equation of motion can be written as

$$\partial_t^2 \mathcal{Q} + 2\gamma \partial_t \mathcal{Q} + \omega_0^2 \mathcal{Q} = F_{\rm d}/m, \tag{4.354}$$

where ω_0 and γ are the resonant frequency and damping rate, and m is a molecule mass.

The external electric field is due to traveling pump and Stokes waves,

$$E(t,z) = \tfrac{1}{2}[\mathcal{E}_p e^{i(k_p z - \omega_p t)} + \mathcal{E}_s e^{i(k_s z - \omega_s t)} + c.\,c.], \tag{4.355}$$

It follows from (4.355) that

$$E^2(t,z) = \tfrac{1}{2}[\mathcal{E}_p \mathcal{E}_s^* e^{i(k_p - k_s)z} e^{-i(\omega_p - \omega_s)t} + NR + c.\,c.], \tag{4.356}$$

where "NR" stands for non-resonant terms we are not interested in. We seek a driven solution to the molecular vibration in the form

$$\mathcal{Q}(t,z) = \tfrac{1}{2}\mathcal{Q}_\omega e^{i(k_p - k_s)z} e^{-i(\omega_p - \omega_s)t} + c.\,c. \tag{4.357}$$

On substituting from Eq. (4.357) into (4.354) we obtain that

$$\mathcal{Q}_\omega = \frac{\epsilon_0 (d\alpha/d\mathcal{Q})_0 \mathcal{E}_p \mathcal{E}_s^*}{2m(\omega_0^2 - \omega_\Delta^2 - 2i\gamma\omega_\Delta)}. \tag{4.358}$$

Here we introduced the Raman frequency change as

$$\omega_\Delta = \omega_p - \omega_s. \tag{4.359}$$

The Raman interaction is only efficient near resonance such that $\omega_\Delta \approx \omega_0$. Assuming the pump and Stokes frequency difference falls in the vicinity to resonance, it follows that

$$\omega_0^2 - \omega_\Delta^2 - 2i\gamma\omega_\Delta \simeq 2\omega_0(\omega_0 - \omega_\Delta - i\gamma). \tag{4.360}$$

On substituting from Eq. (4.360) into (4.358), we obtain

$$\mathcal{Q}_\omega = -\frac{\epsilon_0 (d\alpha/d\mathcal{Q})_0 \mathcal{E}_p \mathcal{E}_s^*}{4m\omega_0[(\omega_\Delta - \omega_0) + i\gamma]}. \tag{4.361}$$

We can now determine the induced polarization,

$$P_{NL} = Np_{NL} = \epsilon_0 N \left(\frac{d\mathcal{Q}}{d\alpha}\right)_0 \mathcal{Q}E, \tag{4.362}$$

which can be expressed in terms of the Stokes, pump, and non-resonant frequency components as

$$P_{NL} = \tfrac{1}{2}[\mathcal{P}_{NL}(\omega_s)e^{-i\omega_s t} + \mathcal{P}_{NL}(\omega_p)e^{-i\omega_p t} + NR + c.\,c.] \tag{4.363}$$

We can infer from Eqs. (4.355), (4.357), (4.361) through (4.363) that the polarization component oscillating at the Stokes frequency is given by the expression

$$\mathcal{P}_{NL}(\omega_s) = -\frac{\epsilon_0^2 N(d\alpha/d\mathcal{Q})_0^2 |\mathcal{E}_p|^2 \mathcal{E}_s}{8m\omega_0[(\omega_\Delta - \omega_0) - i\gamma]} e^{ik_s z}. \tag{4.364}$$

By the same token, the pump frequency component to polarization takes the form

$$\mathcal{P}_{NL}(\omega_p) = -\frac{\epsilon_0^2 N(d\alpha/d\mathcal{Q})_0^2 |\mathcal{E}_s|^2 \mathcal{E}_p}{8m\omega_0[(\omega_\Delta - \omega_0) + i\gamma]} e^{ik_p z} \tag{4.365}$$

On the other hand, the third-order polarization corresponding to the annihilation of a Stokes photon and creation of a pump photon stimulated by the presence of a pump photon can be written as

$$\mathcal{P}_{NL}(\omega_s) = \frac{3\epsilon_0}{2}\chi_s^{(3)}(-\omega_s;\omega_p,-\omega_p,\omega_s)|\mathcal{E}_p|^2\mathcal{E}_s e^{ik_s z} \tag{4.366}$$

It then follows on comparing Eqs. (4.364) and (4.366) that the nonlinear susceptibility of this process is

$$\chi_s^{(3)}(-\omega_s;\omega_p,-\omega_p,\omega_s) = -\frac{\epsilon_0 N(d\alpha/d\mathcal{Q})_0^2}{12m\omega_0[(\omega_\Delta - \omega_0) - i\gamma]}. \tag{4.367}$$

Similarly, the pump frequency polarization can be expressed as

$$\mathcal{P}_{NL}(\omega_p) = \frac{3\epsilon_0}{2}\chi_p^{(3)}(-\omega_p;\omega_s,-\omega_s,\omega_p)|\mathcal{E}_s|^2\mathcal{E}_p e^{ik_p z}, \tag{4.368}$$

and the corresponding nonlinear susceptibility takes the form

$$\chi_p^{(3)}(-\omega_p;\omega_s,-\omega_s,\omega_p) = -\frac{\epsilon_0 N(d\alpha/d\mathcal{Q})_0^2}{12m\omega_0[(\omega_\Delta - \omega_0) + i\gamma]}, \tag{4.369}$$

Thus,

$$\chi_p^{(3)} = \chi_s^{(3)*} = \chi_s^*. \tag{4.370}$$

Let us now write down coupled-wave equations for the stimulated Raman scattering process,

$$2ik_j\partial_z\mathcal{E}_j = -\mu_0\omega_j^2\mathcal{P}_{NL}(\omega_j)e^{-ik_j z}, \qquad j = p, s. \tag{4.371}$$

Explicitly, we obtain for the pump and Stokes field amplitudes the equations

$$i\frac{d\mathcal{E}_p}{dz} = -\frac{3\omega_p^2}{4k_p c^2}\chi_s^*|\mathcal{E}_s|^2\mathcal{E}_p, \tag{4.372}$$

and

$$i\frac{d\mathcal{E}_s}{dz} = -\frac{3\omega_s^2}{4k_s c^2}\chi_s|\mathcal{E}_p|^2\mathcal{E}_s. \tag{4.373}$$

Assume that the amplitude of the pump field is very large and can be treated as undepleted during the SRS process. Under the undepleted pump approximation, the Stokes field is governed by the equation

$$i\frac{d\mathcal{E}_s}{dz} = -\frac{3\omega_s^2\chi_s|\mathcal{E}_p|^2}{4k_s c^2}\mathcal{E}_s. \tag{4.374}$$

After a simple algebra, Eq. (4.374) can be cast into the Stokes intensity evolution equation as

$$\frac{dI_s}{dz} = \frac{3\omega_s I_p \mathrm{Im}\{\chi_s\}}{2\epsilon_0 n_p n_s c^2} I_s. \tag{4.375}$$

Eq. (4.375) can be integrated, yielding an exponential growth of the Stokes mode,

$$I_s(z) = I_{s0}\exp(g_R I_p z), \tag{4.376}$$

where the gain factor can be expressed as

$$g_R \equiv \frac{3\omega_s \mathrm{Im}\{\chi_s\}}{2\epsilon_0 n_p n_s c^2}, \tag{4.377}$$

where

$$\mathrm{Im}\{\chi_s\} = \frac{\epsilon_0\gamma N(d\alpha/d\mathcal{Q})_0^2}{12m\omega_0[(\omega_\Delta-\omega_0)^2+\gamma^2]}. \tag{4.378}$$

The gain factor in Eq. (4.377) can be expressed as

$$g_R = g_{R0}\mathcal{L}(\omega_\Delta), \tag{4.379}$$

where

$$g_{R0} = \frac{\omega_s N(d\alpha/d\mathcal{Q})_0^2}{8m\omega_0\gamma c^2 n_p n_s}, \tag{4.380}$$

is a gain factor at the line center and the gain spectrum is Lorentzian,

$$\mathcal{L}(\omega_\Delta) = \frac{\gamma^2}{[(\omega_\Delta-\omega_0)^2+\gamma^2]}. \tag{4.381}$$

Typical values of center-line gain factors for gases are around a few cm/GW. For instance, $g_{R0} \approx 1.5$ cm/GW for molecular hydrogen H_2.

Whenever pump depletion cannot be neglected, coupled pump and Stokes wave dynamics must be studied using the full coupled-wave equations

$$\frac{dI_s}{dz} = \frac{3\omega_s \mathrm{Im}\{\chi_s\}}{2\epsilon_0 n_p n_s c^2} I_p I_s, \tag{4.382}$$

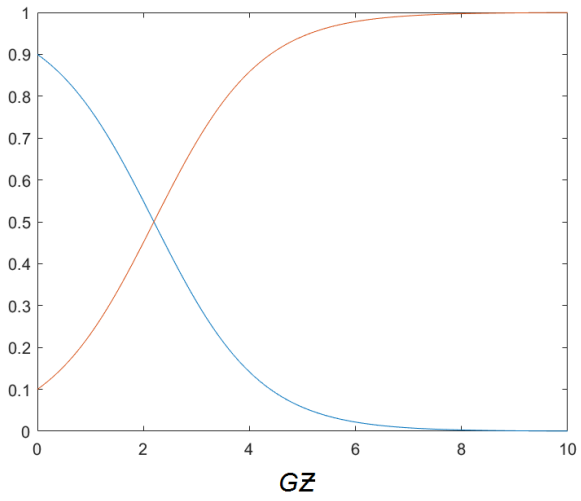

Figure 4.30: Photon number fractions in the Stokes (red) and pump (blue) pulses as functions of Gz beyond the undepleted pump approximation with $x = 0.1$.

and

$$\frac{dI_p}{dz} = -\frac{3\omega_s \mathrm{Im}\{\chi_s\}}{2\epsilon_0 n_p n_s c^2} I_p I_s. \tag{4.383}$$

It follows from Eqs. (4.382) and (4.383) after some algebra that

$$\frac{1}{\omega_p}\frac{dI_p}{dz} + \frac{1}{\omega_s}\frac{dI_s}{dz} = 0. \tag{4.384}$$

Eq. (4.384) implies that

$$\mathcal{N}_s + \mathcal{N}_p = \mathcal{N}_{p0} + \mathcal{N}_{s0} = \mathcal{N}_0 = const, \tag{4.385}$$

where $\mathcal{N}_j = I_j/\hbar\omega_j$ is a photon flux of the pump (Raman) beam. In other words, the total photon flux is conserved because in an elementary act of Raman scattering a death of a pump photon corresponds to birth of a Stokes photon and vice versa.

Eq. (4.385) can be used to eliminate the Stokes intensity, say, in favor of the pump intensity viz.,

$$I_s = \mathcal{N}_0 \hbar\omega_s - I_p \omega_s/\omega_p. \tag{4.386}$$

On substituting from Eq. (4.386) into (4.382) and (4.383), we can integrate the latter, yielding

$$\mathcal{N}_p(z)/\mathcal{N}_0 = \frac{(1-x)e^{-Gz}}{x + (1-x)e^{-Gz}}, \tag{4.387}$$

and

$$\mathcal{N}_s(z)/\mathcal{N}_0 = \frac{x}{x + (1-x)e^{-Gz}}. \tag{4.388}$$

Here we introduced the initial photon number fraction $x = \mathcal{N}_{s0}/\mathcal{N}_0$ in the Stokes pulse that indicates the percentage of photons carried by the incident Stokes pulse of the overall input photon number. The total gain is given by

$$G = G_0 \mathcal{L}(\omega_\Delta), \tag{4.389}$$

where

$$G_0 = \frac{\mathcal{N}_0 \hbar \omega_s \omega_p N (d\alpha/d\mathcal{Q})_0^2}{8 m \omega_0 \gamma c^2 n_p n_s}, \tag{4.390}$$

is the gain at the center-line of the gain spectrum. The behavior of the Stokes and pump intensities is sketched in the Fig. 5.4. It is seen either in the figure or from Eqs. (4.387) and (4.388) that the Stokes intensity starts off growing exponentially at short interaction distances. As the interaction distance increases, though, the Stokes mode growth saturates and the pump mode becomes depleted, transferring energy into the Stokes mode and medium molecule vibrations.

We have so far focused on the Stokes mode. Let us include the anti-Stokes mode into our framework as well. To this end, we consider an input field comprised of the there components, the pump, Stokes and anti-Stokes modes such that

$$E(t,z) = \tfrac{1}{2}[\mathcal{E}_p e^{i(k_p z - \omega_p t)} + \mathcal{E}_s e^{i(k_s z - \omega_s t)} + \mathcal{E}_{as} e^{i(k_{as} z - \omega_{as} t)} + c.\,c.]. \tag{4.391}$$

Let us also introduce the Raman frequency change

$$\omega_\Delta = \omega_p - \omega_s = \omega_{as} - \omega_p. \tag{4.392}$$

It follows at once from Eq. (4.391) that

$$E^2(t,z) = \tfrac{1}{4}\{[\mathcal{E}_p \mathcal{E}_s^* e^{i(k_p - k_s)z} + \mathcal{E}_{as} \mathcal{E}_p^* e^{i(k_{as} - k_p)z}] e^{-i\omega_\Delta t} + NR + c.\,c.]. \tag{4.393}$$

Therefore, we seek the driven solution for the generalized molecule vibration coordinate in the form

$$\mathcal{Q}(t,z) = \tfrac{1}{2}\{[\mathcal{Q}_{\omega s} e^{i(k_p - k_s)z} + \mathcal{Q}_{\omega as} e^{i(k_{as} - k_p)z}] e^{-i\omega_\Delta t} + c.\,c.\}. \tag{4.394}$$

On substituting from Eq. (4.394) into (4.354), we obtain for the spectral amplitude of the Stokes mode

$$\mathcal{Q}_{\omega s} = -\frac{\epsilon_0 (d\alpha/d\mathcal{Q})_0 \mathcal{E}_p \mathcal{E}_s^*}{4 m \omega_0 [(\omega_\Delta - \omega_0) + i\gamma]}, \tag{4.395}$$

and for the anti-Stokes one

$$\mathcal{Q}_{\omega as} = -\frac{\epsilon_0 (d\alpha/d\mathcal{Q})_0 \mathcal{E}_{as} \mathcal{E}_p^*}{4 m \omega_0 [(\omega_\Delta - \omega_0) + i\gamma]}. \tag{4.396}$$

The nonlinear polarization then can be expressed as

$$P_{NL} = \tfrac{1}{2}[\mathcal{P}_{NL}(\omega_s) e^{-i\omega_s} + \mathcal{P}_{NL}(\omega_{as}) e^{-i\omega_{as}} + \mathcal{P}_{NL}(\omega_p) e^{-i\omega_p} + c.\,c.], \tag{4.397}$$

where the Stokes and anti-Stokes components take the form

$$\mathcal{P}_{NL}(\omega_s) = \frac{\epsilon_0^2 N (d\alpha/d\mathcal{Q})_0^2 e^{ik_s z}}{8 m \omega_0 [(\omega_\Delta - \omega_0) - i\gamma]} \left(|\mathcal{E}_p|^2 \mathcal{E}_s + \mathcal{E}_p^2 \mathcal{E}_{as}^* e^{i\Delta k z} \right), \tag{4.398}$$

and

$$\mathcal{P}_{NL}(\omega_{as}) = \frac{\epsilon_0^2 N (d\alpha/d\mathcal{Q})_0^2 e^{ik_{as}z}}{8m\omega_0[(\omega_\Delta - \omega_0) + i\gamma]} \left(|\mathcal{E}_p|^2 \mathcal{E}_{as} + \mathcal{E}_p^2 \mathcal{E}_s^* e^{i\Delta kz}\right). \tag{4.399}$$

The coupled-mode equations can then be written as

$$2ik_j \partial_z \mathcal{E}_j = -\mu_0 \omega_j^2 \mathcal{P}_{NL}(\omega_j) e^{-ik_j z}, \qquad j = p, s, as, \tag{4.400}$$

or explicitly for the Stokes mode:

$$i\partial_z \mathcal{E}_s = -\xi_s \left(|\mathcal{E}_p|^2 \mathcal{E}_s + \mathcal{E}_p^2 \mathcal{E}_{as}^* e^{i\Delta kz}\right), \tag{4.401}$$

and for the ant-Stokes mode:

$$i\partial_z \mathcal{E}_{as} = -\xi_{as} \left(|\mathcal{E}_p|^2 \mathcal{E}_{as} + \mathcal{E}_p^2 \mathcal{E}_s^* e^{i\Delta kz}\right). \tag{4.402}$$

Here

$$\xi_s = \frac{\epsilon_0 \omega_s N (d\alpha/d\mathcal{Q})_0^2}{16m\omega_0 n_s c[(\omega_\Delta - \omega_0) - i\gamma]}, \tag{4.403}$$

$$\xi_{as} = \frac{\epsilon_0 \omega_{as} N (d\alpha/d\mathcal{Q})_0^2}{16m\omega_0 n_{as} c[(\omega_\Delta - \omega_0) + i\gamma]}, \tag{4.404}$$

are the corresponding coupling constants and the wave-vector mismatch is defined as

$$\Delta k = 2k_p - k_s - k_{as}. \tag{4.405}$$

In the undepleted pump approximation and with very large wave-vector mismatch, the fast oscillating second term on the r. h. s of Eqs. (4.401) and (4.402) can be dropped and the resulting decoupled wave equations for the Stokes and anti-Stokes modes can be written as

$$i\partial_z \mathcal{E}_s = -\kappa_s |\mathcal{E}_p|^2 \mathcal{E}_s, \tag{4.406}$$

and

$$i\partial_z \mathcal{E}_{as} = -\kappa_{as} |\mathcal{E}_p|^2 \mathcal{E}_{as}. \tag{4.407}$$

The equation for the Stokes mode is equivalent to Eq. (4.375) describing exponential gain, and the anti-Stokes mode evolution is governed by

$$\frac{dI_{as}}{dz} = -\gamma_{as} I_p I_{as}, \tag{4.408}$$

where the anti-Stokes loss factor is defined as

$$\gamma_{as} = \gamma_{as0} \mathcal{L}(\omega_\Delta), \tag{4.409}$$

with the center-line loss factor given by

$$\gamma_{as0} = \frac{\omega_{as} N (d\alpha/d\mathcal{Q})_0^2}{8m\omega_0 \gamma c^2 n_{as} n_p}. \tag{4.410}$$

It follows from Eqs. (4.408) through (4.410) that for sufficiently large phase mismatch, the anti-Stokes mode decays exponentially with the decrement γ_{as},

$$I_{as} = I_{as0} \exp(-\gamma_{as} I_p z). \tag{4.411}$$

Thus unless one takes care to phase-match the anti-Stokes mode, it exponentially decays on propagation. This is the reason one usually focuses on the Stokes mode.

4.15 Transient stimulated Raman scattering

We present a semiclassical theory[2] of transient SRS in a hollow-core photonic crystal fiber (HCPCF) geometry. We consider a single-mode HCPCF filled with a molecular gas such as hydrogen. The single-mode HCPCF use guarantees a very large interaction length as light diffraction is arrested and its energy is squeezed into a tight fiber mode. Further, a properly engineered HCPCF can ensure all higher-order Stokes mode suppression such that the SRS excitation process engages only the first-order Stokes mode, thereby allowing to focus on the basic two-mode, pump and Stokes, situation. Quantum mechanically, a pump pulse photon absorption promotes a molecule from its initial state, labelled as "1", to one of the intermediate excited states, labelled as "i", that are far off resonance with both laser and Stokes pulses. As the excited molecule emits a photon at the Stokes frequency, it descends to a final state "3" which differs from the ground state. The released energy $\hbar(\omega_{i1} - \omega_{i3})$ excites molecular vibration/rotation; ω_{i1} and ω_{i3} are transition frequencies characterizing dipole allowed transitions from the initial and final levels, respectively, to any intermediate level. The appropriate energy level diagram is sketched in Fig. 4.31

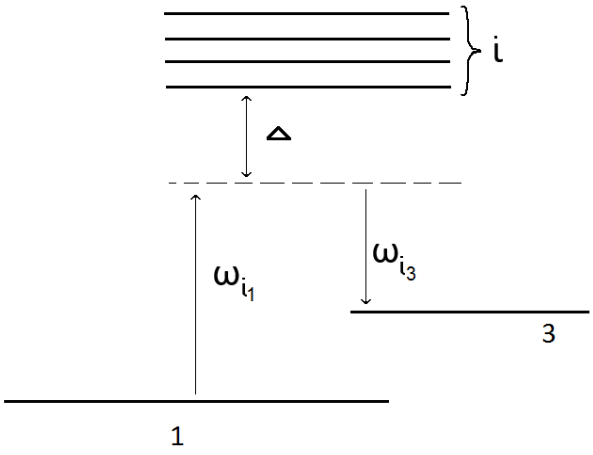

Figure 4.31: Energy level diagram for stimulated Raman scattering.

We will make two assumptions. First, the pump and Stokes pulse frequencies are tuned to exact Raman resonance such that $\omega_{31} \equiv \omega_3 - \omega_1 = \omega_p - \omega_s$, where $\omega_{1,3} = E_{1,3}/\hbar$ describe initial/final energies, $E_{1,3}$ in frequency units, and ω_p as well as ω_s are pump and Stokes pulse frequencies, respectively. The exact resonance implies that $\omega_{i1} - \omega_{i3} = \omega_p - \omega_s$. The exact Raman resonance is desirable to increase SRS efficiency and it can be attained in HCPCFs thanks to homogeneous line broadening there. This is because molecule collisions with the fiber core walls are the dominant mechanism of

[2]Some quantum mechanics background is required to understand the material of this section–see, for instance, Chaps. 2, 3, 4 & 14 of "Quantum Mechanics for Scientists & Engineers," by D. A. B. Miller, Cambridge University Press, 2008.

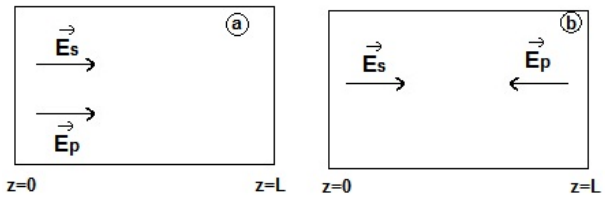

Figure 4.32: Forward-and backward-propagating SRS geometries

spectral line broadening in the system for sufficiently high gas pressures. The second assumption, corresponding to realistic experimental conditions, is weak excitation such that all excited level populations–including that of the final level–are negligible. The lack of population transfer implies that

$$\rho_{11} \simeq 1; \qquad \rho_{33} \simeq 0, \tag{4.412}$$

and consequently, the off-diagonal density matrix elements (coherences) are small as well,

$$\rho_{i1}, \rho_{i3}, \rho_{31} \ll 1. \tag{4.413}$$

The density matrix evolution is governed by the Schrödinger equation that reads

$$\partial_t \rho_{mn} = -(\gamma_{mn} + i\omega_{mn})\rho_{mn} - \tfrac{i}{\hbar}\textstyle\sum_k (V_{mk}\rho_{kn} - \rho_{mk}V_{kn}). \tag{4.414}$$

Here $\omega_{mn} \equiv \omega_m - \omega_n$ and we introduced a phenomenological damping rates γ_{mn}; V_{ij} is a matrix element of the dipole interaction Hamiltonian.

We will consider two experimentally feasible regimes: the co-propagating regime when pump and Stokes pulses propagate in the same direction and counter-propagating regime of the pump pulse propagating the direction opposite to the Stokes pulse propagation direction. To increase the Raman interaction efficiency, one has to maximize the pulse profile overlap. In the co-propagating geometry with the pump and Stokes pulses travelling together at the same speed $\beta_{1p} = \beta_{1s} = \beta$, which can be engineered by designing a dispersion flat fiber at the frequency range of interest, this can be achieved for nearly identical temporal profiles of the two pulses. In the counter-propagating geometry, one usually takes a long pump pulse which allows a passing by short Stokes pulse extract as much energy from it as possible. The two excitation regimes are sketched in Fig. 4.33.

The interaction Hamiltonian can then be written in the usual rotating-wave approximation in the compact form, encompassing both regimes as

$$\hat{V} = \tfrac{1}{2}\left[\mathcal{E}_p e^{i(\pm k_p z - \omega_p t)} d_{i1} |i\rangle\langle 1| + \mathcal{E}_s e^{i(k_s z - \omega_s t)} d_{i3} |i\rangle\langle 3| + h.\,c.\right] \tag{4.415}$$

Here $+(-)$ sign in the first term on the r.h.s. corresponds to the co-propagating (counter-propagating) geometry of Fig. 4.32; $\mathcal{E}_p$ and $\mathcal{E}_s$ are the pump and Stokes pulse amplitudes, respectively, and d_{i1} and d_{i3} are the corresponding dipole matrix

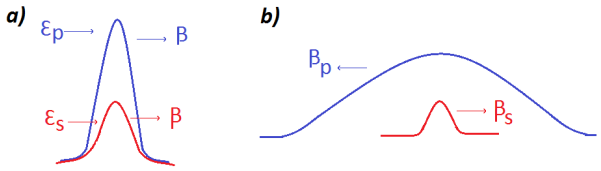

Figure 4.33: Forward-and backward-propagating SRS excitation geometries.

elements. Finally "h.c." is a shorthand for Hermitian conjugate. It follows at once from Eq. (4.415) that the only nonzero matrix elements of $\hat{V}$ are

$$V_{i1} = \tfrac{1}{2} d_{i1} \mathcal{E}_p e^{i(\pm k_p z - \omega_p t)}, \qquad V_{1i} = V_{i1}^*; \tag{4.416}$$

and

$$V_{i3} = \tfrac{1}{2} d_{i3} \mathcal{E}_s e^{i(k_s z - \omega_s t)}, \qquad V_{3i} = V_{i3}^*, \tag{4.417}$$

The corresponding density operator matrix elements obey the evolution equations

$$\partial_t \rho_{i1} = -(\gamma_{i1} + i\omega_{i1})\rho_{i1} - \tfrac{i}{\hbar}(V_{i1} + \rho_{31} V_{i3}), \tag{4.418}$$

$$\partial_t \rho_{i3} = -(\gamma_{i3} + i\omega_{i3})\rho_{i3} - \tfrac{i}{\hbar} V_{i1} \rho_{31}^*, \tag{4.419}$$

and

$$\partial_t \rho_{31} = -(\gamma_{31} + i\omega_{31})\rho_{31} - \tfrac{i}{\hbar} \textstyle\sum_i (V_{3i}\rho_{i1} - \rho_{3i} V_{i1}). \tag{4.420}$$

Here we took into account the approximations introduced by Eqs. (4.412) and (4.413). Further, transforming to the interaction picture by introducing slowly varying coherences viz.,

$$\rho_{i1} = \tilde{\rho}_{i1} e^{i(\pm k_p z - \omega_p t)}, \qquad \rho_{i3} = \tilde{\rho}_{i3} e^{i(k_s z - \omega_s t)}, \tag{4.421}$$

and

$$\rho_{31} = \tilde{\rho}_{31} e^{i(k_p - k_s)z} e^{-i(\omega_p - \omega_s)t}, \tag{4.422}$$

we can transform the density matrix evolution equations to

$$\partial_t \tilde{\rho}_{i1} = -[\gamma_{i1} + i\Delta]\tilde{\rho}_{i1} - \tfrac{i d_{i1} \mathcal{E}_p}{2\hbar} - \left(\tfrac{i d_{i3} \mathcal{E}_s}{2\hbar}\right) \tilde{\rho}_{31} \tag{4.423}$$

$$\partial_t \tilde{\rho}_{i3} = -[\gamma_{i3} + i\Delta]\tilde{\rho}_{i3} - \left(\tfrac{i d_i 1 \mathcal{E}_p}{2\hbar}\right) \tilde{\rho}_{31}^*, \tag{4.424}$$

and

$$\partial_t \tilde{\rho}_{31} = -\gamma_{31}\tilde{\rho}_{31} - \tfrac{i}{2\hbar} \textstyle\sum_i (d_{3i} \mathcal{E}_s^* \tilde{\rho}_{i1} - d_{i1} \mathcal{E}_p \tilde{\rho}_{3i}). \tag{4.425}$$

Here we introduced $\Delta = \omega_{i3} - \omega_s = \omega_{i1} - \omega_p$.

Let us now recall that all intermediate levels are far off resonance with the two dipole-allowed transitions. Mathematically, this implies large frequency detuning such that

$$\gamma_{i1} \ll \Delta, \qquad \gamma_{i3} \ll \Delta. \tag{4.426}$$

We can then adiabatically eliminate the intermediate levels. This term implies that the far-off resonance density matrix elements $\tilde{\rho}_{i1}$ and $\tilde{\rho}_{i3}$ rapidly oscillate around their local equilibrium values, determined by the pulse field amplitudes and the molecular coherence between the initial and final states, ρ_{31}. We can then formally drop the time derivatives on the l.h.s of Eqs. (4.423) and (4.424) to obtain

$$\tilde{\rho}_{i1} = -\frac{d_{i1}\mathcal{E}_p}{2\hbar\Delta} - \frac{d_{i3}\mathcal{E}_s}{2\hbar\Delta}\tilde{\rho}_{31}, \tag{4.427}$$

and

$$\tilde{\rho}_{i3} = -\frac{d_{i1}\mathcal{E}_p}{2\hbar\Delta}\tilde{\rho}^*_{31}. \tag{4.428}$$

It follows from Eq. (4.413) that to the leading order in the small parameter, $\tilde{\rho}_{31}$, the off-diagonal matrix elements read

$$\tilde{\rho}_{i1} \simeq -\frac{d_{i1}\mathcal{E}_p}{2\hbar\Delta}, \qquad \tilde{\rho}_{i3} \simeq 0. \tag{4.429}$$

On substituting from Eq. (4.429) into (4.425), we arrive at

$$\partial_t\tilde{\rho}_{31} = -\gamma_{31}\tilde{\rho}_{31} - \frac{i}{4\hbar^2}\sum_i\left(\frac{d_{3i}d_{i1}}{\Delta}\right)\mathcal{E}_p\mathcal{E}_s^*. \tag{4.430}$$

Finally, recalling that at Raman resonance $\omega_{i1} - \omega_{i3} = \omega_p - \omega_s$, implying that $\Delta = \frac{1}{2}(\omega_{i1}+\omega_{i3}-\omega_p-\omega_s)$, introducing the Raman transition dipole moment matrix element by the expression,

$$r_{\text{eff}} = \frac{1}{\hbar}\sum_i\frac{d_{3i}d_{i1}}{(\omega_{i1}+\omega_{i3}-\omega_p-\omega_s)}, \tag{4.431}$$

and rescaling the dipole matrix elements d_{i1} and d_{i3}, we obtain for the Raman density matrix element $\tilde{\rho}_{31}$, the governing equation

$$\partial_t\sigma = -\gamma\sigma + \left(\tfrac{ir_{\text{eff}}}{4\hbar}\right)\mathcal{E}_p\mathcal{E}_s^*. \tag{4.432}$$

Here we redefined $\tilde{\rho}_{31} = \sigma$ and $\gamma_{31} = \gamma$ to simplify the notation.

Recall now that as we show in Secs. 3.1 and 3. 2, in the absence of group-velocity dispersion of the fiber–or in cases the dispersion length is so long that dispersion is negligible–pulses propagate inside fibers with their group velocities. On the other hand, we describe the effect of pure nonlinearities on plane wave propagation within the framework of coupled-wave theory. Combining the two effects, slowly-varying envelope evolution equations for the Stokes and pump fields take the form

$$2ik_s(\partial_z\mathcal{E}_s + \beta_{1s}\partial_t\mathcal{E}_s) = -\mu_0\omega_s^2\mathcal{P}_{NL}(\omega_s)e^{-ik_sz}, \tag{4.433}$$

and

$$2ik_p(\pm\partial_z\mathcal{E}_p + \beta_{1p}\partial_t\mathcal{E}_p) = -\mu_0\omega_p^2\mathcal{P}_{NL}(\omega_p)e^{\mp ik_pz}, \tag{4.434}$$

where $\beta_{1p,s}$ are group velocities of the pump and Stokes pulses. The nonlinear polarization field can then be expressed as

$$P_{NL} = N\langle\hat{d}\rangle = \mathcal{P}_{NL}(\omega_p)e^{-i\omega_pt} + \mathcal{P}_{NL}(\omega_s)e^{-i\omega_st} + c.c.. \tag{4.435}$$

Here the average dipole moment is determined by

$$\langle \hat{d} \rangle = \mathrm{Tr}\{\rho \hat{d}\}, \tag{4.436}$$

where the dipole moment operator reads

$$\hat{d} = \sum_i d_{i1}|1\rangle\langle i| + d_{i3}|3\rangle\langle i| + h.c. \tag{4.437}$$

It then follows from Eqs. (4.435) through (4.437) after some straightforward albegra that

$$\mathcal{P}_{NL}(\omega_p) = N \sum_i d_{i1}\tilde{\rho}_{i1} e^{ik_p z}, \tag{4.438}$$

and

$$\mathcal{P}_{NL}(\omega_s) = N \sum_i d_{i3}\tilde{\rho}_{i3} e^{ik_s z}. \tag{4.439}$$

On substituting the approximate expressions (4.427) and (4.428) for the density matrix elements into Eqs. (4.433) and (4.434) and using Eqs. (4.438) and (4.439), we arrive, after some algebra, at the following set of coupled-wave equations for the pump and Stokes pulse amplitudes,

$$\pm\partial_z \mathcal{E}_p + \beta_{1p}\partial_t \mathcal{E}_p = \left(\frac{i\omega_p N r_{\mathrm{eff}}}{2\epsilon_0 c n_p}\right)\sigma E_s, \tag{4.440}$$

and

$$\partial_z \mathcal{E}_s + \beta_{1s}\partial_t \mathcal{E}_s = \left(\frac{i\omega_s N r_{\mathrm{eff}}}{2\epsilon_0 c n_s}\right)\sigma^* E_p. \tag{4.441}$$

Note that in deriving the last two equations we dropped a term on the l.h.s of Eq. (4.440) linear with respect to $\mathcal{E}_p$. This term arises when the first term on the r.h.s. of Eq. (4.427) is substituted to the r.h.s. of Eq. (4.433). One can show the dropped linear term leads to a common global phase of the pump and Stokes fields which does not affect the Raman dynamics.

Exercise 4.23. *Re-derive the coupled-wave equations for transient SRS by keeping the term linear in the pump pulse amplitude. Show that by a gauge transformation, $\mathcal{E}_p = \tilde{\mathcal{E}}_p e^{i\alpha z}$ and $\mathcal{E}_s = \tilde{\mathcal{E}}_s e^{-i\alpha z}$ with the appropriate α to be determined, the linear term can be eliminated from your equations and Eqs. (4.440), (4.441) can be recovered. Notice also that the Raman density matrix evolution, Eq. (4.432), is unaffected by the gauge transformation.*

Let us now consider co- and counter-propagating cases separately.

Co-propagating geometry. – We assume the fiber is engineered to be dispersion-flat, implying that $\beta_{1p} = \beta_{1s} = \beta_1$. We can then transform to a reference frame co-moving with the pulses and introduce new variable, $\zeta = z$ and $\tau = t - \beta_1 z$. The resulting SRS equations read

$$\partial_\zeta \mathcal{E}_p = \left(\tfrac{i\omega_p N r_{\mathrm{eff}}}{2\epsilon_0 c n_p}\right)\sigma \mathcal{E}_s, \tag{4.442}$$

$$\partial_\zeta \mathcal{E}_s = \left(\tfrac{i\omega_s N r_{\mathrm{eff}}}{2\epsilon_0 c n_s}\right)\sigma^* \mathcal{E}_p, \tag{4.443}$$

and

$$\partial_\tau \sigma = -\gamma\sigma + \left(\tfrac{ir_{\rm eff}}{4\hbar}\right)\mathcal{E}_p\mathcal{E}_s^*. \tag{4.444}$$

We can then introduce the pulse peak optical intensities viz.,

$$I_{s0,p0} = \frac{\epsilon_0 n_{s,p} c|E_{s0,p0}|^2}{2}, \tag{4.445}$$

and proceed normalizing the pulse fields to the peak pump intensity at the source, $\mathcal{E}_p = (2I_{p0}/\epsilon_0 c n_p)^{1/2}\overline{\mathcal{E}}_p$ and $\mathcal{E}_s = (2I_{p0}/\epsilon_0 c n_p)^{1/2}\overline{\mathcal{E}}_s$ and introducing dimensionless distance and time, $Z = \zeta/L_{\rm SRS}$ and $T = \tau/T_{\rm SRS}$. We introduced here characteristic SRS interaction distance and time viz.,

$$L_{\rm SRS} = \left(\frac{N r_{\rm eff}}{2\epsilon_0 c}\sqrt{\frac{\omega_p\omega_s}{n_p n_s}}\right)^{-1}, \quad T_{\rm SRS} = \left(\frac{r_{\rm eff} I_{p0}}{2\hbar\epsilon_0 c n_p}\right)^{-1}. \tag{4.446}$$

The dimensionless SRS equations can then be written as

$$\partial_Z \overline{\mathcal{E}}_p = i\kappa\sigma\overline{\mathcal{E}}_s, \tag{4.447}$$

$$\partial_Z \overline{\mathcal{E}}_s = i\kappa^{-1}\sigma^*\overline{\mathcal{E}}_p, \tag{4.448}$$

and

$$\partial_T \sigma = -\Gamma\sigma + i\overline{\mathcal{E}}_p\overline{\mathcal{E}}_s^*. \tag{4.449}$$

Here $\kappa = \sqrt{\omega_p n_s/\omega_s n_p}$ and $\Gamma = \gamma T_{\rm SRS}$ is a key dimensionless parameter governing the SRS process.

Counter-propagating geometry. – Assuming a dispersion-flat fiber, we can arrive at the dimensionless SRS field equations as

$$-\partial_Z \overline{\mathcal{E}}_p + \delta\,\partial_T \overline{\mathcal{E}}_p = i\kappa\sigma\overline{\mathcal{E}}_s, \tag{4.450}$$

and

$$\partial_Z \overline{\mathcal{E}}_s + \delta\,\partial_T \overline{\mathcal{E}}_s = i\kappa^{-1}\sigma^*\overline{\mathcal{E}}_p, \tag{4.451}$$

where $\delta = \beta_1 L_{\rm SRS}/T_{\rm SRS}$. Note that whereas in the co-propagating case one can transform away the drift term, the latter is not possible in the counter-propagating case even if the two group velocities are identical. Physically, this drift term indicates that any fixed points in pulse profiles, the peak intensity positions, say, shift relative to their positions at the fiber inputs as the Stokes pulse zaps by the pump one.

Let us now briefly discuss order-of-magnitude values of relevant parameters for SRS in HCPCF. For simplicity, we assume the fiber is filled with molecular hydrogen. Typically nanosecond pump pulses, $1 \leq t_p \leq 10$ ns carrying from 10 to 100 μJ are employed. The Raman dipole moment matrix element can be estimated as $r_{\rm eff} \simeq 1.4\times10^{-41}$ C m^2/V. Typical gas densities and relaxation time at 1 bar of pressure are[3] $N \simeq 2\times10^{20}$ cm^{-3} and $T_R = \gamma^{-1} \simeq 5$ ns.

Finally, we can derive an approximate expression for the threshold gain required to jumpstart the SRS process from noise. To this end, we need an expression for a

[3]Source: F. Flora and L. Giudicotti, Appl. Opt. **26**, 4001-4008 (1987).

linear gain in the cw case. The latter can be easily obtained by looking int a cw limit of Eqs. (4.442) through (4.444) in the undepleted pump approximation. Namely, assuming, $\mathcal{E}_p = const$ and letting $\partial_\tau \sigma = 0$, we can derive an expression for the amplified Stokes pulse intensity and comparing with Eq. (4.376), we can infer conclude that

$$g_R = \frac{\omega_s N |r_{\rm eff}|^2}{4\epsilon_0^2 c^2 n_s n_p \hbar \gamma}. \tag{4.452}$$

Exercise 4.24. *Derive Eq. (4.452) and compare with Eq. (4.380).*

We can finally estimate a critical power required for SRS generation with a cw laser source in an HCPCF. The input intensity can be estimated as $I_{p0} \simeq P/A_{\rm eff}$, where P is the pump power and $A_{\rm eff}$ is a an effective HCPCF core area which takes into account the spatial pump mode distribution in the fiber. At the threshold, Raman gain is

$$G = g_R I_{p0} L = G_{\rm th}. \tag{4.453}$$

The threshold gain is determined empirically to fall in the range $20 \leq G_{\rm th} \leq 30$, yielding the power estimate

$$P_{\rm th} \simeq \frac{G_{\rm th} A_{\rm eff}}{g_R L}. \tag{4.454}$$

4.16 Spontaneous Brillouin scattering

Brillouin scattering arises as light scattering from collective oscillation modes in the media such as pressure or acoustic waves. Spontaneous Brillouin scattering is caused by thermal density fluctuations in the media which induce dielectric permittivity fluctuations. The latter, in turn, give rise to macroscopic medium polarization. To describe the phenomenon quantitatively, let us consider the medium density ρ and temperature T as independent thermodynamic variables and express the permittivity fluctuations as

$$\epsilon' = \left(\frac{\partial \epsilon}{\partial \rho}\right)_T \rho' + \left(\frac{\partial \epsilon}{\partial T}\right)_\rho T'. \tag{4.455}$$

We assume that the medium is isotropic which is an adequate model for gases and liquids. The first (large) term on the r.h.s. of Eq. (4.455) describes the contribution due to electrostriction, i. e, the tendency of the dielectric constant to vary with the medium density, whereas the second–smaller–term is due to temperature variations caused by absorption in the medium. In practice, the second term on the r.h.s of Eq (4.455) is negligible for transparent or nearly transparent media which we assume to be the case hereafter. Thus, to good accuracy, we can write

$$\epsilon' = \left(\frac{\partial \epsilon}{\partial \rho}\right) \rho' = \frac{\gamma_e}{\rho} \rho', \tag{4.456}$$

where we dropped the subscript T for notational simplicity and introduced the electrostriction constant γ_e, defined as

$$\gamma_e \equiv \rho \left(\frac{\partial \epsilon}{\partial \rho}\right). \tag{4.457}$$

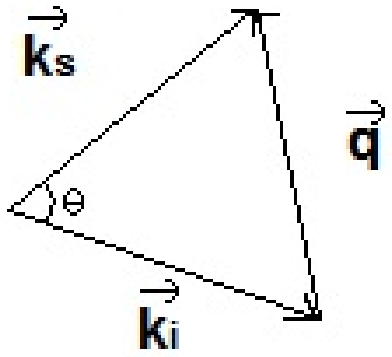

Figure 4.34: Illustrating momentum conservation in a single photon-phonon scattering act.

The induced polarization field reads

$$P_{NL} = \epsilon_0 \epsilon' E, \tag{4.458}$$

where in the absence of the input Stokes mode, the electric field is represented by the pump wave such that

$$E = \tfrac{1}{2}\mathcal{E} e^{i(\mathbf{k}_p \cdot \mathbf{r} - \omega_p t)} + c.c., \tag{4.459}$$

and the density fluctuations constitute a propagating acoustic wave,

$$\rho' = \tfrac{1}{2}\tilde{\rho} e^{i(\mathbf{q}\cdot\mathbf{r} - \Omega t)} + c.c. \tag{4.460}$$

Here $\mathbf{q}$ and Ω are the wave vector and frequency of an acoustic (Brillouin) phonon which are related by the dispersion relation

$$\Omega = |\mathbf{q}| c_s, \tag{4.461}$$

where c_s is the speed of sound.

It follows from Eqs. (4.456) through (4.460) that the induced polarization has two shifted frequencies such that

$$P_{NL} = \tfrac{1}{2}\mathcal{P}(\omega_s) e^{-i\omega_s} + \tfrac{1}{2}\mathcal{P}(\omega_{as}) e^{-i\omega_{as}} + c.c., \tag{4.462}$$

where

$$\omega_s = \omega_p - \Omega, \qquad \omega_{as} = \omega_p + \Omega, \tag{4.463}$$

are the generated Stokes and anti-Stokes frequencies. The Stokes polarization component, for example, can be written explicitly as

$$\mathcal{P}(\omega_s) = \left(\tfrac{\epsilon_0 \gamma_e}{2\rho}\mathcal{E}\tilde{\rho}^*\right) e^{i\mathbf{k}_s \cdot \mathbf{r}}, \tag{4.464}$$

where

$$\mathbf{k}_s = \mathbf{k}_p - \mathbf{q}. \tag{4.465}$$

As $\Omega \ll \omega_p, \omega_s$ due to phonon sluggishness, $c_s \ll c$, it is reasonable to assume that the magnitude of photon momentum does not appreciably change at each scattering event, $k_p \approx k_s$. It then follows from Eqs. (4.461), (4.463) and (4.465) and the geometry of Fig. 5. 6 that

$$\Omega = 2k_p \sin\theta/2, \tag{4.466}$$

where θ is a photon scattering angle. It follows at once from Eq. (4.466) that the most energetically efficient Stokes wave generation–because Ω_B is maximized–takes place in the backward direction, $\theta = \pi$. Moreover, the energy-momentum conservation laws in each scattering event explicitly prohibit Stokes wave generation in the forward direction, $\theta = 0$.

4.17 Brillouin phonon propagation

Let us now briefly examine the generated phonon propagation. As phonons are acoustic waves, their evolution is governed by linearized fluid dynamics equations. We postulate that in 1D geometry we are going to study, the mass and momentum conservation of the fluid can be expressed as

$$\partial_t \rho + \partial_z(\rho v) = 0, \tag{4.467}$$

and

$$\partial_t v + v\partial_z v = -\tfrac{1}{\rho}\partial_z p_{eff} + (\zeta + \tfrac{4}{3}\nu)\partial^2_{zz} v \tag{4.468}$$

Here we assumed that the acoustic wave propagates along the z-axis, ζ and ν are bulk and shear kinematic viscosity coefficients, and the effective pressure can be expressed in the form

$$p_{\text{eff}} = p - \gamma_e \frac{\epsilon_0 E^2}{2}. \tag{4.469}$$

The first term on the r. h. s. of Eq. (4.469) is the static fluid pressure, whereas the second term represents an electrostriction pressure which describes a force per unit area that tends to pull fluid particles toward regions of the strong electric field E. The electrostriction forces arise due to the density dependence of the dielectric constant.

Eqs. (4.467) and (4.468) are not closed until a relationship, the so-called equation of state, between the pressure p and density ρ is specified. To this end, we can express the pressure p in Eq. (4.469) in terms of any two independent thermodynamic variables. In our case, it is convenient to use the density and entropy such that

$$\frac{\partial p}{\partial z} = \left(\frac{\partial p}{\partial \rho}\right)_S \frac{\partial \rho}{\partial z} + \left(\frac{\partial p}{\partial S}\right)_\rho \frac{\partial S}{\partial z}. \tag{4.470}$$

In the absence of heat transfer in transparent media, we can assume that acoustic waves are adiabatic, that is the entropy is conserved, $S = const$. It then follows that the pressure gradient can be expressed as

$$\frac{\partial p}{\partial z} = c_s^2 \frac{\partial \rho}{\partial z}, \tag{4.471}$$

where

$$c_s = \sqrt{\left(\frac{\partial p}{\partial \rho}\right)_S}, \tag{4.472}$$

is the adiabatic speed of sound in the medium.

We can now linearize Eqs. (4.467), and (4.468), subject to the equation of state (4.471), by considering small density ρ' and velocity v deviations from the equilibrium state, $v = 0$–the fluid is at rest–and $\rho = \rho_0$. Thus, we substitute from

$$\rho = \rho_0 + \rho', \qquad \rho' \ll \rho_0, \tag{4.473}$$

into Eqs. (4.467) and (4.468) and keep only terms linear with respect to either ρ' or v, leading to the acoustic approximation:

$$\partial_t \rho' + \rho_0 \partial_z v = 0, \tag{4.474}$$

and

$$\partial_t v = -\left(\frac{c_s^2}{\rho_0}\right)\partial_z \rho' + \left(\frac{\epsilon_0 \gamma_e}{2\rho_0}\right)\partial_z E^2 + (\zeta + \tfrac{4}{3}\nu)\partial_{zz}^2 v \tag{4.475}$$

Taking the time and space derivatives on both sides of Eqs. (4.474) and (4.475), respectively, we can transform our acoustic equations to

$$\partial_{zt}^2 v = -\left(\frac{1}{\rho_0}\right)\partial_{tt}^2 \rho', \tag{4.476}$$

and

$$\partial_{tz}^2 v = -\left(\frac{c_s^2}{\rho_0}\right)\partial_{zz}^2 \rho' + \left(\frac{\epsilon_0 \gamma_e}{2\rho_0}\right)\partial_{zz}^2 E^2 + \frac{(\zeta + \frac{4}{3}\nu)}{\rho_0}\partial_{tzz}^3 \rho'. \tag{4.477}$$

In deriving Eq. (4.477), we eliminated the fluid velocity on the r. h. s., with the help of Eq. (4.474). Equating the mixed velocity derivatives from Eq. (4.476) and (4.477), we eliminate the velocity field and arrive at the wave equation for the density variations alone in the form

$$\partial_{tt}^2 \rho' - c_s^2 \partial_{zz}^2 \rho' - \Gamma \partial_{tzz}^3 \rho' = -\tfrac{1}{2}\epsilon_0 \gamma_e \partial_{zz}^2 E^2. \tag{4.478}$$

Here we introduced the effective damping rate,

$$\Gamma = \zeta + \frac{4}{3}\nu. \tag{4.479}$$

The electrostriction term on the r.h.s of Eq. (4.478) plays the role of a driving source.

Let us focus on the acoustic wave propagation in the absence of driving, $E = 0$. Eq. (4.478) with $E = 0$ has a plane-wave solution of the form,

$$\rho' \propto e^{i(qz - \Omega t)}. \tag{4.480}$$

On substituting from Eq. (4.480) into (4.478) with E=0, we arrive at the dispersion relation

$$-\Omega^2 + c_s^2 q^2 - i\Gamma \Omega q^2 = 0. \tag{4.481}$$

Or,

$$q^2 = \frac{\Omega^2/c_s^2}{1 - \frac{i\Gamma\Omega}{c_s^2}} \simeq \frac{\Omega^2}{c_s^2}\left(1 + \frac{i\Gamma\Omega}{c_s^2}\right), \tag{4.482}$$

where we assumed that $\Gamma\Omega c_s^2 \ll 1$. At the same level of approximation, we can obtain the wave number as

$$q \simeq \Omega/c_s + i\alpha/2, \tag{4.483}$$

where we introduced the inverse phonon damping length α as

$$\alpha = \Gamma q^2/c_s. \tag{4.484}$$

We can now estimate characteristic parameters of Brillouin acoustic waves noticing that as follows from Eqs. (4.465) for backward propagating Stokes modes, $q \simeq 2k_p \sim 4\pi \times 10^6$ m^{-1} for the pumping wavelength of the order of 1μm. Assuming further typical values: $\Gamma \sim \zeta \sim \nu = \eta/\rho_0$ with $\rho_0 \sim 10^3$ kg/m^3 and the dynamic sheer viscosity $\eta \sim 10^{-3}$ N s/m^2 as well as $c_s \sim 10^3$ m/s, we estimate the Brillouin frequency to be $\Omega/2\pi \sim qc_s/2\pi \sim 2$ GHz, and the inverse damping length $\alpha \sim 1.6 \times 10^5$ m^{-1}, implying that phonons are damped over a characteristic length α^{-1} of just 5 μm. Thus, generated ultrasound phonons are strongly damped over a characteristic length over which the fluid density or the applied electric field amplitude changes.

4.18 Stimulated Brillouin scattering

Consider now the situation when both the pump and Stokes pulses are present and their coupling through the electrostriction causes sound wave generation. Resonance interaction of the sound waves with the pump and Stokes modes causes amplification of the latter at the expense of the former. This process is known as *stimulated Brillouin scattering* (SBS). The electric field can be expressed as

$$E(t,z) = \tfrac{1}{2}[\mathcal{E}_p(t)e^{i(k_p z - \omega_p t)} + \mathcal{E}_s(t)e^{i(-k_s z - \omega_s t)} + c.\,c.], \tag{4.485}$$

where $\mathcal{E}_p$ and $\mathcal{E}_s$ are slowly varying pump and Stokes pulse amplitudes, and we assume that the Stokes mode propagates in the backward direction to maximize the SBS efficiency. The electrostriction coupling is specified by the term

$$E^2(t,z) = \tfrac{1}{2}[\mathcal{E}_p\mathcal{E}_s^* e^{i(k_p+k_s)z}e^{-i(\omega_p-\omega_s)t} + NR + c.\,c.], \tag{4.486}$$

where NR, as before, stands for non-resonant terms. The generated acoustic wave can be described in terms of the medium density variations as

$$\rho' = \tfrac{1}{2}\tilde{\rho}e^{i(qz-\Omega t)} + c.c. \tag{4.487}$$

Here,

$$q = k_p + k_s \simeq 2k, \qquad \Omega = \omega_p - \omega_s, \tag{4.488}$$

where $k = k_p \simeq k_s$.

On substituting from Eq. (4.485) through (4.487) into the acoustic wave equation (4.478), we obtain

$$-2i\Omega\partial_t\tilde{\rho} + (\Omega_B^2 - \Omega^2 - i\Gamma\Omega q^2)\tilde{\rho} = \tfrac{1}{2}\epsilon_0\gamma_e q^2\mathcal{E}_p\mathcal{E}_s^*, \tag{4.489}$$

where $\Omega_B = c_s q$. In deriving Eq. (4.489) we dropped the spatial derivative of $\tilde{\rho}$ because generated Brillouin phonons are ultrasound, and hence are strongly damped, as we showed in the previous section. Introducing $\Gamma_B = \Gamma q^2$ and assuming $\Omega \simeq \Omega_B$ to ensure resonant SBS enhancement, we can simplify,

$$\Omega_B^2 - \Omega^2 - i\Gamma\Omega q^2 \simeq 2\Omega_B(\Omega_B - \Omega - i\Gamma_B/2). \tag{4.490}$$

Combining Eqs. (4.489) and (4.490), we arrive, after a simple rearrangement, at

$$\partial_t\tilde{\rho} = -(\Gamma_B/2 + i\Delta)\tilde{\rho} + \left(\tfrac{i\epsilon_0\gamma_e k^2}{\Omega_B}\right)\mathcal{E}_p\mathcal{E}_s^*, \tag{4.491}$$

where we introduced frequency detuning as

$$\Delta = \Omega_B - \Omega. \tag{4.492}$$

Eq. (4.491) is the material evolution equation for the SBS process.

The coupled-wave equations for the pump and Stokes pulses can be derived in strict analogy with the SRS wave equations. Specifically, starting from Maxwell's equations an applying SVEA, we obtain

$$2ik_s(-\partial_z\mathcal{E}_s + \beta_s\partial_t\mathcal{E}_s)e^{-ik_s z} = -\mu_0\omega_s^2\mathcal{P}_{NL}(\omega_s), \tag{4.493}$$

and

$$2ik_p(\partial_z\mathcal{E}_p + \beta_p\partial_t\mathcal{E}_p)e^{ik_p z} = -\mu_0\omega_p^2\mathcal{P}_{NL}(\omega_p). \tag{4.494}$$

Here β_s and β_p are the inverse group velocities of the Stokes and pump pulses. The induced polarization field can be expressed as

$$\mathcal{P}_{NL} = \tfrac{1}{2}\mathcal{P}_{NL}(\omega_s)e^{-i\omega_s t} + \tfrac{1}{2}\mathcal{P}_{NL}(\omega_p)e^{-i\omega_p t} + c.c., \tag{4.495}$$

where using Eqs. (4.456), (4.458) and (4.487), we obtain, by analogy with Eq. (4.464),

$$\mathcal{P}_{NL}(\omega_s) = \left(\tfrac{\epsilon_0\gamma_e}{2\rho_0}\right)\mathcal{E}_p\tilde{\rho}^* e^{-ik_s z}, \tag{4.496}$$

and

$$\mathcal{P}_{NL}(\omega_p) = \left(\tfrac{\epsilon_0\gamma_e}{2\rho_0}\right)\mathcal{E}_s\tilde{\rho}e^{ik_p z}. \tag{4.497}$$

On substituting from Eqs. (4.496) and (4.497) into Eqs. (4.494) and (4.495), we obtain, after simple algebra, the following equations

$$2ik_s(-\partial_z\mathcal{E}_s + \beta_s\partial_t\mathcal{E}_s) = -\frac{\omega_s^2}{c^2}\left(\frac{\gamma_e}{2\rho_0}\right)\mathcal{E}_p\tilde{\rho}^*, \tag{4.498}$$

and

$$2ik_p(\partial_z\mathcal{E}_p + \beta_p\partial_t\mathcal{E}_p) = -\frac{\omega_p^2}{c^2}\left(\frac{\gamma_e}{2\rho_0}\right)\mathcal{E}_s\tilde{\rho}. \tag{4.499}$$

Introducing $\omega = \omega_p \simeq \omega_s$, $n = n_p \simeq n_s$, we can cast Eqs. (4.498) and (4.499) to

$$-\partial_z \mathcal{E}_s + \beta_s \partial_t \mathcal{E}_s = \left(\frac{i\omega\gamma_e}{4cn\rho_0}\right) \mathcal{E}_p \tilde{\rho}^*, \tag{4.500}$$

and

$$\partial_z \mathcal{E}_p + \beta_p \partial_t \mathcal{E}_p = \left(\frac{i\omega\gamma_e}{4cn\rho_0}\right) \mathcal{E}_s \tilde{\rho}. \tag{4.501}$$

Eqs. (4.500) and (4.501), together with Eq. (4.491) form the basis for quantitative description of SBS.

In the cw limit, the stationary solution to Eq. (4.491) can be easily obtained dropping the time derivative of $\tilde{\rho}$, yielding

$$\tilde{\rho}_{ss} = \frac{i\epsilon_0 \gamma_e k^2 \mathcal{E}_p \mathcal{E}_s^*}{\Omega_B(\Gamma_B/2 + i\Delta)}. \tag{4.502}$$

On substituting from Eq, (4.502) into (4.500) and (4.501), and dropping the time derivatives of the field amplitude, we obtain

$$\partial_z \mathcal{E}_s = -\frac{\epsilon_0 \omega \gamma_e^2 k^2}{4\Omega_B cn\rho_0(\Gamma_B/2 - i\Delta)} |\mathcal{E}_p|^2 \mathcal{E}_s, \tag{4.503}$$

and

$$\partial_z \mathcal{E}_p = -\frac{\epsilon_0 \omega \gamma_e^2 k^2}{4\Omega_B cn\rho_0(\Gamma_B/2 + i\Delta)} |\mathcal{E}_s|^2 \mathcal{E}_p, \tag{4.504}$$

The latter can be transformed to the evolution equations for the optical intensities, by analogy with the SRS case, yielding

$$d_z I_s = -g_B I_s I_p, \tag{4.505}$$

and

$$d_z I_p = -g_B I_s I_p, \tag{4.506}$$

where we introduced the SBS gain coefficient as

$$g_B = g_{B0} \frac{\Gamma_B^2/4}{\Gamma_B^2/4 + \Delta^2}. \tag{4.507}$$

In Eq. (4.507), g_{B0} is the center-line gain defined as

$$g_{B0} = \frac{\omega^2 \gamma_e^2}{nc^3 c_s \rho_0 \Gamma_B}. \tag{4.508}$$

Let us estimate a typical value of g_{B0}. Consider CS_2 at 1 μ as a characteristic medium for SBS. Taking typical values $\omega/2\pi = 3 \times 10^{14}$ Hz, $\gamma_e = 2.4$, $n \simeq 1.7$, $c_s \simeq 10^3$ m/s, $\rho_0 \simeq 1300$ kg/m^3, and $\Gamma_B^{-1} \simeq 4 \times 10^{-9}$ s, we obtain an estimate $g_{B0} \simeq 0.2$ cm/MW.

In the undepleted pump approximation, $I_p = const$ and a straightforward integration of Eq. (4.505) yields,

$$I_s(z) = I_s(L) \exp[g_B I_p (L - z)]. \tag{4.509}$$

It follows at once from Eq. (4.509) that the Stokes mode intensity grows exponentially on its propagation backward from the exit to the interaction volume towards its entrance.

Whenever pump depletion is no longer negligible, Eqs. (4.505) and (4.506) must be considered together. It can be easily inferred that

$$d_z I_s = d_z I_p, \tag{4.510}$$

implying that

$$I_p(z) = I_s(z) + C, \tag{4.511}$$

where $C = I_{p0} - I_{s0}$ is determined by initial conditions. Eliminating the pump intensity

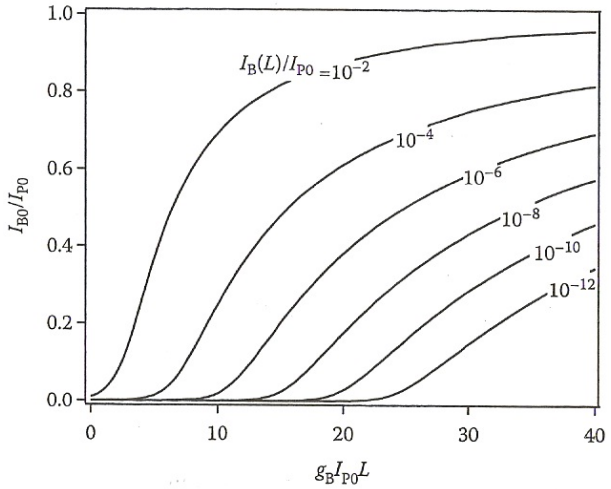

Figure 4.35: Intensity transfer characteristics of SRS beyond the undepleted pump approximation.

from Eq. (4.505) with the help of Eq. (4.516), we obtain

$$d_z I_s = -g_B I_s (I_s + C). \tag{4.512}$$

Eq. (4.512) can be readily integrated yielding

$$I_s(z) = \frac{I_{s0}(I_{p0} - I_{s0})}{I_{p0} \exp[g_B z (I_{p0} - I_{s0})] - I_{s0}}. \tag{4.513}$$

However, as the Stokes mode propagates backwards, we must express the Stokes intensity at the input I_{s0} in terms of its value at the output $I_s(L)$ which serves as the proper initial condition. It follows from Eq. (4.513) that

$$I_s(L) = \frac{I_{s0}(I_{p0} - I_{s0})}{I_{p0} \exp[g_B L (I_{p0} - I_{s0})] - I_{s0}}, \tag{4.514}$$

which is a transcendental equation giving the unknown reflection coefficient at the input, I_{s0}/I_{p0} in terms of $I_s(L)/I_{p0}$. Instead of solving it however, we can simply plot $g_B I_{p0} L$ as a function of I_{s0}/I_{p0} and swap the axes. The result is displayed in Fig 5.7. It is seen from the figure that significant pump depletion takes place when the overall gain $G = g_B I_{p0} L$ exceeds the value of 20.

In general, there are two possible SBS setups illustrated in Fig. 5.8. If both pump and Stokes fields are present–as is seen in Fig. 5.8 on the left–the process is referred to as SBS amplification whereby the initially Stokes mode is amplified while propagating in the backward direction. In the second instance, shown in Fig. 5.7 on the right,

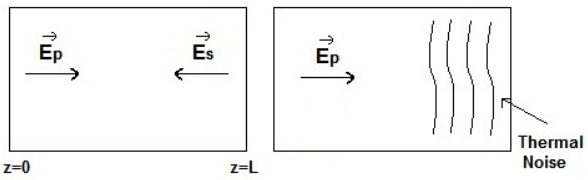

Figure 4.36: Illustrating two SBS modalities: SBS amplification (left) and SBS generation (right).

no Stokes component is initially present and SBS generation starts off from thermal noise near distributed throughout the interaction region. The process then starts as spontaneous Brillouin scattering triggered by thermal noise. The key metric for such SBS generation efficiency is the reflection coefficient defined as

$$R = \frac{I_{s0}}{I_{p0}}. \tag{4.515}$$

In the initial stage of the process pump depletion is negligible. Hence, the Stokes intensity at the output face $z = 0$ is related to its magnitude at the input $z = L$ according to Eq. (4.509):

$$I_{s0} = I_s(L)e^G, \tag{4.516}$$

where the overall gain at the Brillouin resonance is defined as

$$G = g_{B0} I_{p0} L. \tag{4.517}$$

A convenient figure-of-merit to indicate a threshold for the SBS generation is $R_{th} = 0.01$, i. e., the generated Stokes mode at the output has the intensity equal to 1% of the input pump intensity. Experiments carried out with a variety of SBS materials show that G_{th} lies in a fairly narrow interval from 25 to 30 under rather general conditions.

We can finally estimate a critical power required for SBS generation with a focused cw laser beam. The input intensity can be estimated as $I_{p0} \simeq P/\pi w_0^2$, where P is the pump power and w_0 is a spot-size of the focused beam. The characteristic interaction length for a focused beam is determined by its Rayleigh range, $z_R \simeq k_p w_0^2$, assuming the beam to be Gaussian. Substituting this to Eq. (4.517) with $L \sim z_R$, we arrive at

$$G \simeq 2 g_{B0} P/\lambda_p. \tag{4.518}$$

The critical power is determined by $G = G_{th}$ such that

$$P_{th} \simeq \frac{G_{th}\lambda_p}{2g_{B0}}. \tag{4.519}$$

For CS_2, for example, $g_{B0} \simeq 0.2$ cm/MW and using $G_{th} = 28$ and $\lambda_p = 1$ μm, we arrive at $P_{th} \simeq 7$ kW.